Identification of a novel subnetwork involved in eye size variation between *Drosophila melanogaster* and *D. mauritiana*

Dissertation

for the award of the degree
Doctor rerum naturalium (*Dr.rer.nat.*)

Division of Mathematics and Natural Sciences
of the Georg-August-Universität Göttingen

within the doctoral program *International Max Planck Research School for Genome Science* of the Georg-August University School of Science (GAUSS)

submitted by

Ting-Hsuan Lu
from Chiayi, Taiwan

Göttingen, December 2021

Thesis Committee

Dr. Nico Posnien (Supervisor)
Dept. of Developmental Biology, Johann-Friedrich-Blumenbach-Institute of Zoology and Anthropology, Georg-August-University Göttingen

Prof. Dr. Gregor Bucher
Dept. of Evolutionary Developmental Genetics, Johann-Friedrich-Blumenbach-Institute of Zoology and Anthropology, Georg-August-University Göttingen

Prof. Dr. Christoph Bleidorn
Dep. Animal Evolution and Biodiversity, Johann-Friedrich-Blumenbach-Institute of Zoology and Anthropology, Georg-August-University Göttingen

Members of the Examination Board

Reviewer: Dr. Nico Posnien
Dept. of Developmental Biology, Johann-Friedrich-Blumenbach-Institute of Zoology and Anthropology, Georg-August-University Göttingen

Second Reviewer: Prof. Dr. Gregor Bucher
Dept. of Evolutionary Developmental Genetics, Johann-Friedrich-Blumenbach-Institute of Zoology and Anthropology, Georg-August-University Göttingen

Further members of the Examination Board

Prof. Dr. Christoph Bleidorn
Dep. Animal Evolution and Biodiversity, Johann-Friedrich-Blumenbach-Institute of Zoology and Anthropology, Georg-August-University Göttingen

Prof. Dr. Halyna Shcherbata
Research Group Gene Expression and Signaling, Institute of Cell Biochemistry, Medizinische Hochschule Hannover

Prof. Daniel J. Jackson
Dept. of Geobiology, Geoscience Centre, Georg-August-University Göttingen

Dr. Gerd Vorbrüggen
Research Group Molecular Cell Dynamics, Max Planck Institute for Biophysical Chemistry

Date of the oral examination: February 24th, 2022

Declaration

I herewith declare, that I prepared the Dissertation

"Identification of a novel subnetwork involved in eye size variation between *Drosophila melanogaster* and *D. mauritiana*"

on my own and with no other sources and aids than quoted.

_____ Göttingen, February 24th, 2022

Ting-Hsuan Lu

What man sees depends both upon what he looks at and also upon what his previous visual-conception experience has taught him to see.

(Thomas S. Kuhn)

Acknowledgement

This study started in the autumn time in 2017, when all the leaves fall, flowers dropped, and temperature decreased; whereas it stopped in the end of the winter time, when everything comes back to life.

My study cannot be finished without all the helps from others. First of all, I would like to thank my supervisor Dr. Nico Posnien, who provides me this opportunity to work in this challenging and exciting project. He always supports me and shares great idea with me. He encourages me to join the scientific meetings, method courses, summer schools, which always provides me new aspects to learn. Not only the scientific point of view, had I learnt also the way to lead and trust others. Whenever I knocked the door or sent a message, he always opened the door (or Zoom) and started our discussion with very warm greeting.

And, I would like to appreciate all the help from my Thesis Committee members. Thanks to Prof. Gregor Bucher who joined the TAC meeting and always pointed out crucial aspects. Thanks to Prof. Halyna Shcherbata for really helpful advices to reshape my projects in the beginning. Thanks to Prof. Christopher Bleidorn for kindly willing to join with short notice and all the helpful discussions. I would also like to thank Dr. Gerd Vorbrüggen and Prof. Daniel Jackson, who agrees to serve in my examination board.

I would never start the journey if without the big help from IMPRS-GS and GGNB office, especially thanks to Dr. Henriette Irmer. As the first batch in IMPRS-GS, everything would be impossible without her. Thanks to all the peers in the IMPRS-GS for fruitful discussion in our formal retreat or informal meet up. I also appreciated the opportunity from GGNB which provides me extra funding to finish my work and all the method courses and workshops.

Besides, I enjoyed my time in the big family in department of Developmental Biology in these 4 years. Every annual progress report in the department always helps me to reconstruct my project and my scientific mindset. Therefore, I would like to thank Prof. Ernst Wimmer, Prof. Sigrid Hoyer-Fender and Dr. Marita Büscher. As well as, I sincerely thank to all of our department assistances, especially Elke in fly crossing and mites checking; Birgit and Merle for all the administrative supports; Beate and Tarek for the microscope and IT helps.

In addition, I would also like to thank all the wonderful lab mates in the Posnien lab, Amel, Gordon, and Linh, for creating a nice atmosphere in exchanging idea and helping each other. A big thanks

to Dr. Elisa Buchberger for all her help when I first joined the lab and the time afterward, and for introducing me to join GGNB Times Newsletter editorial board; and also thank Dr. Micael Reis for his mathematic knowledge (and also funny stories). I am grateful to supervise some honor students during the PhD study, Yi-Ching Lai (enhancer test assay), Jan Ahrend (ISH for *Rat1*), and Lena Reim (functional analyses of partial candidate genes).

As well as, I thank all the members in the department who sharing their stories, technologies, equipment, skills and food, as well as providing some useful suggestions on my experiments to solve my problems. In the long way of the study, it was my pleasure to have those great lab mates, Cera, Constanza, Gordon, Annka and Erica, for sharing the difficulties, happiness and good movies from time to time. I would also like to give my special thanks to nice colleague and best friend, Dr. Felix Quade, for cooking together and sharing useful information.

I would also like to thank our collaborators, Prof. Alistair P. McGregor and his whole group in Oxford for sharing their experiences and techniques. Especially, I would like to thank Dr. Pedro Gaspar for teaching me all the knowledges.

Thanks to all of my friends for making Göttingen as a second home, Felicia, Sheng-an, Wen-Shen, Po-Yin, Chao-Chin, Luby, Chichak and Julia. I also thank to Dr. Guan-Ting Liu and Dr. Yu-Chih Lin for their advices in applying the PhD program. Thanks to Kai-Chih, Ning-Cheng and Pei-Yu, for lasting friendship and their interests from far away. Also, thanks to "Zubi's" for giving me every joyful Friday.

It is my pleasure to have my best friends, Shih-Han and An-Chun aside, who shares happiness and warms me up when I am in the dark. A great thank goes to Dr. Ming-Cheng Wu, Prof. Kuang-Hui Lu and Prof. Maurice Ku in Taiwan for nice scientific conversation and advices every time when we met.

Finally, the greatest thank goes to my dearest Mom, Dad, my sister (Dr. Yen-Ting Lu) for their countless loves and endless supports during my study. With all of you having my back, the difficulties became less hard. Thank you for encouraging me to develop my interests and trusting me no matter what decision I made.

Author contribution

Ting-Hsuan Lu and Nico Posnien conceptualized the project. Ting-Hsuan Lu designed and performed the experiments, derived the new network model regulating eye/head development and analysed the data. Jan Ahrend assisted with ISH for *Rat1*, and Lena Reim assisted with overexpression experiments via TRiP/CRISPR system and RNAi using *elav*-Gal4, *tsh*-Gal4 and *dpp*-Gal4. Gordon Wiegleb generated and analysed the sn-RNAseq data and he provided the plots used in this thesis. Ting-Hsuan Lu wrote the thesis in consultation with Nico Posnien.

Table of Contents

List of Figures

List of Tables

List of Abbreviations

AEL	After Egg Laying
ASE	allele-specific expression
Atac1	*Ada2a-containing complex component 1*
ATACseq	Assay for Transposase-Accessible Chromatin sequencing
Ato	Atonal
Bace	*beta-site APP-cleaving enzyme*
BDSC	Bloomington *Drosophila* Stock Center
bHLH	basic Helix-Loop-Helix
CCDC43	*coiled-coil domain containing 43*
cka	*Connector of kinase to AP-1*
da	*daughterless*
dac	*dachshund*
dac	*dachshund*
DAPI	4', 6-diamidino-2-phenylindole
DAVID	Database for Annotation, Visualization and Integrated Discovery
DE	disc proper
df	Differentiation Expression
dpp	BMP2/*4 gene decapentaplegic*
Drak	*Death-associated protein kinase related*
D-V	Dorsal-Ventral
EAB	eye-antennal border
EAD	eye-antennal disc
Exp	Expression
ey	*eyeless*
eya	*eyes absent*
eyg	*eye gone*
Fas3	*Fasciclin 3*
FFLs	feed-forward-loops
FOXO	Forkhead box, sub-group O
GeneMANIA	Gene Function Prediction using a Multiple Association Network Integration Algorithm
GEO	Gene Expression Omnibus
Gl	*Glass*
GO	Gene Ontology
GRN	Gene Regulatory Network
G-TRACE	Gal4 technique for real-time and clonal expression
GWAS	Genome-wide association studies
HAT	histone acetyltransferase
HCR	Hybridization Chain Reaction
hh	*hedgehog*
Hpo	Hippo
HyA	Hybridization buffer A

HyB	Hybridization buffer B
IGB	Integrated Genome Browser
IGV	Intergrative Genomics Viewer
INT	Interommatidial cells
ISH	*in situ* hybridization
JNK	regulate c-Jun-amino-terminal-(NH2)-Kinase
Klu	Klumpfuss
LI	first larval instar
LII	second larval instar
LIII	Third larval instar
Mad	Mothers against dpp
MAPK	mitogen-activated protein kinases
Med	Medea
Megf8	*Multiple EGF like domains 8*
MF	morphogenetic furrow
MF_SoxN	morphogenetic furrow with SoxN expression
OreR	OregonR
Pax6	Paired box protein 6
PBS	Phosphate-buffered saline
PE	peripodial epithelium
PFA	paraformaldehyde
PG	Perineurial glia
PhR	Photoreceptors
Pnr	Pannier
PPN	pre-proneural domain
PSED	*Pax-six-eya-dac*
QTL	quantitative trait loci
Rat1	*Rat1 5′-3′ exoribonuclease*
Rca1	Regulator of Cyclin A1
RDGN	retinal determination gene network
Ribo	cells that express ribosomal genes
RNAi	RNA interference
RNAseq	RNA sequencing
Rrp7A	Ribosomal RNA-processing protein 7A (
Rtnl1	*Reticulon-like1*
rux	*roughex*
salr	*spalt-related*
SmiFISH	single molecule inexpensive fluorescence *in situ* Hybridization
SMW	Second mitotic wave
SNP	single nucleotide polymorphism
sn-RNAseq	single-nucleus RNA sequencing
so	*sine oculis*
TFs	transcription factors
TRiP-CRISPR	Transgenic RNAi Project-CRISPR
Trl	*Trithorax-like*

tsh	*teashirt*
Ubx	Ultrabithorax
upd	*unpaired*
Upd/Jak/STAT	the Upd involved Janus kinase (JAK)-signal transducer and activator of transcription (STAT)
VDRC	Vienna Drosophila Resource Center
wg	*wingless*
WG_SPG	wrapping glia and subperineural glia cells
Wts	Warts
Yki	Yorkie
z	*zeste*
zen	*zerknullt*

1. Summary

The Mendelian genetics concept relies on simple genotype-phenotype relationships with few genes having major effects on the phenotype. However, many traits evolve by a combination of variation in many genomic loci with minor phenotypic effects. Therefore, it is challenging to reveal individual genes underlying natural variation in quantitative traits. Most genes do not act individually, but they are interconnected in gene regulatory networks (GRNs). Revealing variable nodes and modules within GRN, thus has the potential to gain mechanistic insights into phenotypic evolution. The insect head that harbours the compound eyes is a complex quantitative trait that is highly variable in *Drosophila*. The formation of the insect compound eye is determined by a complex GRN composed of more than 5,000 genes. To reveal the molecular and developmental basis of natural variation in eye size and head shape, I studied head development in *Drosophila melanogaster* and *D. mauritiana*. Eye size varies in these two species due to differences in ommatidia number and a trade-off between eye size and interstitial head cuticle has been observed. To reveal novel candidate genes, I integrated several unbiased genome wide datasets, such as developmental gene expression (RNAseq), chromatin accessibility (ATACseq) and quantitative trait loci mapping data. This integrative approach unravelled 65 candidate genes, which I validated functionally for their functional involvement in eye development applying an RNA interference screen. Phenotypically relevant candidate genes were used to reconstruct a novel GRN module that contains predominantly genes with variable expression between species. The addition of few extra genes to this network allowed me to propose developmental processes that may be variable. I tested one of these hypotheses functionally to show that Jim, Pnr and Upd are co-expressed during head and eye development, suggesting a novel role of Jim during this process. Overall, my finding shows that a GRN-centric approach is highly powerful to reveal the mechanisms underlying the evolution of complex organ development.

2. Introduction

2.1 Evolution of complex traits

Morphological, physiological, and behavioural traits are variable across animals in nature. The phenotype is defined by a series of intricate and interconnected molecular processes which transfer information stored in the genome of an organism. This concept of phenotype-genotype association was already established in the early 1900's (Johannsen, 1911). For some phenotypes/traits, the association is rather simple, meaning that variation in one or few genes is related with variation in the phenotype. For instance, variation in the stripe pattern in cichlid fishes is defined by variation in the *agouti-related peptide 2* gene (Kratochwil et al., 2018). Such "simple" traits suggest that genotype-phenotype associations are predictable (Stern and Orgogozo, 2009). However, many traits vary continuously, and the genetic basis of such quantitative traits is complex with many genes contributing. An example for such a polygenic trait is the number of sensory bristles of *Drosophila melanogaster*, which are altered by a collection of genes (Mackay, 1995). Genome-wide association studies (GWAS) results for a number of quantitative traits suggest that many (polygenic model), if not all (omnigenic model), genes influence a certain phenotype (Boyle et al., 2017). The omnigenic model furthermore suggests that associated genes/loci do not act alone on the phenotype and that each gene also contributes to more than one phenotype. Additionally, each gene has only a minor impact (i.e. effect size) on the phenotype (Boyle et al., 2017; Tautz et al., 2020). Support for this model comes from mapping approaches which often reveal many genetic variants associated with quantitative trait differences, for instance, pupal length in *Drosophila* (Reeves and Tautz, 2017; Zhang et al., 2021). Therefore, identification of individual genes associated with quantitative phenotypic differences is often impossible. One solution could be revealing network modules and sub-networks related to certain biological processes via analysing different quantitative genetics data (Fagny and Austerlitz, 2021). One such process could be development as

Evo-devo over the last decades established that variation in developmental processes influence the evolutionary changes (see review in (Müller, 2007; Hall, 2012). And thus, Gene Regulatory Networks (GRNs) controlling these processes are important for variation in adult traits (Fagny and Austerlitz, 2021). Therefore, the major goal of this PhD thesis was revealing variable GRN modules that underlie developmental processes related to adult morphological variation.

2.2 Evolution of the visual system

Many animals rely on their visual system to obtain relevant environmental information, such as detection of prey, predators, or mates (Land and Nilsson, 2006). The morphology of the visual system is extremely variable to adapt to different environmental conditions. Such morphological variation in the visual system can vary the optical performance, which is related to the lifestyle of certain species (Nilsson, 2009). For instance, the separated binocular eyes (i.e. Holoptic eyes) in Damselflies, *Calopteryx*, are correlated with their frontal target tracking system. While in many dragonflies, the eyes are fusing compound eyes (i.e. Dichopic eyes) at the dorsal surface that facilitates intercepting prey from below (Supple et al., 2020). This correlation is also evident in an extreme example, which is the loss of eyes in cave fish, *Astyanax mexicanus*, which is an adaptation to the darkness of caves (Rétaux and Casane, 2013). The eye evolution can increase the ecological fitness of animals. A theoretical model from Nilsson and Pegler in 1994 demonstrated that an eye can evolve gradually by numerous slight modifications in less than 400,000 generation (Nilsson and Pelger, 1994). The quick evolution of eye morphology and function is best exemplified in cave fish, where the loss happened within one to five million years (Gross, 2012; Gross et al., 2015).

The different morphologies of eyes allow defining 65 eye types (v. Salvini-Plawen and Mayr, 1977). In general, these eye types can be categorized in two major groups, camera eyes (single lens eyes) and compound eyes (multiple lenses eyes), and both of them allow high resolution vision (Figure 2.1, A and B). Due to the diversity in eye morphologies, it was thought that eyes evolved 40-65 times

independently (v. Salvini-Plawen and Mayr, 1977). However, molecular data suggests that the visual systems of animals are based on the same core molecular machinery. Eyes evolved from an eyespot to a camera eye or a compound eye (Schwab, 2018). All visual systems contain a light-sensitive membrane (i.e. retina), light-sensitive proteins (i.e. opsins) with highly conserved structure (Porter, 2016) and the development of visual systems is based on a highly conserved homeobox gene family, *pax6* (Halder et al., 1995; Tyas et al., 2006; Fishman, 2008; Schwab, 2018). These conserved essential components support that the eyes have evolved from the common ancestor of all animals.

The compound eyes of insects are especially exciting as they are composed of many ommatidia. Each ommatidium consists of a rhabdom with a lens on top and pigment cells (Cagan, 2009). Those eyes, which provide a high-resolution image, have evolved from simple tasks (light detection) (Figure 2.1, A) (Nilsson, 2009, 2013). Compound eyes which facilitate complex behavioural tasks evolved independently in crustaceans and insects (Figure 2.1, B) (Nilsson, 2009, 2013) and they can be further categorized into apposition compound eyes and superposition compound eyes (Nilsson, 1989; Land and Nilsson, 2012). The apposition compound eyes are made by multiple microlensphotoreceptors (i.e. ommatidia) sitting next to each other and having pigment throughout what results in an isolated image for each ommatidium (e.g. Chelicerata, Crustacea and Instecta) (Figure 2.1, B) (Land and Fernald, 1992). On the contrary, the superposition compound eyes, which are found in many nocturnal insects (e.g. moths and beetles), have a wide clear zone between the retina and the lenses that bundle information from multiple ommatidia (Warrant, 1999). The earliest recorded compound eyes belong to Trilobite, *Schmidtiellus reetae* Bergström, at the Cambrian period around 540 million years ago, which was found in 1973 (Figure 2.1, C) (Schoenemann et al., 2017; Schoenemann and Clarkson, 2021). The early creatures in the Cambrian were coloured, which supports the importance of vision at that time. So, the very first eye must have

existed even before that (Parker, 2004; Fishman, 2008). However, there are not many fossils that can elucidate visual system evolution, since complete eye structures are hardly preserved (Schoenemann et al., 2017). Although the first compound eyes were not found yet, the apposition compound eyes of trilobites are believed to be an early common ancestor eye of insects (Schoenemann and Clarkson, 2020). Hence, the visual system of animals and specifically insects, is an important and highly variable complex morphological structure. Therefore, I use the morphology of the visual system as model to study genotype-phenotype associations of complex traits.

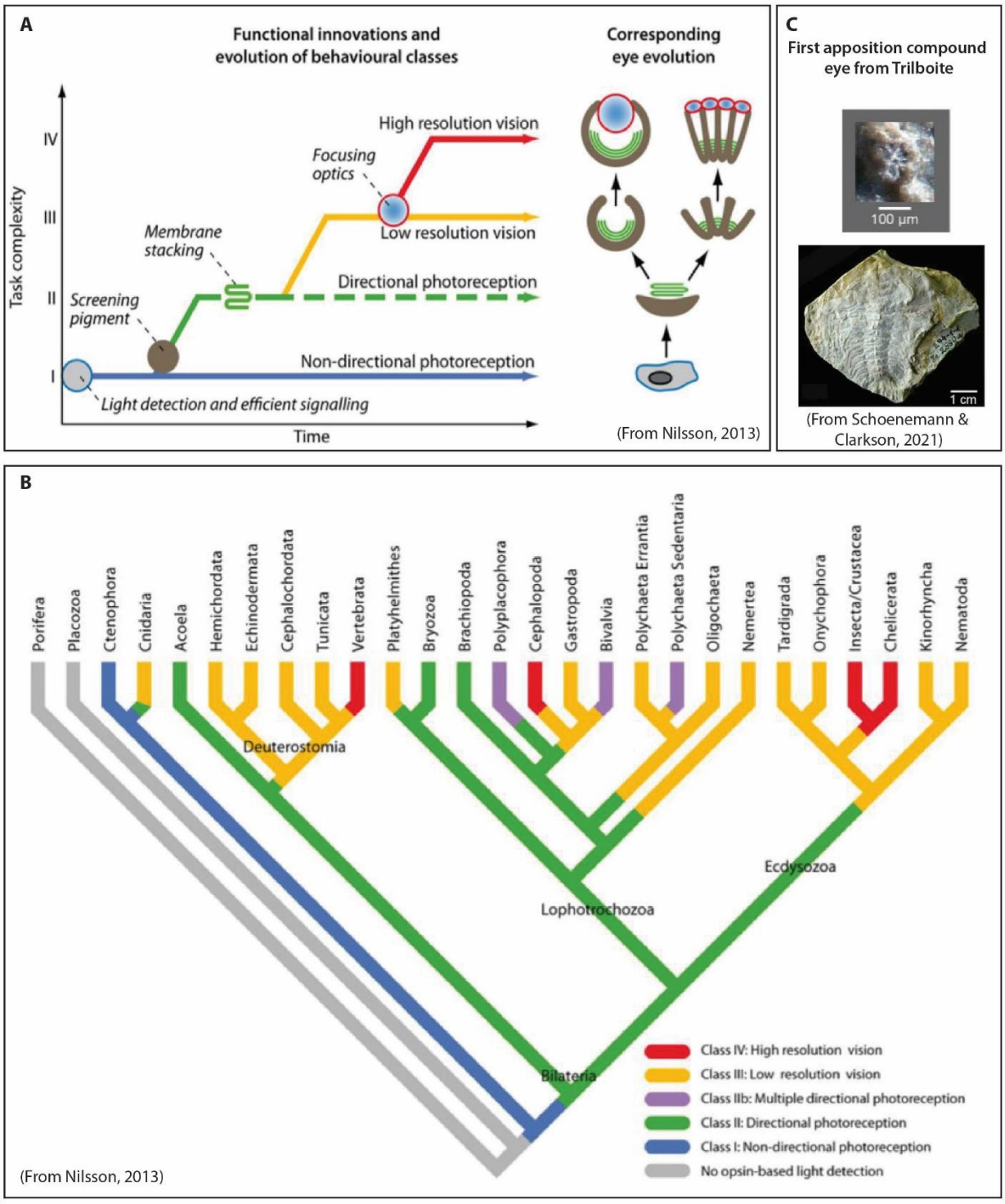

Figure 2.1. The evolution of animals' eyes **(A)**, **(B)** from Nilsson, 2013. **(C)** The first compound eyes from Trilobite photo modified from Schoenemann and Clarkson, 2021.

2.3 Variation of eye size among insects

Although compound eyes are the dominant eye type across all Insecta, the size and shape of compound eyes are very variable. The eyes of *Pipunculidae* flies cover almost the entire head with

about 4,500 ommatidia (Figure 2.2, A) and *Myrmecia* ants have the largest eyes in the ants' world with 3,000 ommatidia (Narendra et al., 2011). In contrast, individuals of a subterranean ant species of the genus *Crematogaster* only have one ommatidium (Figure 2.2, B) (Hosoishi, 2019; Casares and McGregor, 2020).

In many insects, the number of ommatidia (i.e. the eye size) correlates with visual activity (Gonzalez-Bellido et al., 2011; Land and Nilsson, 2012) and thus with ecological needs. In Australian *Myrmecia* ants, the number of ommatidia correlates with periods of activity during day or night, respectively: Night-active ants have bigger eyes with more ommatidia (Narendra et al., 2011). The correlation between eye size and the lifestyle is also evident in honeybees, where the enlarged eyes of *Apis florea* drones are related to its specific mating flight times (Streinzer et al., 2013).

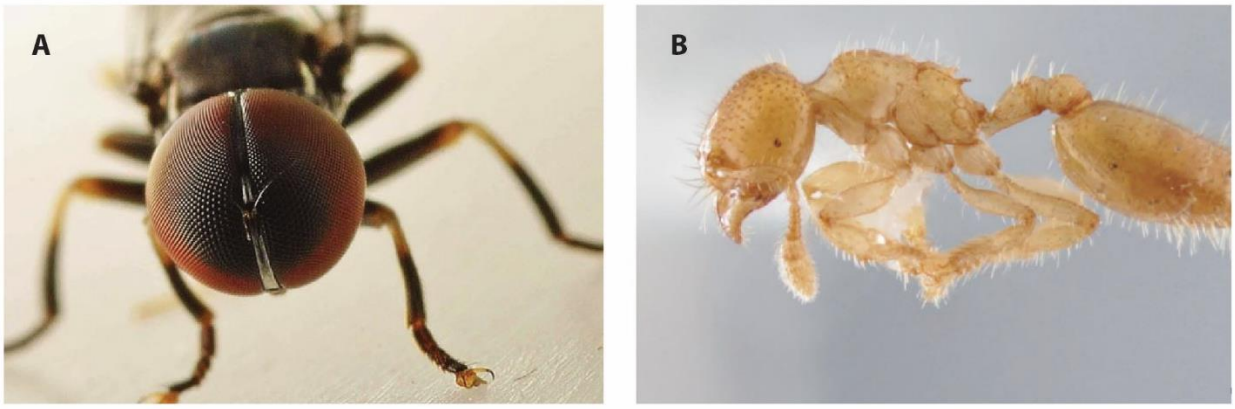

Figure 2.2. (A) The eyes of *Pipunculidae* flies with more than 4,500 ommatidia (Figure from Casares and McGregor, 2020) **(B)** The eye of Crematogaster with only one ommatidium (Figure from Hosoishi, 2019).

The structure and function of compound eyes is very well studied in the insect model system *Drosophila melanogaster*. The compound eyes of *D. melanogaster* are composed of about 800 ommatidia. One ommatidium contains six large photoreceptor cells that obtain motion signals and two central small photoreceptors on top of each other for colour vision. The subsequent neural pathways transmit the orientation, motion and colour visual stimulus into the lamina and trigger the corresponded behaviour (Rister et al., 2007).

Intriguingly, recent studies showed that extensive variation in eye size across *Drosophila* species, including *D. melanogaster*, exists in nature (Posnien et al., 2012; Arif et al., 2013; Keesey et al., 2019; Gaspar et al., 2020; Reis et al., 2020). A broad survey across 62 species within *Drosophila* was done by Kessey and colleagues in 2019 showing that eye size varies in flies with similar body sizes in many pairwise species comparisons (Keesey et al., 2019). Interestingly, a trade-off between the visual (i.e. eye lobes) and the olfactory (i.e. antennal lobes) system seems to exist in *Drosophila*: flies with bigger eyes tend to rely more on the visual system (e.g. species with light-dependent courtship behaviour), while flies with smaller eyes tend to use more the olfactory system (Keesey et al., 2019; Ramaekers et al., 2019). Although it is well established that variation in sensory systems is highly associated with adaptation to new environments (Gaspar et al., 2020; Özer and Carle, 2020), it remains unknown how such a trade-off is regulated on the molecular and developmental level.

Eye size (i.e. eye surface area) differences have been shown to be positively correlated with the number of ommatidia in the species examined by Keesey and colleagues (i.e. *D. americana*, *D. busckii*, *D. pseudotalamancana*, *D. funebris*, *D. melanogaster*, *D. suzukii*, *D. pseudoobscura* and *D. subobscura*) (Keesey et al., 2019, 2020). Similar correlations were observed for the eye size variation in *D. melanogaster* and *D. mauritiana* (Posnien et al., 2012). However, variation in eye size between *D. melanogaster* and *D. simulans* is caused by differences in the surface area of facets (Posnien et al., 2012; Gaspar et al., 2020; Torres-Oliva et al., 2021). Therefore, eye size can be influenced by the number of ommatidia or the size of ommatidia (Posnien et al., 2012; Gaspar et al., 2020).

2.4 Eye and head development in *D. melanogaster*

The *Drosophila* adult head, including the compound eyes, develops from larval eye-antennal discs (Figure 2.3). The eye-antennal discs originate from a few embryonic cells (i.e. eye precursors) which form an unpatterned monolayer epithelium at 13-15 h After Egg Laying (AEL) (first instar larvae) (Mandaravally Madhavan and Schneiderman, 1977). Throughout larval development, the different

organ precursors are specified, the discs grow extensively, and photoreceptor cells differentiate in the retinal region (see review in (Casares and Almudi, 2016)).

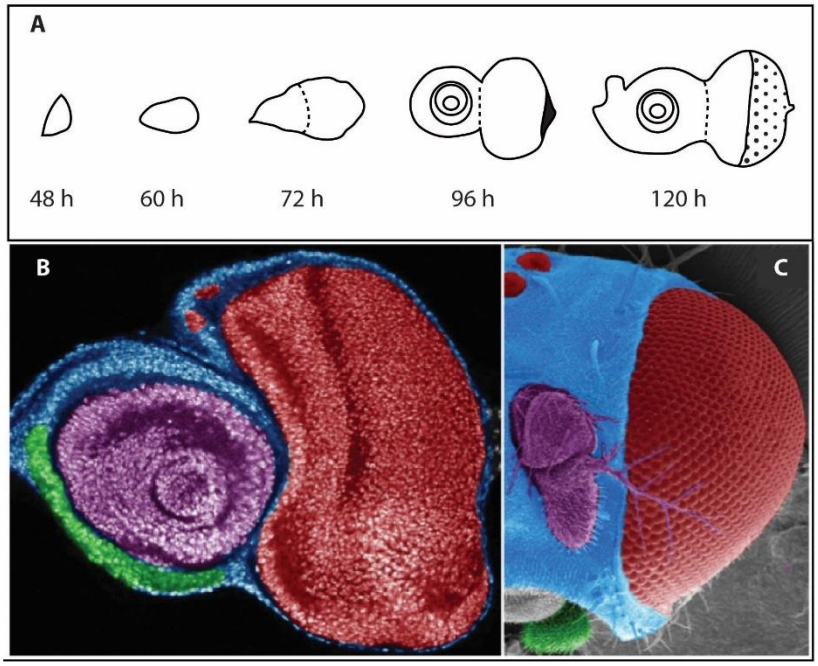

Figure 2.3. (A) Schematic overview of eye-antennal disc development. **(B-C)** The fate map of the late L3 eye-antennal disc (B) and corresponding adult structures (C) (Figure from Casares and McGregor, 2020).

During early larval stages, the highly conserved *pax6/eyeless (ey)* gene is expressed throughout the eye-antennal disc (Halder et al., 1998). Growth of the disc and opposing morphogen gradients result in the activation of *cut* expression in the future antennal region (Dong et al., 2002) and *ey* expression gets restricted to the future retinal region (Halder et al., 1998). Ey activates a number of target genes, which are connected among each other and with *ey* in a complex gene regulatory network, the retinal determination gene network (RDGN) (Figure 2.4). Loss-of-function of genes in the RDGN lead to severe eye reduction or complete eye loss phenotypes. Those genes are assumed as "master regulatory genes" (Desplan, 1997), which also include *eye gone* (*eyg*) (Yao and Sun, 2005), *sine oculis* (*so*) (Weasner et al., 2007), *eyes absent* (*eya*) (Bonini et al., 1993, 1997) and *dachshund* (*dac*) (Shen and Mardon, 1997). Ey is on top of the RDGN controlling the cell growth, specification, and patterning via regulating all the other "master regulatory genes" (Halder et al., 1995; Gehring, 1996). The RDGN

is not a linear regulation pathway, because the target genes of Ey actually work as a circuitry with regulatory loops (Figure 2.4) (Desplan, 1997; Kumar, 2009a; Sánchez-Aragón et al., 2019). For example, Eya-So-Dac act as a complex which is confirmed in previous studies (Pignoni et al., 1997; Chen et al., 1999; Wang and Sun, 2012).

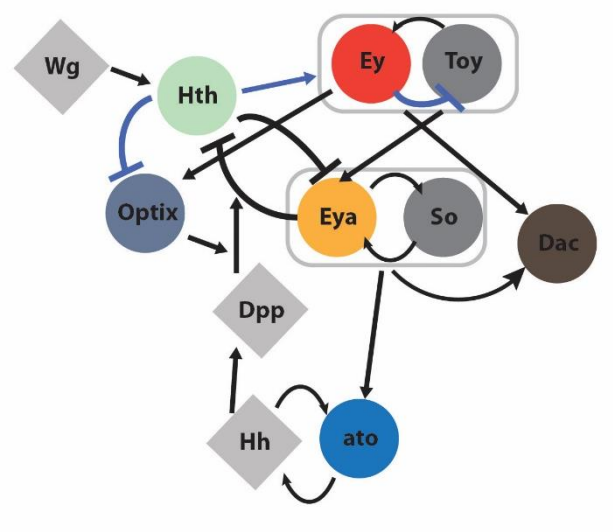

Figure 2.4. Scheme of genetic interactions of the RDGN. The genes in the boxes represent genes that interact. The black links represent validated regulation, while the blue links show suggested relationships (Figure modified from Sánchez-Aragón et al., 2019).

Once the eye-antennal disc is subdivided into the different head regions, the retinal part of the disc is composed of two main regions along the anterior-posterior axis: In the anterior part adjacent to the antennal region, cells proliferate, while a dynamic wave of differentiation is established in the posterior part of the retinal region. The cells within this wave change their shape to form a visible indentation, the so-called morphogenetic furrow (MF). The MF moves from posterior to anterior across the retinal part of the eye-antennal disc (Ready et al., 1976; Wolff and Ready, 1991). *so* and *eya*, are expressed in the posterior region of the eye-antennal disc before the MF forms (Bonini et al., 1993; Bessa et al., 2002), and induce the initiate of the MF from the posterior region (Figure 2.5, B) (Pignoni et al., 1997). In general, the cells posterior to the MF differentiate, while those anterior to the MF proliferate (Figure 2.5, A). It is confirmed that *hedgehog* (*hh*) and BMP2/4 *gene decapentaplegic* (*dpp*) act in a feed-forward-loop (FFP) to differentiate the photoreceptors, which results in a

forward-moving wave of differentiation (Figure 2.5, B) (Rogers et al., 2005; Casares and Almudi, 2016). Additionally, the Upd/Jak/STAT pathway represses *wingless (wg)* expression to trigger the initiation of the MF (Figure 2.5, B) (Vollmer et al., 2017). The ectopic misexpression of *upd* results in the more photoreceptors, which leads to larger eye (Bach et al., 2003; Tsai et al., 2007). Those findings suggest that the overexpression of *upd* messes up the initiation of MF and leads to the larger eye in *Drosophila*. At the end of larval development, the pool of dividing cells is used up and the final eye size is more or less defined.

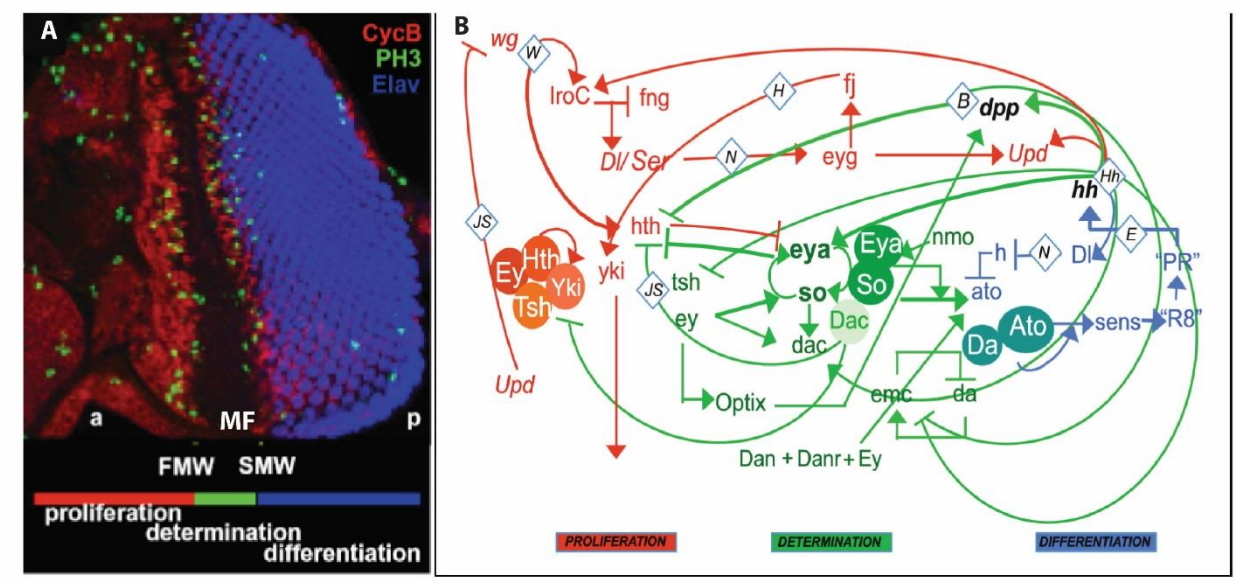

Figure 2.5. (A) Morphogenetic furrow (MF) in the developing eye-antennal disc. **(B)** The gene regulatory networks posterior (right) and anterior (left) to the MF region. a, anterior; p, posterior; FMW, First Mitotic Wave; SMW, Second Mitotic Wave (Figures from Casares and Almudi, 2016).

A recent re-analysis of the role of Ey during retinal development revealed an interesting novel process in which this protein is involved (Baker et al., 2018). Baker and colleagues showed that a critical function of Ey in initiating the MF is based on its expression in the peripodial epithelium (PE), an epithelial layer that covers the disc proper (DP) (Auerbach, 1935). Since the function of the PE had been underestimated by the researchers for decades (see review in book (2020)), our knowledge about the function of the PE is still limited. Intriguingly, however, other crucial genes involved in eye and head patterning are expressed in the PE. For instance, the GATA transcription

factor Pannier (Pnr) is expressed in the PE throughout larval eye-antennal disc development (Oros et al., 2010) and loss- and gain-of-function experiments showed that Pnr is required for establishing the dorsal-ventral boundary in the eye-antennal discs through regulating its downstream genes, *wingless* (*wg*), *mirror* and *fringe* (Maurel-Zaffran and Treisman, 2000).

In summary, the eye-antennal disc is determined by the interaction of many well-known developmental gene products, which are organized in the RDGN and control various developmental processes, such as disc growth, patterning and differentiation of photoreceptors. Additionally, the PE may play an important role during retinal development that has been poorly acknowledged.

2.5 Genetic basis of eye size and head shape variation

Recent studies attempted to unravel the genetic architecture of inter- and intra-specific eye size and head shape variation in *Drosophila* (Arif et al., 2013; Norry and Gomez, 2017; Gaspar et al., 2020). In general, those findings suggest a complex architecture with multiple genes involved. For instance, several quantitative trait loci (QTL) on the X chromosome have been identified for eye size variation between *D. simulans* and *D. mauritiana* (Arif et al., 2013) and a large group of genes have been linked to intra-specific variation in *D. melanogaster* (Carreira et al., 2013, 2016; Norry and Gomez, 2017). In contrast, Ramaekers and colleagues identified a single nucleotide polymorphism (SNP) in the *eyeless* locus that explain a considerable portion of variation in eye size among *D. melanogaster* laboratory strains (Ramaekers et al., 2019). Interestingly, the observed variation in *ey* expression during eye and head development could explain, both the increase in eye size and the reduction of interstitial head cuticle size (Ramaekers et al., 2019), suggesting that the same genetic variant can simultaneously affect both traits. Support for this analysis comes from a mapping study in *D. melanogaster* populations that revealed at least one QTL that had opposite effects on both head traits (Norry and Gomez, 2017). However, an inter-specific mapping analysis in *D. simulans* and

D. mauritiana revealed distinct QTL for eye size and interstitial head cuticle size variation (Arif et al., 2013).

Overall, *D. mauritiana* and *D. melanogaster* are excellent models to study the molecular and developmental basis of eye size variation because eye size varies due to ommatidia number differences and a trade-off between retinal tissue and head cuticle has been observed (Posnien et al., 2012; Buchberger et al., 2021). And, the data obtained so far revealed contrasting results and they suggest that natural variation in *Drosophila* eye and head morphology is as a polygenic trait with many loci contributing to the phenotypic differences. However, the exact developmental mechanisms are not well understood. Therefore, in my study, I started to reveal the GRN modules and subnetworks underlying the eye size variation between *D. melanogaster* and *D. mauritiana*.

2.6 Potential developmental mechanisms underlying eye size and head shape variation in *Drosophila*

The eye size variation is negatively correlated with the size of other head tissues, such as the interstitial head cuticle on head (e.g. face width and size of antenna) (Posnien et al., 2012; Arif et al., 2013; Norry and Gomez, 2017; Ramaekers et al., 2019; Gaspar et al., 2020; Buchberger et al., 2021; Torres-Oliva et al., 2021). In general, those findings suggested that this trade-off is defined during the development of the eye-antennal disc as the adult eye/head morphology forms from it. Accordingly, adult flies with larger eyes should also contain larger eye fields in the developing eye-antennal discs (Posnien et al., 2012; Ramaekers et al., 2019; Gaspar et al., 2020).

In the previous findings, several genes have been identified as essential genes in the developing eye-antennal discs, which participate in regulating the eye size and correlate with the trade-offs. For instance, it was confirmed that the differential expression of *pnr* affects the ommatidia number and interstitial cuticle size between *D. melanogaster* and *D. mauritiana* (Buchberger et al., 2021). And

a SNP affecting the regulation of *ey* expression modifies the proportion between the antennal and eye region (Ramaekers et al., 2019).

Additionally, the posterior-to-anterior progression of the MF affects the eye size in adult flies (Casares and McGregor, 2020). This means, the more anterior the MF moves across the eye-antennal disc, the more rows of ommatidia form, which results in bigger eye size (Casares and McGregor, 2020). Therefore, it has been suggested that genes involved in the MF initiation and progression in the developing eye-antennal discs also correlate with the determination of eye size in the adult fly (see review in (Kumar, 2012)). In summary, variation in multiple developmental processes can influence the eye size in the adult of *Drosophila*, such as the differentiation of eye primordium, the rate of proliferation, the speed of cell differentiation and the size of ommatidia (Casares and McGregor, 2020).

Besides the well-studied processes that regulate eye and head development, many more genes are involved in the morphogenesis of the visual system. For instance, when mapping putative regulatory interactions of genes involved in eye-antennal disc development, the resulting complex GRN is composed of 5,632 genes (Potier et al., 2014). For many parts of this network, a thorough understanding of related developmental processes and the potential to contribute to natural morphological variation is unknown. Therefore, I aimed to reveal genes, network modules and sub-networks and related developmental processes that contribute to variation in eye size and head shape between *D. melanogaster* and *D. mauritiana*.

3. Materials and Methods

3.1 Candidate Genes

3.1.1 Identification the candidate genes

To reveal putative candidate genes involved in the eye size and head shape variation between *Drosophila melanogaster* and *D. mauritiana*, multiple unbiased genome wide datasets were integrated (see Figure 4.1): First, all genes expressed during eye-antennal disc development were identified from a previously published RNAseq dataset for *D. melanogaster* (Torres-Oliva et al., 2018) (Figure 4.1 A). Among the expressed genes, I extracted those genes that were previously shown to be differentially expressed between *D. melanogaster* and *D. mauritiana* at padj < 0.05 at at least one of the three studied stages (72 h, 96 h, and 120 h After Egg Laying (AEL)) (Buchberger et al., 2021) (Figure 4.1 B). Next, I asked, whether differentially expressed genes were also positional candidates obtained by previously published quantitative trait loci (QTL) mapping data that revealed genomic regions associated with intra-specific variation in eye size and head shape in *D. melanogaster* (Carreira et al., 2013, 2016; Norry and Gomez, 2017). Note that intra-specific variation in *D. melanogaster* is also caused by differences in ommatidia number (Carreira et al., 2013, 2016; Norry and Gomez, 2017) and larger eyes form at the expense of interstitial cuticle, as observed between *D. melanogaster* and *D. mauritiana* (Posnien et al., 2012). Positional candidate genes located in QTL regions (Table 3.1) were identified by mapping the QTL region on genomic coordinates onto the *D. melanogaster* genome (version 6.13) by using Integrated Genome Browser (IGB, version 9.1.2) (Figure 4.1 C). Once the coordinated genes (FlybaseID) were found and extracted, the gene names were annotated by using the Database for Annotation, Visualization and Integrated Discovery (DAVID, https://david.ncifcrf.gov/conversion.jsp). The obtained positional

candidate genes were compared to the list of differentially expressed genes using the "Relationship Tools" in Microsoft Access (version 2019). This data integration resulted in 256 genes (Figure 4.1).

Table 3.1 Published quantitative trait loci associated with eye size variation. Chr, chromosome

Approach	**Chr.**	**Coordinates/Genes**	**Source**
QTL	2L	5,943,642-9,279,771	Norry & Gomez, 2017
Quantitative Complementation Tests	2L	*Fasciclin 3*, *Reticulon-like 1*	Carreira et al., 2016
Quantitative genetic analyses	2R	*CG43340*	Carreira et al., 2013
	3L	*jim*	
	X	*Drak*	

The number of differentially expressed positional candidate genes was further reduced by integrating two types of information: **1)** All differentially expressed positional candidate genes with the GO term "eye-antennal disc morphogenesis" (GO: 0007455) and/or "compound eye morphogenesis" (GO: 0001745) were added to the final candidate gene list (Figure 4.1 D). Note that one positional candidate gene (*wg*) that was not differentially expressed but had the GO term "compound eye morphogenesis" (GO: 0001745) was added to the candidate gene list as well (Figure 4.1 D). **2)** To distinguish between genes which were differentially expressed due to changes in their own regulatory region (i.e. divergence in *cis*) and those with changes in expression or function of factors controlling their expression (i.e. divergence in *trans*), I integrated information from an allele-specific expression dataset that has been established and analysed previously (Torres-Oliva, 2016). Specifically, all differentially expressed positional candidate genes with signature of *cis*-regulatory divergence at at least one of the three studied stages were included in the final candidate gene list (Figure 4.1 E).

Additional candidate genes were obtained by including putative regulators of *pnr* because this gene has been identified as crucial factor involved in eye size and head shape variation between *D. melanogaster* and *D. mauritiana* (Buchberger et al., 2021)(Figure 4.1 F). To this end, the open chromatin regions in the *pnr* locus were identified from a previously established chromatin accessibility dataset (ATACseq) (Buchberger, 2019). Those regions were mapped to the reference genome (dm6) using Intergrative Genomics Viewer (IGV, version 2.10.0) and the sequences were extracted. Sequences for all open chromatin regions were combined into one FASTA file and MEME suite (version 5.4.1) was used to predict motifs for potential transcription factors.

3.1.2 Reconstruction of gene regulatory networks

To analyse potential functional interactions of the identified candidate genes, several gene regulatory networks (GRNs) were constructed using the GeneMANIA (Gene Function Prediction using a Multiple Association Network Integration Algorithm, version 3.5.2) tool (Warde-Farley et al., 2010; Franz et al., 2018) (Figure 4.9) in the Cytoscape app (version 3.8.2). One network was constructed for the candidate genes and *pnr*, which were defined as nodes and edges were based on information stored in common databases: **(i)** predicted interactions (based on known functional relationships from another organism in Integrated Interactions Database), **(ii)** shared protein domains (e.g. from InterPro, SMART and Pfam databases), **(iii)** co-expression (from Gene Expression Omnibus (GEO) and publications (e.g. (Beckstead et al., 2005; Zhao et al., 2010; Guruharsha et al., 2011)), **(iv)** co-localization (Frise et al., 2010), **(v)** genetic interaction (from BioGRID and IRefIndex) and **(vi)** physical interaction (from BioGRID and IRefIndex).

To test if the connectivity of the candidate gene GRN was different from networks based on randomly selected genes, several additional networks were constructed using the procedure described above.

The nodes for these random networks were based on genes selected from gene lists obtained throughout my screening pipeline (Table 4.1). From each gene list I randomly selected 19 genes (i.e., the same number as candidate genes) and the random selection and network reconstruction was performed ten times for each gene list (Figure 3.1. A). To avoid the technical bias, I constructed the networks including those gene lists associated with wing tissues as outgroup comparison. The candidate gene based GRN was compared to the random networks based on connectivity (i.e., number of edges) and the quality of predicted connections (i.e. source of edge information) (Figure 3.1 B). I analysed the quality of networks by comparing the percent of number of edges of each data source (e.g., physical interaction) in relation to the total number of edges (Figure 3.1 C).

To provide a broader regulatory context to the candidate gene network, additional 20 genes were added to the network using the GeneMANIA tool. Those 20 genes were automatically chosen because they had the biggest impact on increased connectivity within the candidate gene based GRN (Figure 3.1 D).

Since this extended candidate gene network (incl. the 20 additional genes) was based on predicted interactions from multiple databases without directionality of the edges, I eventually assessed putative direct interactions between some nodes of the network. To this end, I predicted transcription factor binding motifs in genomic regions that were accessible during eye-antennal disc development as inferred by ATACseq data from three stages (Buchberger et al., 2021) (Figure 3.1 F). Open chromatin peaks in putative regulatory regions of the 19 candidate genes were extracted. A BED file containing 14,511 ATACseq peaks, which were found among three developmental stages (Buchberger et al., 2021), was uploaded into the genome browse, IGV. Peak sequences in putative regulatory regions (i.e. up to 5 kb upstream of transcription start, in introns and in intergenic regions) were extracted as FASTA file

and the MEME suite (version 5.4.1) (Bailey and Elkan, 1994) https://meme-suite.org/meme/tools/meme) was used to search for individual motifs in those sequences and motifs were aggregated using MAST (motifs with E-value < 0.05) (Bailey and Gribskov, 1998). Identified motifs were annotated to transcription factors (TFs) using the motif comparison tool Tomtom (version 5.3.3) (Gupta et al., 2007) based on motif databases (e.g. OnTheFly, Fly Factor Survey, FLYREG, iDMMPMM and DMMPMM). Information of putative direct TF binding motifs was used to infer direct and directional interactions between candidate genes within the extended network (Figure 3.1 G). For instance, if the motif of gene 1 was found in an open chromatin region of gene 2, a direct interaction from gene 1 gene 2 was added to the network. Note that additional genes predicted to regulate the expression of *jim* and with GO term "compound eye morphogenesis (GO: 0001745)" or/and eye-antennal disc morphogenesis" (GO: 0007455) were added to the extended network based on the motif search.

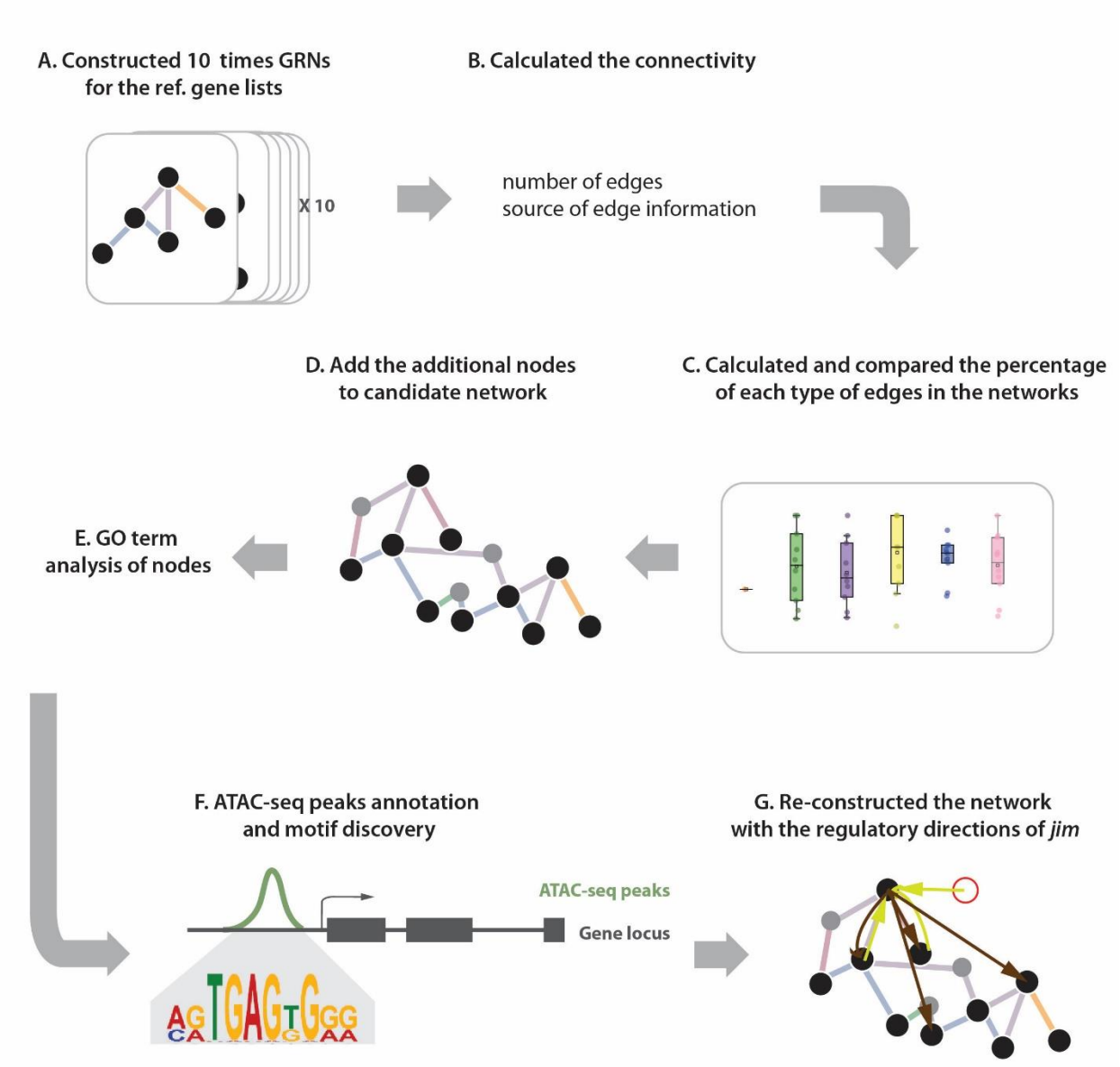

Figure 3.1. The workflow for network construction. The grey arrow represents the direction of workflow.

3.1.3 GO term enrichment analysis

To understand the biological function of the candidate genes, as well as the 20 genes that were added to the GRN to increase connectivity within the network, I used the GO enrichment tool (WEB-based GEne SeT AnaLysis Toolkit) (http://www.webgestalt.org/) (Wang et al., 2017) (Figure 3.1 E). I applied the Over Representation Analysis method and searched for their gene ontology in biological process.

3.2 Functional validation experiments

3.2.1 Fly husbandry and crosses

All fly stocks and crosses were kept on standard food under 12/12 (day/night (hr)) cycle at 18°C, 25°C, or 29°C depending on the experiment. For crosses, five to seven males were placed in food vials with 10 to 15 virgin females. For egg collections, males and virgins were transferred to small cages which were covered with apple agar plates and yeast.

3.2.2 RNA interference using UAS/Gal4 binary expression system

For the RNA interference (RNAi) screen I employed the UAS/ Gal4 system (Brand and Perrimon, 1993). Crosses were performed at 25°C and 29°C using virgins of the *eyeless (ey)*-Gal4 driver line (BDSC #5535) and males of UAS-RNAi lines (see Table 3.2). When available, I used three UAS-RNAi lines from the Vienna Drosophila Resource Center (VDRC) and Bloomington *Drosophila* Stock Center (BDSC), respectively. The expression of the *ey*-Gal4 driver line in the eye-antennal disc was confirmed by crossing females with males of the reporter line UAS-stinger-GFP (BDSC #84277).

To study the genetic interaction between *jim* and *pnr* using RNAi, I crossed the 10 females of *pnr*-Gal4 lines to five males of Jim UAS-RNAi lines (see Table 3.2). The expression of the *pnr*-Gal4 driver line in the eye-antennal disc was confirmed previously (Buchberger et al., 2021). On the contrary, I crossed the 10 virgin females of *jim*-Gal4 lines with five males of UAS-RNAi lines of *pnr* (BDRC #101522). Moreover, to study the function of Jim specifically in the peripodial epithelium, I performed the loss-of-function of *jim* with *c311*-Gal4 driver line (BDSC #5937). The expression of *c311*-Gal4 driver line in the peripodial epithelium was previously confirmed (Baker et al., 2018). To confirm the effect of RNAi, I also crossed five males of UAS-RNAi lines (i.e., for Bace, Trl and Atac1) with 10 females of other Gal4 lines (*tsh*-Gal4, *elav*-Gal4, and *dpp*-Gal4), whose expression is confirmed previously (see Table 3.3).

Table 3.2 UAS-RNAi lines used in this work.

VDRC/ BDSC ID	Library	Gene
2842	VDRC	*CG9555*
43571	VDRC	*Aasdh*
105626	VDRC	*Aasdh*
61984	BDSC	*Aasdh*
36092	VDRC	*Atac1*
108992	VDRC	*Atac1*
57250	BDSC	*Atac1*
15541	VDRC	*Bace*
110785	VDRC	*bchs*
45028	VDRC	*bchs*
80438	BDSC	*brk*
12371	VDRC	*CG11050*
107837	VDRC	*CG11050*
38460	VDRC	*CG11236*
57486	BDSC	*CG11236*
102250	VDRC	*CG13795*
107513	VDRC	*CG14275*
108103	VDRC	*CG16947/ Rchy1*
58099	BDSC	*CG16947/ Rchy1*
38946	VDRC	*CG31898*
108688	VDRC	*CG31898*
110244	VDRC	*CG42370*
24052	VDRC	*CG42370*
22019	VDRC	*CG5160*
106081	VDRC	*CG5160*
27660	BDSC	*CG5160*
108197	VDRC	*CG6739*
107040	VDRC	*CG7231*
8018	VDRC	*CG7466/ Megf8*
42462	VDRC	*CG7466/ Megf8*
24097	VDRC	*CG8419*
107626	VDRC	*CG8419*
109500	VDRC	*CG9107*
43547	BDSC	*CG9107*
29050	VDRC	*CG9147*
101971	VDRC	*CG9147*
16877	VDRC	*CG9150*
24047	VDRC	*CG9498*
108362	VDRC	*CG9498*
77398	BDSC	*CG9510/ Argl*

46378	VDRC	*CG9555*
11730	VDRC	*CG9568*
102426	VDRC	*CG9568*
51025	BDSC	*CG9568*
104628	VDRC	*CG9586*
102759	VDRC	*chic*
106971	VDRC	*cka*
35799	BDSC	*cort*
7779	VDRC	*crol*
33370	BDSC	*CSN8*
102550	VDRC	*dachs*
12555	VDRC	*dachs*
26319	BDSC	*da*
105258	VDRC	*da*
51297	VDRC	*da*
31987	BDSC	*dar1*
107263	VDRC	*Drak*
32960	VDRC	*Drak*
44524	VDRC	*gl*
51474	BDSC	*Gpdh*
33680	VDRC	*grh*
101428	VDRC	*grh*
28820	BDSC	*grh*
55926	BDSC	*grk*
330460	VDRC	*jim*
12698	VDRC	*jim*
45622	VDRC	*Kfase*
45634	VDRC	*lectin-28C*
104201	VDRC	*lectin-28C*
28385	BDSC	*milt*
3247	VDRC	*mtsh*
3248	VDRC	*mtsh*
33155	VDRC	*pes*
100391	VDRC	*pes*
50612	BDSC	*pes*
102440	VDRC	*Piezo*
2796	VDRC	*Piezo*
28554	BDSC	*prg*
7628	VDRC	*pvf2*
7629	VDRC	*pvf2*
61955	BDSC	*pvf2*
27254	VDRC	*Rat1*
105380	VDRC	*Rat1*

57176	BDSC	*Rat1*
35489	VDRC	*Rca1*
17168	VDRC	*Rps13*
105496	VDRC	*Rps13*
3424	VDRC	*SLC5A11*
104177	VDRC	*SLC5A11*
56958	BDSC	*spz3*
35611	VDRC	*Tep2*
106997	VDRC	*Tep2*
26740	BDSC	*tgo*
10735	VDRC	*tgo*
106479	VDRC	*Trf*
17198	VDRC	*Trl*
106433	VDRC	*Trl*
55642	BDSC	*x16*
29446	VDRC	*z*
35208	VDRC	*z*
31615	VDRC	*z*
12649	VDRC	*zen*
102915	VDRC	*zen*

Table 3.3 Gal4 lines used in this work.

Gene	ID	Library	Ref.
eyeless	5535	BDSC	Figure 4.5
pnr	42374	VDRC	(Buchberger et al., 2021)
c311	5937	BDSC	Figure 4.19 (Baker et al., 2018)
jim	40079	BDSC	Figure 4.15
jim	63926	BDSC	
jim	62748	BDSC	
Teashirt (Tsh)	3040	BDSC	(Bessa and Casares, 2005)
elav	541	BDSC	Supplementary Figure 3
dpp	1553	BDSC	(Skottheim Honn et al., 2016)

3.2.3 Overexpression of candidate genes using the TRiP-CRISPR system

Overexpression of candidate genes in the eye-antennal disc was performed using the TRiP-CRISPR system that is based on the activation driven by dCas9-VPR (Lin et al., 2015). I crossed 10 females of dcas9 driver lines with five males of each TRiP-Overexpressed lines (Table 3.4) to induce overexpression or ectopic expression in the specific region of the disc.

Table 3.4 TRiP-CRISPR lines used in this work.

Gene	ID	Library	Type
elav	67058	BDSC	dcas9 driven in *Elav* positive cells
pnr	67077	BDSC	dcas9 driven in *Pnr* positive cells
dpp	67045	BDSC	dcas9 driven in *Dpp* positive cells
Trl	79865	BDSC	*Trl* overexpression
jim	79944	BDSC	*jim* overexpression
Bace	79473	BDSC	*Bace* overexpression
Atac1	80008	BDSC	*Atac1* overexpression

3.2.4 Lineage tracing using G-TRACE

The G-TRACE system (Evans et al., 2009) was used to analyse the Gal4-based cell lineage. I crossed males of the G-TRACE line (BDSC #28281) with females of *pnr*-Gal4 lines (BDSC #42374) or *jim*-Gal4 lines (BDSC #62748). The eye-antennal discs of F1 offspring larva in 120 h AEL were dissected and I performed Immunohistochemistry with anti-RFP (rabbit) and anti-GFP (chicken) antibodies (see table 3.5) following the protocol in chapter 3.3.1.

Table 3.5. Primary antibodies used in this work.

Used antibodies	Dilution Concentration
Anti-Pnr (rabbit) (Proteintech, Rosemont, IL, USA) (Buchberger, 2019)	1:200
Anti-GFP (chicken) (Abcam)	1:1000
Anti-RFP (rabbit) (Abcam)	1:1000
Anti-Bace (rabbit) (kindly provided by Dr. Doris Kretzschma, Oregon Institute of Occupational Health Sciences, USA, Bolkan et al, 2012)	1:500
Anti-Elav (Rat) (Developmental Studies Hybridoma Bank, DSHB)	1:500

3.2.5 Analysis of adult head phenotypes

The effects of gain- and loss-of-function experiments on adult head and eye formation were analysed in F1 adult flies 10 to 14 days after eclosion. The flies were sorted by the sex and morphology of wings as only flies with normal none-curly wings should elicit RNAi effects according to the balancer of

parental flies. For *ey*-Gal4 crosses, adult flies without curly wings were analysed; while for *jim*-Gal4 crosses, all of the adult flies were analysed. Flies were decapitated and images of the heads were taken with the QCapture-Pro software (version 7, QImaging Corporation, USA) using a stereoscope (Leica M205 FA). For loss-of-function of *jim* (Figure 4.4, L) and the RNAi driven by *jim*-Gal4 (Figure 4.19), the images of the heads were taken with Zeiss Zen software (version 3.3, Zeiss GmbH, Germany) using the Axioplan microscope (Zeiss GmbH, Germany).

For the RNAi screen, I established a phenotype score by measuring and analysing the size of eye region with Fiji 2.1.0 (Figure 4.4, N). The phenotype scores were calculated as percent of size of the eye area in each adult individual (average number of analysed heads was 8) compared to the wildtype eye area (*D. melanogaster* OreR, analysed individuals are 3). For the *jim-pnr-upd* experiment, I measured the size of eye region with Fiji 2.1.0 comparing the crosses with UAS-stinger-GFP (BDSC #84277) (Figure 4.19).

3.2.6 Analysis of eye-antennal disc phenotypes

The effects of gain- and loss-of-function experiments on eye-antennal disc development was assessed by analysing the morphology of eye-imaginal discs. I dissected the specific time points to obtain the corresponding stage of larval discs at 72 h (early LIII stage), 96 h (mid LIII stage), and 120 h (late LIII stage) AEL. The eye-antennal discs of the *ey*-Gal4 crosses were stained with anti-Elav (Rat) antibody (Table 3.5) to label the developing photoreceptor cells and Phalloidin (1:200) for actin filaments staining to mark the morphological structure of eye-antennal discs (see detail steps in chapter 3.3.1). For the *jim* or *pnr* loss-of-function experiment (Figure 4.16), the analysed eye-antennal discs were stained with anti-Pnr (rabbit) antibody to detect the Pnr expression and DAPI (4', 6-diamidino-2-phenylindole) for nuclear acid staining. For the *pnr* loss- and gain- of-function, the analysed eye-antennal discs were stained with anti-Pnr antibody and Phalloidin and the distance from the

dorsal rim of the disc to the morphogenetic furrow (MF) was measured using Fiji 2.1.0 (Figure 4.18). For the other loss-of-function experiments, the eye-antennal discs were stained with anti-Elav antibody, DAPI and Phalloidin for comparing the morphological structure of eye-antennal discs.

3.3 Analysis of spatial and temporal gene and protein expression

3.3.1 Immunohistochemistry

To analyse spatial and temporal protein expression, I adapted an immunohistology protocol from Klein 2008 (Klein, 2008). The eye-antennal discs were dissected with the mouth hooks and the brain still attached in cold 1x Phosphate-buffered saline (PBS) solution for less than 20 minutes and were fixed with 4% paraformaldehyde (PFA) in PBS for 20 minutes at room temperature. Starting from this step on, all the incubation steps were performed on rockers or rotators at room temperature. I replaced the 4% PFA with 1X PBS solution and kept the tissue at 4°C. The eye-antennal discs were incubated in PBT solution, which contained 0.3% Triton X-100 dissolved in 1x PBS and washed three times for 20 minutes. I replaced the PBT solution with blocking solution (4% serum albumin and 5% goat serum in PBT) and incubated for 30 minutes to remove the unspecific protein-antibody interaction. Next, I replaced the blocking solution with corresponding primary antibodies for 90 minutes and washed with PBT three times for 20 minutes. Before I added the secondary antibodies, I incubated the tissue in blocking solution again for 30 minutes. Then, I incubated the discs under corresponding secondary antibodies and/or Alexa Fluor 488 Phalloidin (Table 3.6). Following by PBT washing step again for two times is to remove the unbounding antibodies. And I stained the nucleolus with DAPI (1:1000) by 10 minutes incubation. After that, I washed the tissue once with PBT and once with 1x PBS solution. To finalize the staining, I replaced the solution with mounting medium (80% glycerol + 4% n-propyl gallate in PBS) and incubated it over-night at 4°C. The eye-antennal discs would be dissected and

mounted on the microscope slides. The images were taken using Zeiss LSM-980 confocal laser scanning microscope (Zeiss GmbH, Germany), and staining signal were visualized and analysed with Zeiss Zen software (version 3.3, Zeiss GmbH, Germany).

Table 3.6. Secondary antibodies used in this work.

Used antibodies	**Dilution Concentration**
Anti-chicken-488 (Invitrogen,USA)	1:1000
Anti-chicken-555 (Life Technologies, USA)	1:1000
Anti-rabbit-647 (Invitrogen,USA)	1:500
Anti-rat-647 (Life Technologies, USA)	1:1000

3.3.2 chromogenic *in situ* hybridization

Spatial and temporal mRNA expression in developing eye-antennal discs was analysed using chromogenic *in situ* hybridization. To this end, digoxygenin labelled RNA probes were synthesized as follows: Total RNA was isolated from *D. melanogaster* (OregonR) LIII larvae using the ZR Tissue & Insect RNA Microprep Kit (ZYMO Research) and RNA was reverse-transcribed to complementary DNA (cDNA) using the TAKARA PrimeScript RT Reagent Kit (Takara Bio USA, Inc.). Gene-specific primers were designed (Primer3 as implemented in Geneious Prime version 2019.0.4), synthesized by Integrated DNA Technologies, Inc. and used to amplify gene fragments by PCR using Advantage 2 PCR Kit (Takara Bio USA, Inc.). I aimed for 700-1000 bp fragments (Table 3.7). PCR fragments were cloned into pCR™-TOPO® vector (Invitrogen) from which fragments were amplified with T7 (5'-GAATTGTAATACGACTCACTATAGG-3') and Sp6 (5'-GATTTAGGTGACACTATAGA-3') primers, respectively. Depending on the orientation of the gene fragments in the vector, antisense and sense *in*

situ probes were synthesized using the Dig labeling mix (Roche) and T7 or Sp6 Polymerase (Roche), respectively.

Table 3.7. Primers used to clone the *Rat1* gene.

Gene		Primers	Temp. (°C)	Fragment size
Rat1	Forward Reverse	5'-CGCCGATCTCATCATGTTGG-3' 5'-TGAAGCCATCCTCCCACAAT-3'	60	896

After dissecting the larval discs at the certain time point (72 h, 96 h, and 120 h AEL), I fixed the tissue with 4% PFA for 20 minutes at room temperature followed by three times washing with PBT. The eye-antennal discs were treated with Proteinase K (10 µg/ml, five minutes) and washed with an ascending series of methanol:PBT from 1:3, 1:1, 3:1 and 1:0. The eye-antennal discs were stored in methanol at -20°C or directly processed. The eye-antennal discs were transferred back to PBT by washing with an ascending series of methanol:PBT from 3:1, 1:1, and 1:3. Subsequently, the eye-antennal discs were incubated in PBT:Hybridization buffer B (HyB) (with 50% Formamide, 5x SSC, 0.1% Tween20) at 3:1, 1:1, and 1:3 dilutions for 10 minutes each followed by two times HyB for 10 minutes each at 65°C. HyB was replaced with Hybridization buffer A (HyA) (100 µg/ml denatured herring sperm DNA and 50 µg/ml heparin in HyB) for 10 minutes incubation followed by a 1 hour incubation in HyA at 65°C. 0.5µl Dig-lablled RNA probe was diluted in 100µl HyA and discs were incubated in this solution over-night at 65°C. The next day, the eye-antennal discs were rinsed in HyB and transferred back to PBT using a HyB:PBT dilution series of 3:1, 1:1, and 1:3 at 65°C. And the eye-antennal discs were trenafered into PBT and washed for two times for 10 minutes in room tempterature. Subsequently the eye-antennal discs were incubated in blocking solution for 20 minutes followed by incubation with alkaline phosphatase coupled anti-DIG antibody (Life technologies) (1:2000 in blocking solution) for 90 minutes. The

antibody was removed by washing three times for 20 minutes with PBT. The eye-antennal discs were transferred to AP buffer (100 mM NaCl, 50 mM $MgCl_2$ and 100 mM Tris-HCl pH 9.5) by rinsing three times for five minutes each. Finally, the reaction mix (4.5 µl nitro blue tetrazolium (NBT) + 3.5 µl 5-bromo-4-chloro-3-indolyl-phosphate (BCIP) + 1 ml AP Buffer-Tween20) was added and incubated in the dark to start the colour reaction, which was regularly observed. To stop the reaction, the eye-antennal discs were rinsed three times with PBT. The eye-antennal discs were mounted in 80% Glycerol for imaging with the Zeiss Imager Z2 scanning microscope.

3.3.3 Single molecule inexpensive fluorescence *in situ* Hybridization (SmiFISH)

Because of the limitation of the chromogenic *in situ* hybridization in the eye-antennal disc, I performed the single molecule inexpensive fluorescence *in situ* Hybridization (SmiFISH) approach to detect the expression pattern of *Rca1* and *Trl*. The following steps were modified from the protocol provided by Calvo and his colleagues (Calvo et al., 2021). The probes were generated by Biosearch Technologies stellaris RNA FISH probe designer tool (LGC, Biosearch Technologies https://biosearchtech.com) (Supplementary table 1 and 2). The eye-antennal discs were fixed with 4% PFA for 20 minutes and washed with PBT (0,05% Tween20 in 1x PBS) three times for 10 minutes. The eye-antennal discs were washed with a 1:1 with PBT:Stellaris Wash Buffer (10% 20x SSC and 10% deionised formamide) for 10 minutes. The eye-antennal discs were washed later with Stellaris Wash Buffer two times for five minutes. And the eye-antennal discs were incubated in warm Stellaris Wash Buffer (37°C) two times for 30 minutes. During the incubating time, probe mixtures were prepared (2 µl of the gene-specific probe mix (100 µM), 2,5 µl 100µM labelled FLAP sequence, 5 µl 10x NEB Buffer 3 and 40,5 µl nuclease-free water) and incubated in a thermo cycler with the following sequence: 85°C for three minutes, 65°C for three minutes, 25°C for five minutes. Then, the eye-antennal discs were incubated with 4 µM

probe/FLAP duplex mix in Stellaris Hybridization Buffer (dextran sulphate, 20x SSC and deionised formamide) overnight on 37°C in the dark. The next day, the eye-antennal discs were rinsed with Stellaris Wash Buffer and washed four times for 15 minutes with Stellaris Wash Buffer at 37°C. The next step was to wash the eye-antennal discs with PBT three times for 10 minutes in the dark at room temperature. The eye-antennal discs were subjected to immunohistochemistry as described in chapter 3.3.1 to counter-stain with anti-Elav antibody.

3.3.4 Hybridization Chain Reaction (HCR)

An additional alternative method to analyse mRNA expression *in situ* is the hybridization chain reaction (HCR) (Choi et al., 2014). The probes were designed and synthesized by the Molecular Instruments, Inc. (UAS) (https://www.molecularinstruments.com/). The HCR was performed and followed by the modified protocol from Bruce et al, 2021 (Bruce et al., 2021). First, I dissected the eye-antennal discs in cold RNase-free PBS. I fixed the tissue with 4% PFA for 45 minutes at room temperature, followed by washing with PBT (0.1% Tween20 in 1X PBS) four times (two times in 10 minutes and two times in five minutes). The discs were washed with the Detergent Solution (1% SDS, 0.5% Tween20, 50mM Tris-HCl in pH 7.5, 1mM EDTA in pH 8.0 and 150 mM NaCl in distilled H_2O) for 30 minutes at 37°C. The following hybridization steps were performed in 37°C. The eye-antennal discs were incubated in the hybridization buffer (with 30% formamide, 5x SSC, 9 mM citric acid in pH6, 0.1% Tween20, 50 µg/mL heparin, 1X Denhardt's solution, and 5% dextran sulphate) for 30 minutes. After preparing the 2 pmol solution of each probe mixture in hybridization buffer, the eye-antennal discs were incubated with the probe overnight (12-16 h). The following day, the excess probes were washed off with probe wash buffer (with 30% formamide, 5xSSC, 9 mM pH6 citric acid, 0.1% Tween20, and 50 µg/mL heparin) (four times, 15 minutes for each time). Subsequently, the eye-antennal discs were

washed with 5x SSCT (5x SSC with 0.1% Tween20) two times for five minutes at room temperature. The eye-antennal discs were then incubated in amplification buffer (5x SSC, 0.1% Tween20 and 10% dextran sulfate) for 30 minutes at room temperature. During the pre-amplification steps, the fluorescently labelled hairpins (h1 and h2) were heated at 95°C for 90 seconds and immediately placed in the dark at room temperature for 30 minutes. The pre-amplified eye-antennal discs were placed in the amplification buffer for 30 minutes and incubated with hairpin solution in the dark at room temperature overnight. The next day, the hairpin solution was removed with five times washing by 5X SSCT (three times in five minutes and two times in 30 minutes). The eye-antennal discs were stained with DAPI (1 µg/mL) for 20 minutes. For analysing the expression pattern of *jim*, the eye-antennal disc was post-fixed with 4% PFA again for 20 minutes. And the eye-antennal discs were subjected to immunochemistry as shown in chapter 3.3.1 to counter-stained with anti-Pnr antibody. The eye-antennal discs were mounted in 80% Glycerol for imaging with the Zeiss Imager Z2 scanning microscope (Zeiss GmbH, Germany).

4. Results

4.1 Identification of putative candidate genes involved in eye size and head shape variation between *D. melanogaster* and *D. mauritiana*

To identify candidate genes involved in eye size and head shape variation between *D. melanogaster* and *D. mauritiana*, I integrated several datasets: a comparative developmental transcriptome dataset (Figure 4.1, A and B), published quantitative and/or functional genetics datasets (Figure 4.1, C and D), and other genomic resources (Figure 4.1, E and F).

4.1.1. Differential expression between *D. melanogaster* and *D. mauritiana* during eye-antennal disc development

As variation in adult eye size and head shape between *D. melanogaster* and *D. mauritiana* is the result of differences during eye-antennal disc development (Casares and McGregor, 2020; Buchberger et al., 2021), candidate genes should be expressed during eye-antennal disc development, and they should show differences in expression between species. Therefore, I first re-analysed a transcriptome dataset representing three important stages of eye-antennal disc development (Torres-Oliva et al., 2018). Of the 13,437 genes that were expressed in at least one stage (Figure 4.1, A), 8,556 genes were differentially expressed (padj < 0.05) between the two species (Figure 4.1, B and Table 4.1) (Buchberger et al., 2021).

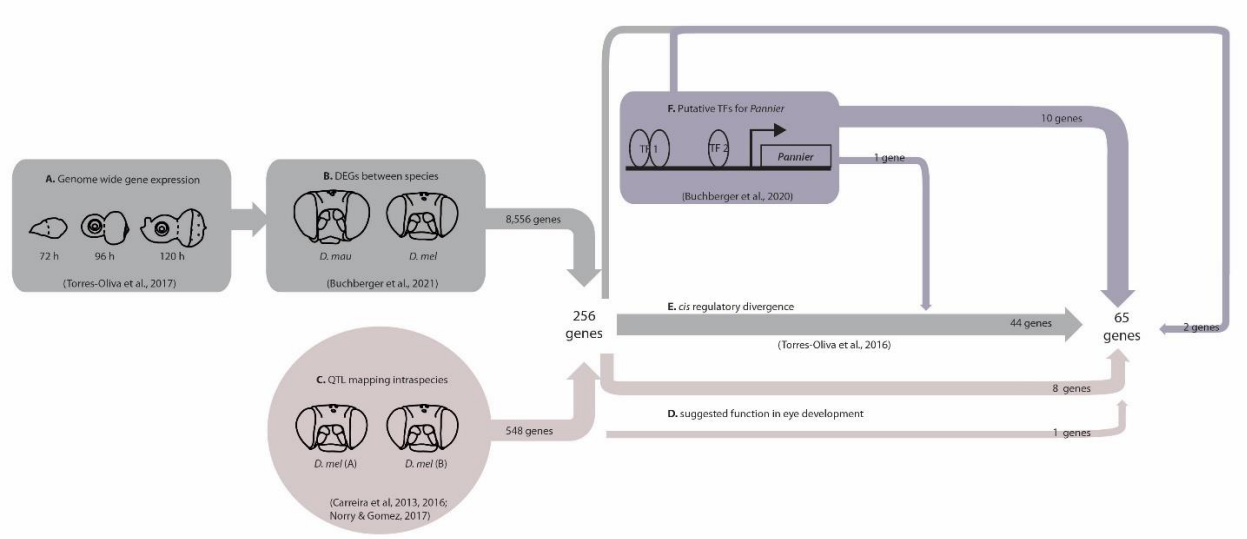

Figure 4.1. The flow chart shows the screening process of candidate genes from several unbiased datasets. **(A-F)** the different datasets used to identify the candidate genes. **(A)** Genome wide gene expression dataset of three developmental stages of eye-antennal discs (Torres-Oliva et al., 2018). **(B)** Differentially expressed genes between *D. melanogaster* (*D. mel*) and *D. mauritiana* (*D. mau*) from Buchberger et al., 2021. **(C)** Eye variation associated genes suggested from the QTL mapping research (Carreira et al., 2013, 2016; Norry and Gomez, 2017). **(D)** Genes with established function during eye development. **(E)** Genes with *cis*-regulatory divergence shown in Torres-Oliva et al., 2016 (Torres-Oliva, 2016). **(F)** Putative regulators for *pannier* obtained from ATACseq data (Buchberger et al., 2021).

4.1.2. Published quantitative genetics datasets

Inter-specific variation in eye size between *D. melanogaster* and *D. mauritiana* is due to differences in ommatidia number and a developmental trade-off between compound eye size and interstitial head cuticle width has been observed (Posnien et al., 2012; Buchberger et al., 2021). Since variation in head morphology among *D. melanogaster* populations shows similar phenotypic characteristics, i.e. ommatidia number differences (Norry and Gomez, 2017) and a trade-off between head compartments (Norry and Gomez, 2017), I incorporated data from previously published quantitative trait locus (QTL) mapping studies, which revealed 548 positional candidate genes responsible for intra-specific eye size and head shape variation in *D. melanogaster* (e.g., *jim*, *Fasciclin 3 (Fas3)*, *Reticulon-like1 (Rtnl1)*) (Figure 4.1, C and Supplementary Table 3) (Carreira et al., 2013, 2016; Norry and Gomez, 2017). A combination of

the QTL data with the developmental RNAseq data showed that 256 of the positional candidate genes were differentially expressed between *D. melanogaster* and *D. mauritiana* (Figure 4.1). A GO term analysis of these 256 genes revealed eight genes with a potential function in "eye-antennal disc development (GO: 0035214)" or "eye-antennal disc morphogenesis (GO:0007455)" and thus these eight genes were included in the finale candidate gene list (Figure 4.1, D, and Supplementary Table 4). Additionally, the GO term analysis also suggested a potential function in "eye-antennal disc development (GO: 0035214)" or "eye-antennal disc morphogenesis (GO:0007455)" for three positional candidates which were not differentially expressed: *CG43340*, *wingless* (*wg*) and *Fascilcin 3 (Fas3*). Therefore, I included these three genes in the final candidate gene list (Figure 4.1, D, and Supplementary Table 4). Note that a function during eye-antennal disc development has been experimentally confirmed for *wg* (Ma and Moses, 1995; Treisman and Rubin, 1995; Royet and Finkelstein, 1996; Wittkorn et al., 2015).

4.1.3. Differentially expressed genes with *cis*-regulatory divergence

Of the 256 positional candidate genes, which were differentially expressed in at least one of the three stages of eye-antennal disc development, I next identified those genes that were differentially expressed due to putative changes in their own regulatory region. To this end, I used an allele-specific expression (ASE) dataset (Torres-Oliva, 2016) that is based on inter-specific F1 hybrids and allows distinguishing between *cis*- and *trans*-regulatory divergence (Torres-Oliva, 2016). 44 genes that showed signatures of *cis*-regulatory divergence in at least one of the three studied developmental stages were added to the final candidate gene list (e.g. *piragua*, *beta-site APP-cleaving enzyme (Bace)*, *TBP-related factor*) (Figure 4.1, E and Table 4.1, 3.1).

4.1.4. Candidate genes involved in *pnr* regulation

Since differential expression of *pnr* has been associated with variation in eye size and head shape between *D. melanogaster* and *D. mauritiana* (Buchberger et al., 2021), I considerrd genes coding for regulators of *pnr* expression as putative candidates. Therefore, I employed chromatin accessibility data (ATACseq) (Buchberger et al., 2021) to identify transcription factor binding motifs in open chromatin regions in the *pnr* locus. This analysis revealed 13 putative regulators (Figure 4.1, F). Among those 13 genes, the GO term analysis also confirmed their potential role in "sequence-specific DNA binding (GO: 0043565)", "DNA binding (GO:0003677)" or "transcription factor activity, RNA polymerase II distal enhancer sequence-specific binding (GO:0003705)" (Supplementary Figure 1 and Supplementary Table 4). Note that two of the 256 differentially expressed positional candidate genes (*jim* and *Mad*; thin grey-purple arrow in figure 4.1) and one of the genes showing *cis*-regulatory divergence (*zeste* (*z*); thin purple arrow in Figure 4.1) seem to be involved in *pnr* regulation.

Table 4.1. Candidate gene lists used to establish the final candidate gene list. The "*" indicates the datasets were used to construct the networks as comparison. The gene lists 7, 8, 9 associated with wing variation are used as outgroup comparison.

Gene lists	Gene numbers
1. Differentially expressed genes in eye-antennal disc (df_EAD)*	8,556
2. Genes underlying eye size in *D. mel* (QTL)*	548
3. Expressed genes in eye-antennal disc & QTL (Exp_EAD_QTL)*	437
4. Differentially expressed genes & QTL (df_EAD_QTL)*	256
4.1 *Cis*-regulatory divergence in eye-antennal disc & QTL & differential expressed in EAD	44
4.2 Gene with known function related to eye development & QTL & differential expressed in EAD	8
4.3 Gene with potential function related to eye development & QTL	3
5. Interaction with eye size related gene, *pannier*	13
5.1 *pannier* related gene with known function related to eye development	2

6.	**Candidate genes in total (Candidate)***	65
6.1	**Genes with RNAi phenotypes or known function in eye development**	18
6.2	**Genes without RNAi phenotypes (No defect)***	47
7.	**Differentially expressed in the wing disc (df_wing)***	2,616
8.	**Expressed genes in wing disc + QTL (Exp_wing_QTL)***	410
9.	**Differentially expressed genes in wing disc + QTL (df_wing_QTL)***	81

In summary, the integration of multiple unbiased genome-wide datasets resulted in 65 candidate genes (Figure 4.1). 63 of 65 genes showed up in at least two sub-datasets, except for *zerknullt* (*zen*), and *Trithorax-like* (*Trl*) (Figure 4.3). Interestingly, 50 of the 65 candidate genes appeared in three sub-datasets. However, there is not much knowledge to support the biological processes that those genes are involved in.

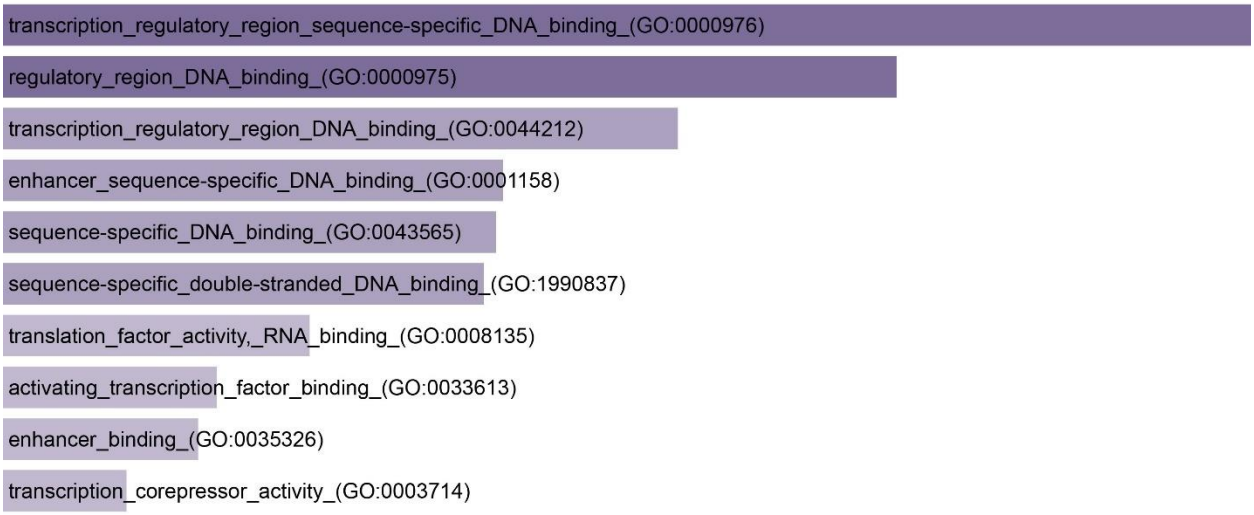

Figure 4.2. GO enrichment analysis of all 65 candidate genes. Among those 65 genes, the most common types of gene ontology are Transcription regulatory region sequence specific DNA binding (GO: 0000976) and Regulatory region DNA binding (GO: 0000975).

4.2. Many candidate genes are crucial for adult eye and head development

The GO enrichment analysis for the 65 candidate genes obtained by integrating multiple datasets suggests that DNA binding activity is the major common biological function of the candidate genes

(Figure 4.2). Six of 65 candidate genes are already well-known to be involved in eye development, which are *Mad* (Wiersdorff et al., 1996; Kim et al., 1997, 2017), *eye absent* (*eya)* (Bonini et al., 1993; Kenyon et al., 2005), *cka* (Neal et al., 2020), *wg* (Ma and Moses, 1995; Treisman and Rubin, 1995; Royet and Finkelstein, 1996; Mosimann et al., 2006; Wittkorn et al., 2015), *da* (Brown et al., 1996; Lim et al., 2008) and *Rca1* (Dong et al., 1997) (Figure 4.3 and Supplementary Table 3). To functionally validate the role of the remaining 59 candidate genes during eye and/or head development, I performed an RNA interference (RNAi) screen employing the Gal4/UAS binary expression system (Brand and Perrimon, 1993). Specifically, I used the *eyeless*-Gal4 (*ey*-Gal4, BDSC #5535) line, which is active in the eye disc from the early stage onwards and to the later stages (Jang et al., 2003; Baker et al., 2018) (Figure 4.6, M), to drive expression of RNAi constructs for the candidate gene of interest. This RNAi screen revealed 12 of 59 tested genes that showed eye and/or head phenotypes (Figure 4.3, 4.4 and 4.6).

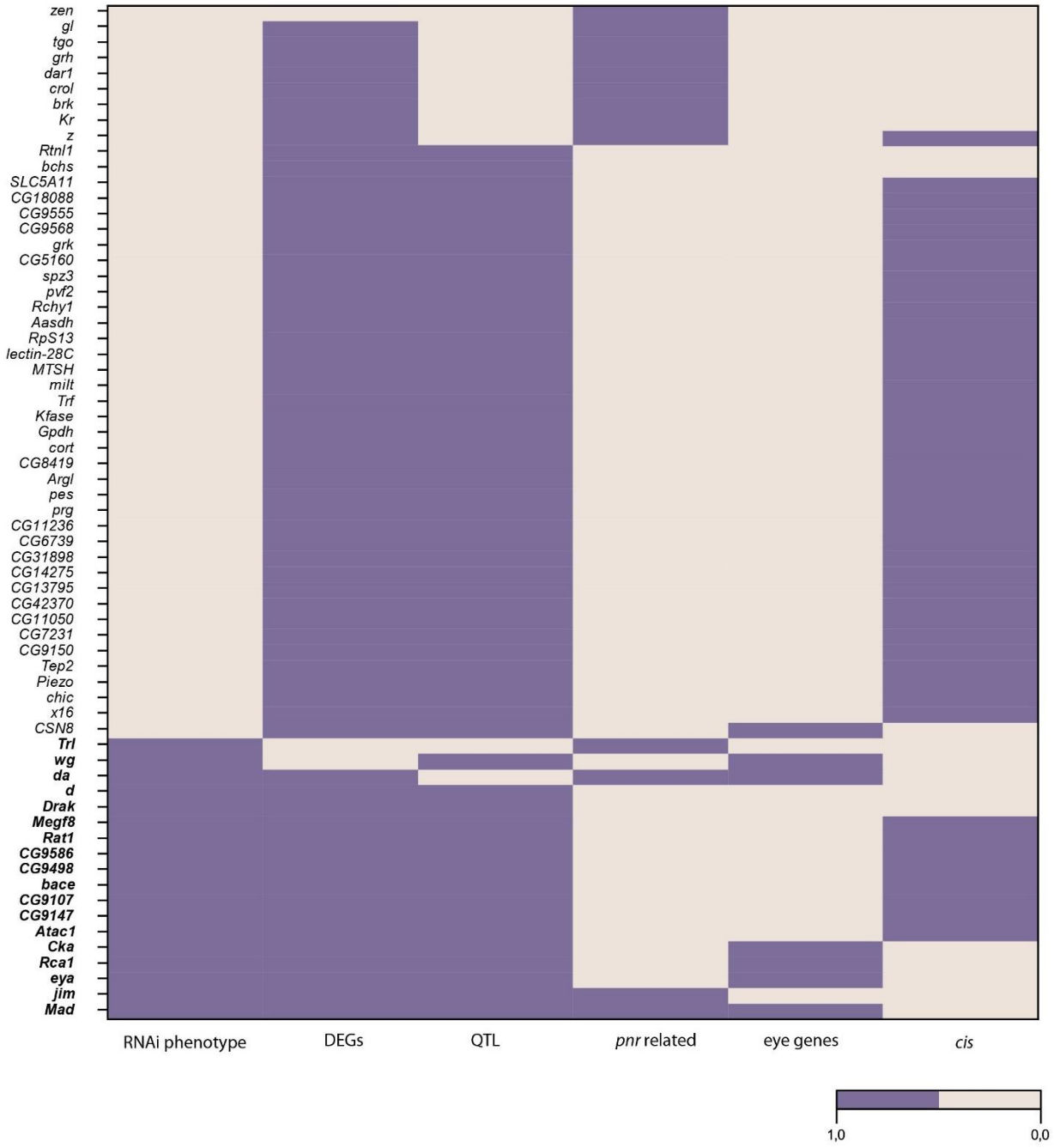

Figure 4.3. Summary of the candidate gene list with their resources. If the genes are shown in the respective resources and it has shown as 1 in this figure (in purple). Labels on the X-axis: RNAi phenotype, RNAi resulted in eye and/or head defects; DEGs, differentially expressed genes between *D. melanogaster* and *D. mauritiana*; QTL, positional candidates associated with eye size differentiation from QTL studies; *pnr* related, putative regulators of *pnr* obtained from ATACseq data; eye genes, the function of those genes in eye development were suggested by the literatures; *cis*, the differentially expression of genes were due to *cis* regulatory divergence.

To quantify the RNAi effects on adult head and eye development, I established a phenotypic score that represents the percentage of eye size in relation to a wildtype eye (Figure 4.4, N and O). The loss-of-function for three genes resulted in severe reduction in eye size (Figure 4.4, C, E, H and O); while one gene only showed subtle reduction (Figure 4.4, K and O). Loss-of-function of most genes caused intermediate to minor eye reduction (Figure 4.4, D, I, L and O). Variation among individuals of the same experiment was high which is expected for RNAi experiments.

The three genes that showed severe eye reduction were *CG9107*, *Trl* and *Drak*. *Drak* that encodes the Death-associated protein kinase (Neubueser and Hipfner, 2010) showed a phenotypic series from minor reduction of the eye field to the complete loss of eyes (Figure 4.4, C and O). Besides the eye phenotype, it is also noted that the bristle pattern was disrupted as well (white arrowhead, Figure 4.4, C). *Trl* that codes for GAGA factor (Bhat et al., 1996) not only led to severe eye loss and extra eye tissue, but also caused defects in other tissues, such as the bristle pattern (white arrowhead, Figure 4.4, E) and extra retinal tissue (red arrow, Figure 4.5, B"). Similarly, an uncharacterized gene, *CG9107*, led to the same severe eye reduction, which was observed at 100% penetrance (Figure 4.4, H). Those flies with smaller eyes also had reduced ventral head cuticle tissue (Figure 4.4, H and 4.5, A"). This loss of ventral head cuticle was not observed for RNAi of other genes. Moreover, *CG9107* RNAi also resulted in a split eye or ectopic ventral eye tissue (red arrow, Figure 4.5, A').

Most intermediate genes resulted in less than 50% reduction in eye area when the expression was interfered (Figure 4.4, A, B, F, G, J and O). *Bace* that codes for an amyloid precursor protein (APP)-cleaving aspartic protease (Bolkan et al., 2012) resulted in loss of ventral eye tissue with a penetrance of 8.3 % (Figure 4.4, A). Besides that, the bristle pattern in the ventral region below the retina was disturbed (white arrowhead, Figure 4.4, A). *Atac1* that codes for a component of a protein

complex involved in chromatin remodelling and histone acetylation (Guelman et al., 2006; Suganuma et al., 2008) resulted in anterior eye reduction upon RNAi (Figure 4.4, B). *dachs* that codes for a myosin protein (Degoutin et al., 2013) resulted in minor eye reduction shown in 61% of adult offspring (Figure 4.4, F). RNAi for the uncharacterized gene *CG9498* showed the partial loss of retinal tissue in the ventral region in 20.6% of the individuals (Figure 4.4, G). *Megf8* that is suggested to be involved in calcium ion binding activity (Larkin et al., 2021) resulted in minor loss of eye in 15.4% of the individuals (Figure 4.4, J). RNAi for *jim* that encodes a zinc finger C_2H_2 transcription factor (Doerflinger et al., 1999) mostly resulted in partial loss of eye tissue (Figure 4.4, O), but some flies with complete eye loss were observed as well (Figure 4.4, L). RNAi for *CG9147* resulted in a broad range of eye reductions (Figure 4.4, I and O) and ectopic antennal tissue was observed in the eye field (Figure 4.5, C). *Rat1* RNAi flies also showed different levels of eye reduction (green arrow in Figure 4.4, D) and some extra antennal tissue in the retina field (black arrow in Figure 4.4, D).

Loss-of-function of *CG9586* only cause subtle reduction of 7% compared to wildtype eyes (Figure 4.4, K and O). Additionally, the eye of loss-of-function individuals showed a rough-eye phenotype. It is important to note that RNAi caused low survival rate with only three survivors.

With the exception of *CG9107* RNAi that caused the reduction or loss of antennal tissue (green arrowhead, 4.5, A and A"), RNAi for all genes that resulted in reduced eye size the antennae were unaffected. This suggests that specific effects were observed. Intriguingly, loss-of-function of *Trl* and *Drak* resulted in antennal duplication (black arrowhead in Figure 4.4, C & E).

Overall, the RNAi screen revealed that 12 of 59 tested candidate genes showed similar phenotypes ranging from mild eye field reduction to eye loss (Figure 4.4, A-L). Together with the six genes that have

been implicated in eye development before, 18 of 65 candidate genes play roles during eye development (Figure 4.3).

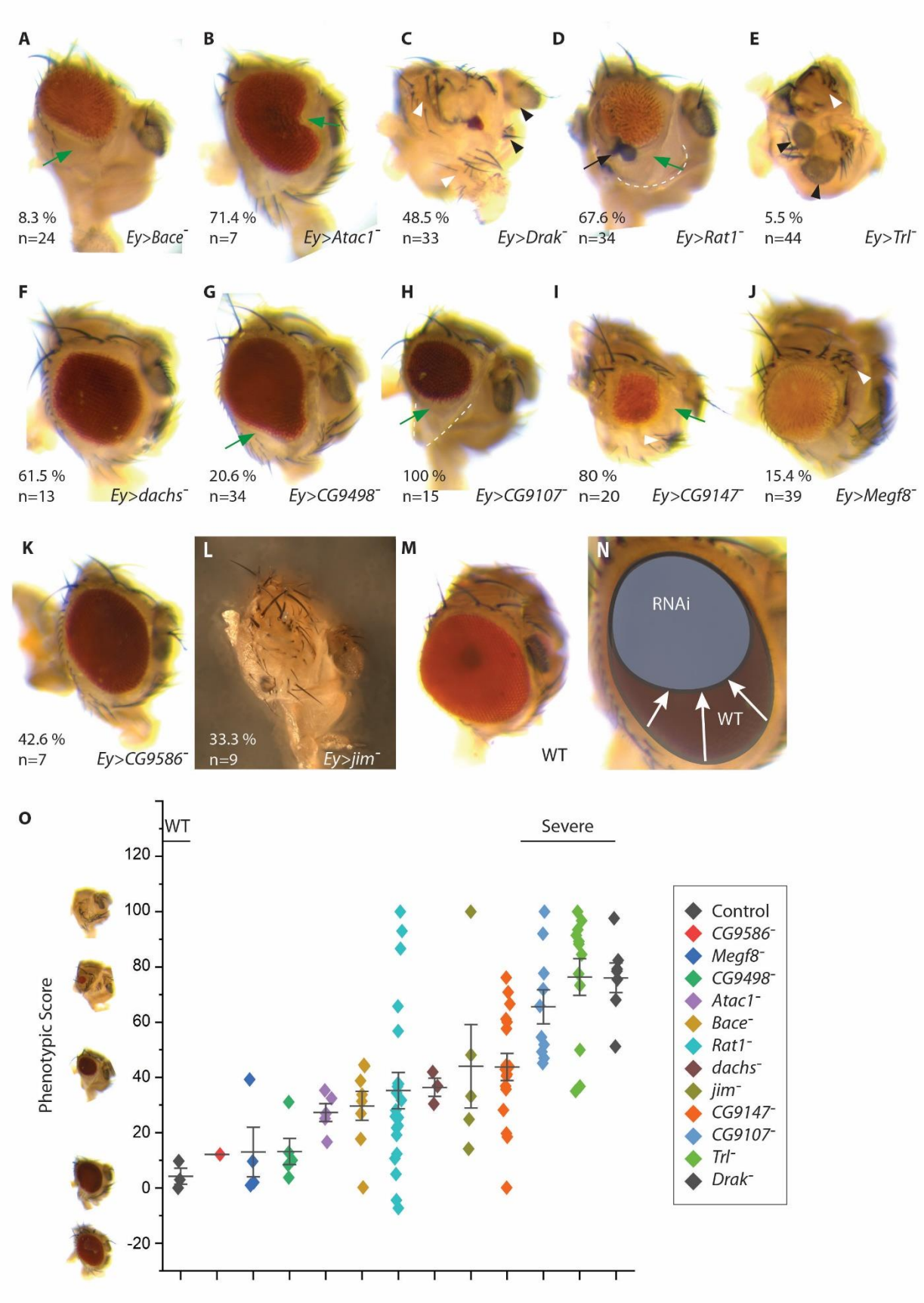
A
8.3 %
n=24
Ey>Bace-
B
71.4 %
n=7
Ey>Atac1-
C
48.5 %
n=33
Ey>Drak-
D
67.6 %
n=34
Ey>Rat1-
E
5.5 %
n=44
Ey>Trl-
F
61.5 %
n=13
Ey>dachs-
G
20.6 %
n=34
Ey>CG9498-
H
100 %
n=15
Ey>CG9107-
I
80 %
n=20
Ey>CG9147-
J
15.4 %
n=39
Ey>Megf8-
K
42.6 %
n=7
Ey>CG9586-
L
33.3 %
n=9
Ey>jim-
M
WT
N
RNAi
WT
O
WT
Severe
Phenotypic Score
120
100
80
60
40
20
0
-20
Control
CG9586-
Megf8-
CG9498-
Atac1-
Bace-
Rat1-
dachs-
jim-
CG9147-
CG9107-
Trl-
Drak-

Figure 4.4. (A-L) Represented adult phenotypes after *ey* > candidate gene-RNAi. For each gene a representative adult head is shown in lateral view. Among the flies without curly wings (n in each panel), the percentage of individuals with the eye phenotypes are shown. as well as the individual number of each crosses (n), except for the numbers of curly wings. The green arrow indicates the reduction of eye tissue, the white arrowhead labels the defect in bristle pattern, the black arrowhead shows extra antennal tissue, the black arrow shows extra antennal tissue in retinal, and the dash line represent the remaining head cuticle tissue. **(M)** Wild type (OreR) head in lateral view. **(N)** Scheme of the calculation of the ratio of eye field reduction. **(O)** The phenotypic scores (%) were determined by the percentage of reduction of eye field. WT, wildtype, severe, with severe phenotype. 0 represents no reduction, while 100 means the eye loss phenotype. In all figures, anterior is to the right.

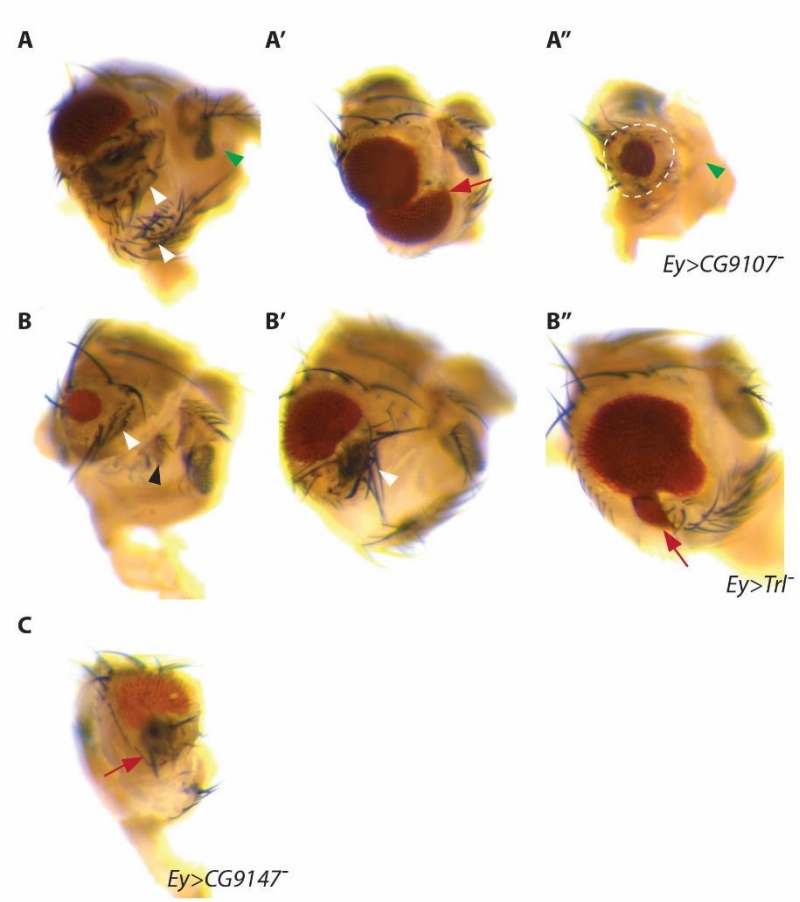

Figure 4.5. Other adult phenotypes after *ey* > candidate gene-RNAi of **(A)** CG9107, **(B)** Trl and **(C)** CG9147. The green arrowhead indicates the reduction or loss of antennal tissue, the white arrowhead labels the defect in bristle pattern, the black arrowhead shows extra antennal tissue, and the red arrow indicates the ectopic tissue growth. The dash line circles the remaining surrounding cuticle. In all figures, anterior is to the left. Related to Figure 4.4.

4.3. Adult phenotypes are linked to perturbation of eye-antennal disc development

To understand the readout of the loss-of-function experiments, I dissected eye-antennal discs of F1 offspring of *ey*-Gal4 X UAS-RNAi crosses and performed immunostaining for Elav and Phalloidin to label differentiating photoreceptors (Koushika et al., 1996) and F-actin (Capani et al., 2001), respectively. Among the 12 genes with RNAi phenotypes, the development of eye-antennal discs in the offspring was severely affected (Figure 4.6) because RNAi for each gene resulted in some individuals with an eye reduction phenotype (Figure 4.6, N). A phenotypic series, including eye reduction, loss of the eye, or reduction of whole disc size were observed for most of genes (Figure 4.6, N). And duplicated antennal tissue was observed for 2 genes (Figure 4.6, N).

In general, the eye-antennal disc phenotypes matched the adult phenotypes. For instance, *Trl* and *CG9107*, two genes that led to severe eye phenotypes in adults (Figure 4.4, O), caused the complete loss of retinal tissue in the developing discs (Figure 4.6, E and N). Similarly, *Drak*, another gene that led to severe eye reduction, as well as antennal duplication in adults (Figure 4.4, C and O), showed dramatically reduced retinal tissue and duplication of antennal tissue in discs (Figure 4.6, C and Interestingly, *Bace* and *Atac1* that caused partially reduction of the eye in adults (green arrow in Figure 4.4, A and B), also led to ectopic growth posterior to antennal region in the disc (Figure 4.6, A and B). However, not all of the antennal phenotype match to the adult eye or/ and head phenotype. It is noted that RNAi for five genes (i.e. *Bace*, *Atac1*, *Rat1*, *dachs*, and *CG9498*) resulted in reduction of the whole eye-antennal disc size (Figure 4.6, N), which was not observed in the adult phenotype (Figure 4.4). Besides that, the RNAi phenotype in the eye-antennal discs showed more frequent than in the adults. Therefore, it is expected that lethality caused by RNAi would lead to the mismatch between developing discs and adults.

To avoid the artefacts, cause by the Gal4 line used, the loss-of-functions of *Trl*, *Bace* and *Atac1* were also activated by the three Gal4 lines *Teashirt* (*Tsh*)-Gal4, *elav*-Gal4 and *dpp*-Gal4, which drive expression in different parts of the eye-antennal disc (Supplementary Figure 3). The observed RNAi phenotypes in eye-antennal discs were partially confirmed for *Bace*, *Atac1* and *Trl*, when three other Gal4-driver lines were used. The strongest effect on eye development was observed when *Trl*, *Bace* or *Atac1*-RNAi was driven by *ey*-Gal4 drivers, while *elav*-Gal4. *teashirt* (*tsh)*- and *dpp*-Gal4 drivers used for driving the RNAi showed no strong effects in the retinal region (Supplementary Figure 3). Note that the analysis of overexpression effect on eye-antennal discs was performed using TRiP-CRISPR lines to confirm the function of Jim, Trl, Bace and Atac1 (see Material and Methods Table 3.4). Since the *ey* driver for TRiP/CRISPR is not available. The used drivers are not in the *ey* positive cells as the RNAi (i.e. *elav*, *pnr* and *dpp*). The crosses resulted in no significant defects (Data not shown).

Taken together, the analysis of RNAi effect on eye-antennal discs confirmed that the 12 candidate genes that have not yet been associated with eye development are involved in this process. Including the six previously analysed genes, 18 of 65 candidate genes were high confidence candidate genes involved in eye size variation between *D. melanogaster* and *D. mauritiana*.

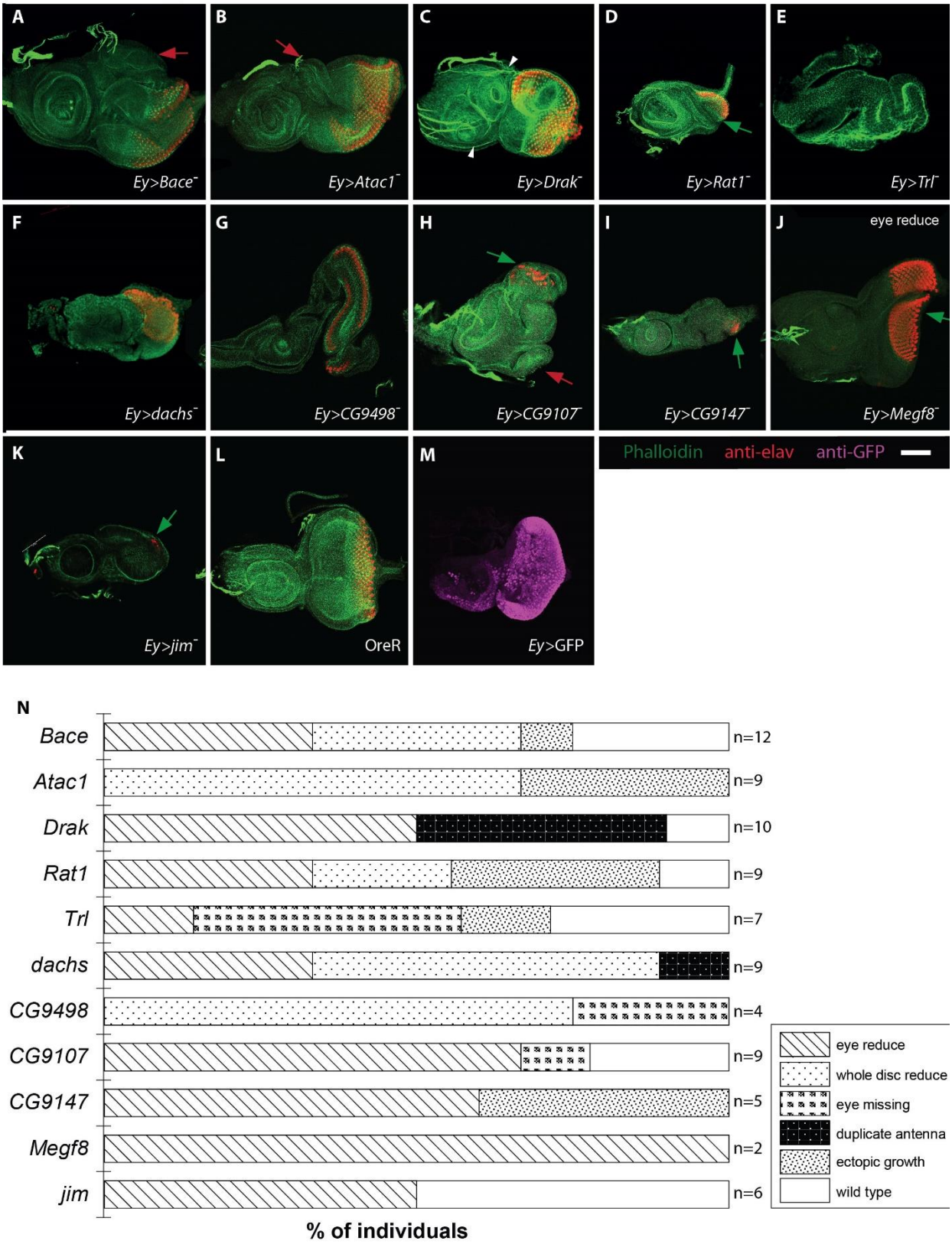

Figure 4.6. (A-J) L3 larval eye-antennal discs of F1 offspring of candidate gene RNAi experiments. The red arrow indicates

the ectopic growth tissues in the eye-antennal discs. The green arrow indicates the eye reduction. **(L)** The larval disc of *D. melanogaster* wild type (OreR). **(M)** Reporter gene expression driven by *ey*-Gal4 in early larval disc. **(N)** Quantification of eye-antennal disc phenotypes shown in percentage of different RNAi phenotype. The individual number of recorded discs is shown as n. In all discs, actin was labelled with Phalloidin (green) and anti-Elav (red) to label the photoreceptors. The scale bar is 50 µm. In all the figures, anterior is to the left.

4.4. Many candidate genes are broadly expressed during eye-antennal disc development

To link the function of the 18 high confidence candidate genes and *pnr* that has previously been revealed as candidate gene (Buchberger et al., 2021) during eye-antennal disc development to potential specific developmental processes, I next analysed their expression in *D. melanogaster* eye-antennal discs using three different datasets and methods: **1)** I assessed the broad expression level from a bulk-RNAseq dataset at three stages (i.e. 72 hrs, 96 hrs and 120 hrs after egg laying, AEL) (Torres-Oliva et al., 2018) (Figure 4.6). **2)** I inferred potential cell types of the compound eye-antennal discs that express the candidate genes employing single-nuclei RNAseq (sn-RNAseq) data for late larval eye-antennal discs (at 120 h AEL) (Gordon Wiegleb, unpublished) (Figure 4.8). **3)** For selected genes, I performed *in situ* hybridisation to analyse the spatial expression (Supplementary Figure 4).

The bulk-RNAseq data revealed that the relative expression level of *Bace* and *Megf8* stayed low during eye development; while some genes, such as *eya*, *dachs*, *CG9586*, *CG9107*, *Trl* and *Rca1* were highly expressed (more than 50 Reads Per Kilobase of transcript per Million mapped reads (RPKM)) (Figure 4.7). The relative expression of many genes increased from 72 h to 96 h and remained constant (i.e. *CG9586*, *dachs*, *Rca1*, *CG9147*, *Atac1* and *pnr*) or decreased (i.e. *eya*, *Trl*, *jim*, *Drak*, *Mad*, *cka* and *Rat1*) at the 120 h stage (Figure 4.7). The relative expression of *CG9498* is the only one that seems to have slightly higher expression at 72 h and its expression drops in the later stage. Additionally, *CG9107* is the only one with lowest expression level in 96 h.

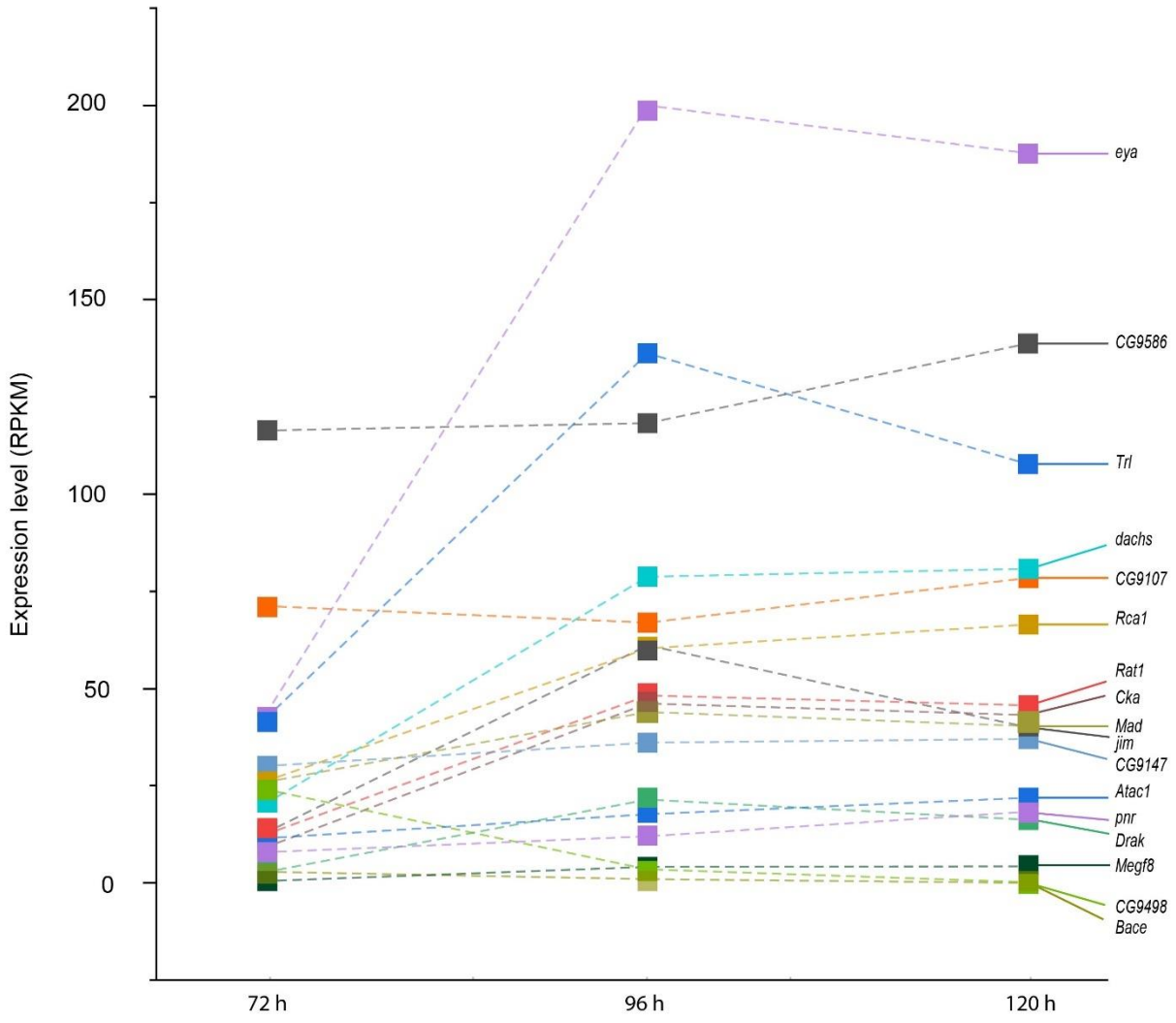

Figure 4.7. The expression of candidate genes among three developmental stages (from 72 h AEL to 120 h AEL) inferred from bulk-RNAseq data. The Y-axis is the expression level, the unit is Reads Per Kilobase of transcript per Million mapped reads (RPKM).

In addition to bulk-RNAseq data, the expression pattern and expression level of each gene were also analysed in sn-RNAseq data (Figure 4.8). Eight of the 19 candidate genes were ubiquitously expressed in the whole eye-antennal disc at relatively low level in 120 h AEL (*CG9586*, *CG9107*, *Rat1*, *Atac*, *Trl*, *Rca1*, *da* and *cka*) (Figure 4.8, A). Four candidate genes were ubiquitously expressed at relatively high level (*Mad*, *Drak*, *jim* and *dachs*) (Figure 4.8, A). For instance, *Drak* is found everywhere in the discs (Figure 4.8, A and C). Three genes (*eya*, *wg*, *pnr*) were highly expressed in specific tissues (Figure 4.8, A). For instance,

eya was highly expressed in cells contributing to the morphogenetic furrow (MF), the pre-proneural domain (PPN), the dorsal region, and Photoreceptors (PhR) (Figure 4.8, D) and *wg* was mainly expressed in the antennal cells, in the dorsal region and in ocelli (Figure 4.8, E). Three genes (*Megf8*, *CG9147* and *CG9498*) were detected in specific tissues at very low expression (Figure 4.8, A). For instance, *CG9498* was only found in a few specific cells in 120 h AEL, which were annotated as wrapping glia and subperineural glia cells (WG_SPG) (Figure 4.8, F). *Bace* expression was not detected in the sn-RNAseq data, most likely due to its low expression level.

The comparison of the two RNAseq datasets showed that many candidate genes were lowly expressed in the eye-antennal disc. However, it is important to note that some discrepancies were observed. For instance, *Rca1* expression was relatively high in the bulk-RNAseq dataset (Figure 4.7) and low in the sn-RNAseq (Figure 4.8, see annotation in Supplementary Figure 2). It is noted that the expression level of *da* and *wg* were not detected in the bulk-RNAseq data (Figure 4.7), although both genes were differentially expressed in the comparative analysis. This discrepancy is most likely due to different normalization methods because the abundance used here is expressed as RPKM value (Torres-Oliva, 2016), while the DEGs search is based on a normalization assuming negative binomial data distribution (Buchberger, 2019). Note that expression of *da* and *wg* was observed in the sn-RNAseq data.

To confirm the data obtained from the two RNAseq approaches, I also performed *in situ* hybridisation and immunostaining to analyse the spatial expression of some candidate genes. The immunostaining for Bace and Rca1 in the eye-antennal discs did not show any specific pattern, correlating to the low expression observed in bulk- and sn-RNAseq data. The *in situ* hybridization of *Rat1* (Supplementary Figure 4, A) matches the sn-RNAseq result that it is expressed in MF and ventral PE. Similarly, I could

confirm *wg* expression in the antennal region, the dorsal region and the eye-antennal border (EAB) in both *in situ* hybridization (Supplementary Figure 4, B) (Ma and Moses, 1995) and sn-RNAseq (Figure 4.8). Also, the low ubiquitous expression with slightly higher expression in photoreceptors (PhR) of *Trl* observed in sn-RNAseq (Figure 4.8) can also be found in the *in situ* hybridization results (white arrowhead in Supplementary Figure 4, B).

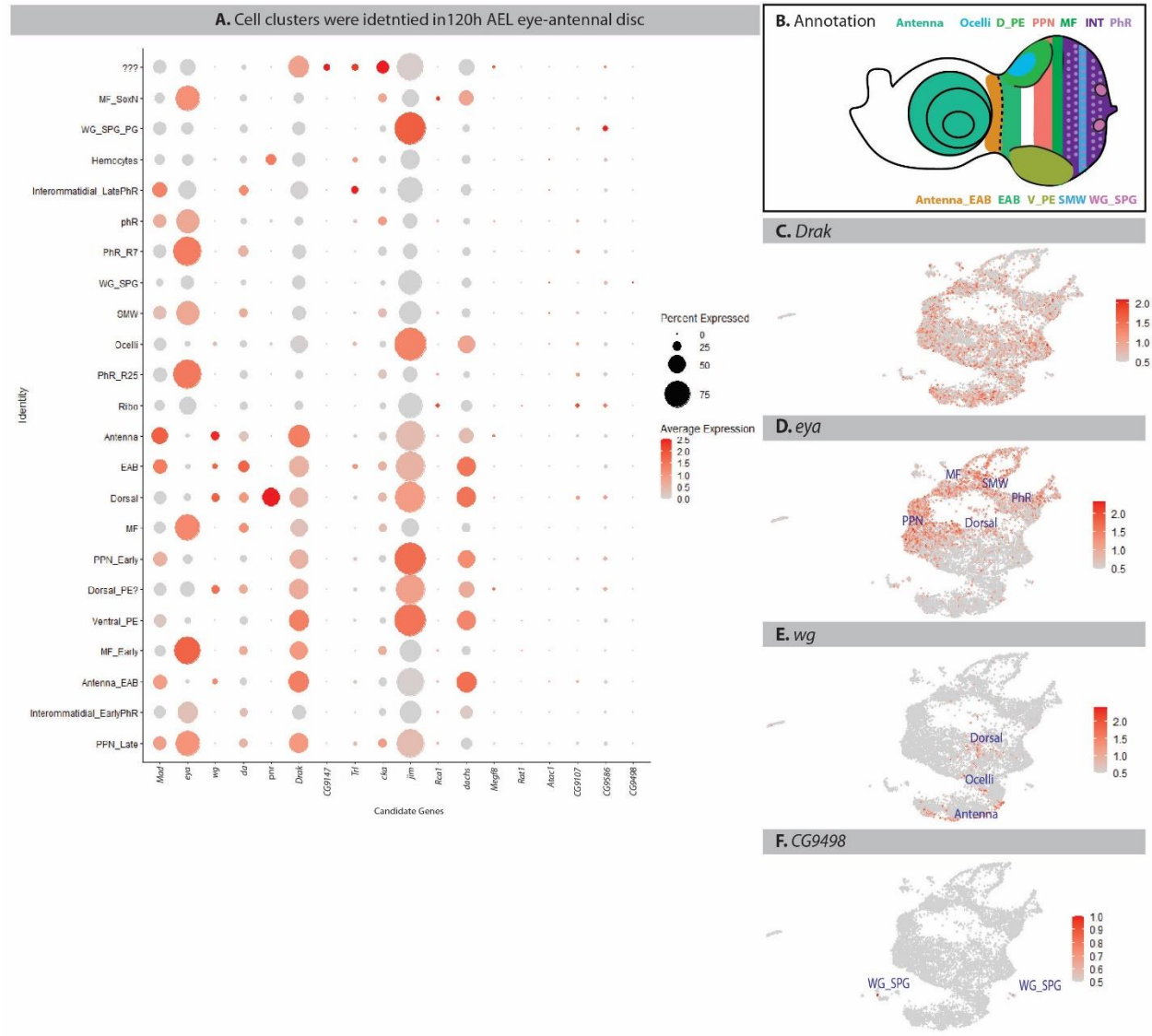

Figure 4.8. (A) Expression of candidate genes observed in sn-RNAseq data of imaginal discs at 120 h AEL. MF, morphogenetic furrow; MF_SoxN, morphogenetic furrow with SoxN expression; WG, Wrapping glia; PG, Perineurial glia; PhR, Photoreceptor; SMW, Second mitotic wave; EAB, Eye-antennal border; PE, Peripodial epithelium; PPN, Pre-proneural domain; Ribo, cells that express ribosomal genes **(B)** Annotated cell cluster for all cells modified from Ariss et al., 2018 (Ariss et al., 2018), V_PE, Ventral Peripodial epithelium; D_PE, Dorsal Peripodial epithelium; INT, Interommatidial cells **(C)** Ubiquitously expressed genes, such as Drak. **(D)** Region specific genes, such as eya. **(E)** Tissue-specifically expressed gene such as wg. Detail annotation in Supplementary Figure 2 **(F)** CG9498 is only expressed in a few cells of WG_SPG. (Figures A, C, D, E, F provided by Gordon Wiegleb, unpublished).

In summary, both bulk-RNAseq and sn-RNAseq provides the expression details of candidate genes in the eye-antennal discs. Because all of the candidate genes showed extremely different expression patterns and levels with one another. This might indicate how is the complexity of gene architectures those genes involved in. Therefore, further investigates are required to dissect the biological function of each candidate gene during eye and head development.

4.5. Network construction of candidate genes allows predicting developmental processes and new genes involved in eye development

4.5.1. Network construction and network connectivity

Since the 18 candidate genes and *pnr* resulted in similar phenotypes upon loss-of-function, I hypothesized that these genes may be functionally related. To test this hypothesis, I constructed a GRN with the 19 genes (Figure 4.9). Connections (edges) between genes (nodes) were based on the following molecular and genetic information stored in various databases (from highest confidence level to lowest confidence): physical interaction, genetic interaction, co-localization, co-expression, shared protein domains and predicted interactions. Note that an edge based on a proven physical interaction has a higher confidence level than a connection inferred from a co-expression.

Only *jim* and *Bace* were not connected to any other candidate gene and *CG9147* and *Rca1* were connected with each other, but not with other genes in the network (Figure 4.9). The remaining 15 genes were present in the same cluster, and they were connected to candidate genes with previously established functions during eye-antennal disc development (i.e. *eya*, *wg*, *cka*, *Mad*, *da* and *pnr*, in red, Figure 4.9).

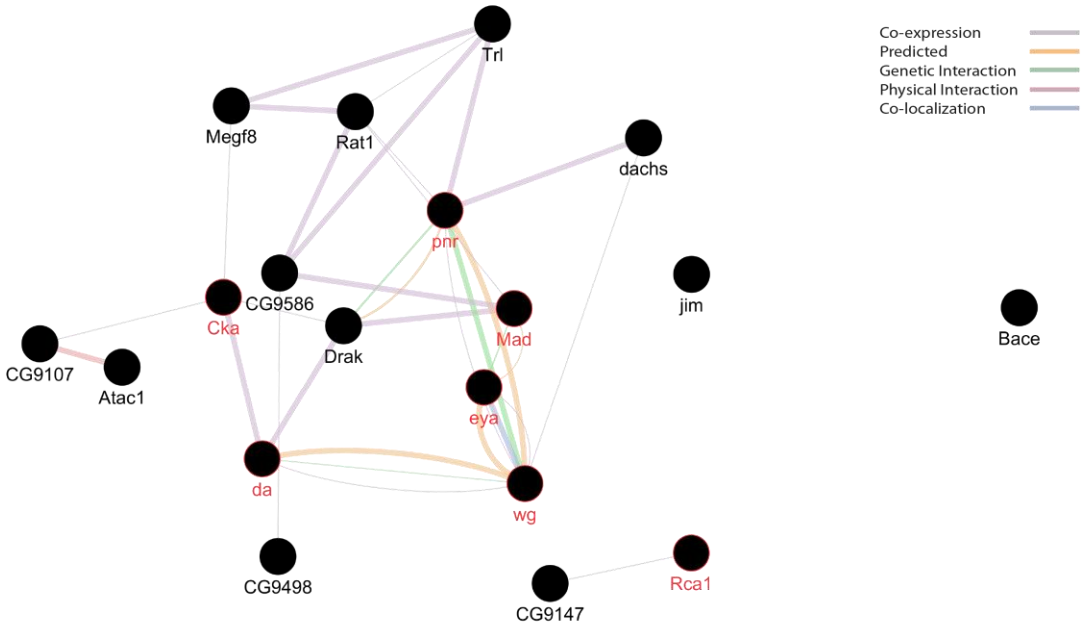

Figure 4.9. The constructed network with 18 candidate genes and *pnr*. The known eye genes are labelled in red. The different types of edges are labelled in respective colour as colour code on the right up. The thickness of the edges reports weights that indicate the predictive value of each dataset. The thicker the edges are, the stronger connection exists between two edges. For instance, the co-expression edge between Pnr and Dachs with the higher strength of data, which supports the associations.

If the high connectivity in the reconstructed GRN is indeed an indication of potentially shared functions, the connectivity should be higher compared to a network of randomly selected genes. To test this idea, I reconstructed several networks from 19 randomly selected genes from various gene lists obtained during the integration of multiple datasets (see Figure 4.1 and Table 4.1 for gene sets that were used for random gene selection) and compared their connectivity (i.e. number of edges) and the quality of predicted connections (i.e. source of edge information) to those of the candidate gene network (Supplementary Figure 5). For instance, I randomly chose 19 genes from the 47 genes (Table

4.1) that did not result in eye or head phenotypes in my RNAi screen (Figure 4.10). This random selection was repeated ten times for each gene list to avoid technical selection biases. The candidate gene network had 33 edges and 66.7 % (22 edges) of them were based on "co-expression" information (Figure 4.9 and Supplementary table 5). The average number of edges in all randomly selected networks was much lower with less than 16 (Figure 4.10) and the dominant edge source was also "co-expression" (Supplementary table 5). The higher connectivity within the candidate gene network was predominantly driven by more edges based on "genetic interactions" (12.12 % vs. none in all other networks) and partially by more "physical interactions" (Figure 4.11 and Supplementary table 5). Besides these high confidence edges, the candidate network was composed by clearly more "predicted interactions", which represent rather low confidence levels. Note that none of the edges in the candidate gene network was based on "shared protein domains", while some randomly selected networks consisted of about 4 % such edges.

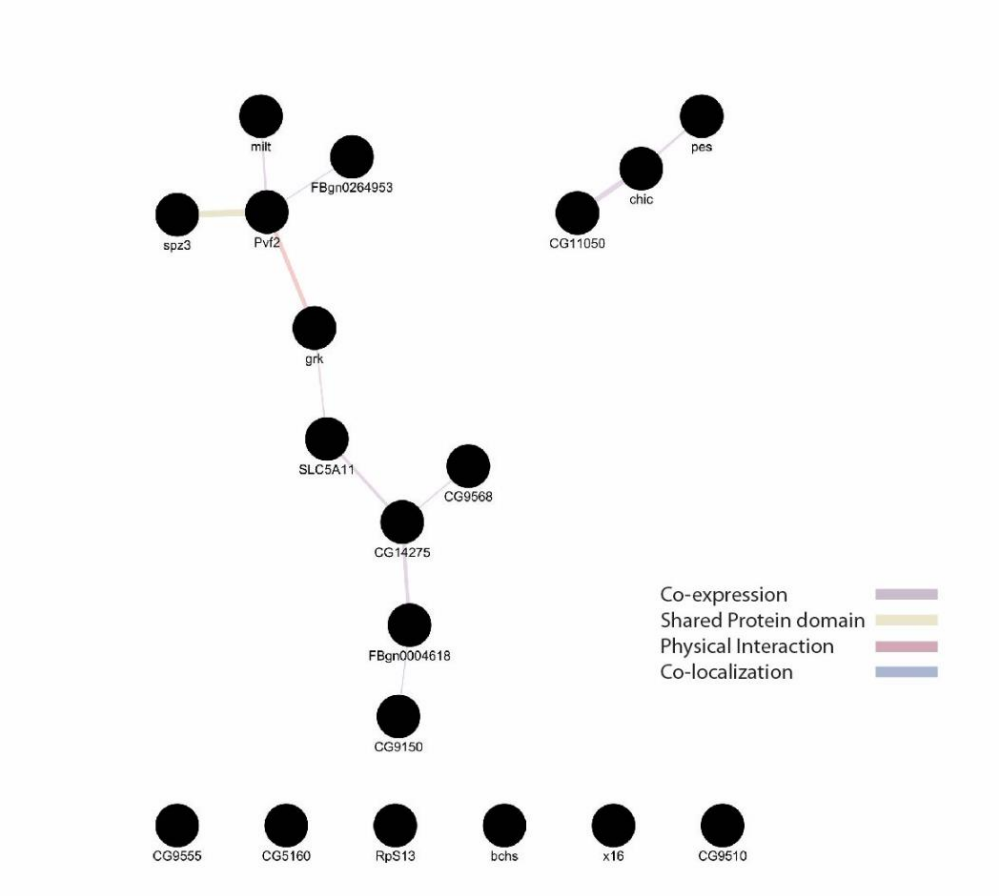

Figure 4.10. 1 of 10 constructed network with 19 randomly selected genes from the 49 genes that did not result in head or eye phenotypes in the RNAi screen.

Overall, this analysis suggests that the gene regulatory network composed of candidate genes shows consistently higher connectivity with more high-quality edges compared to all randomly selected networks.

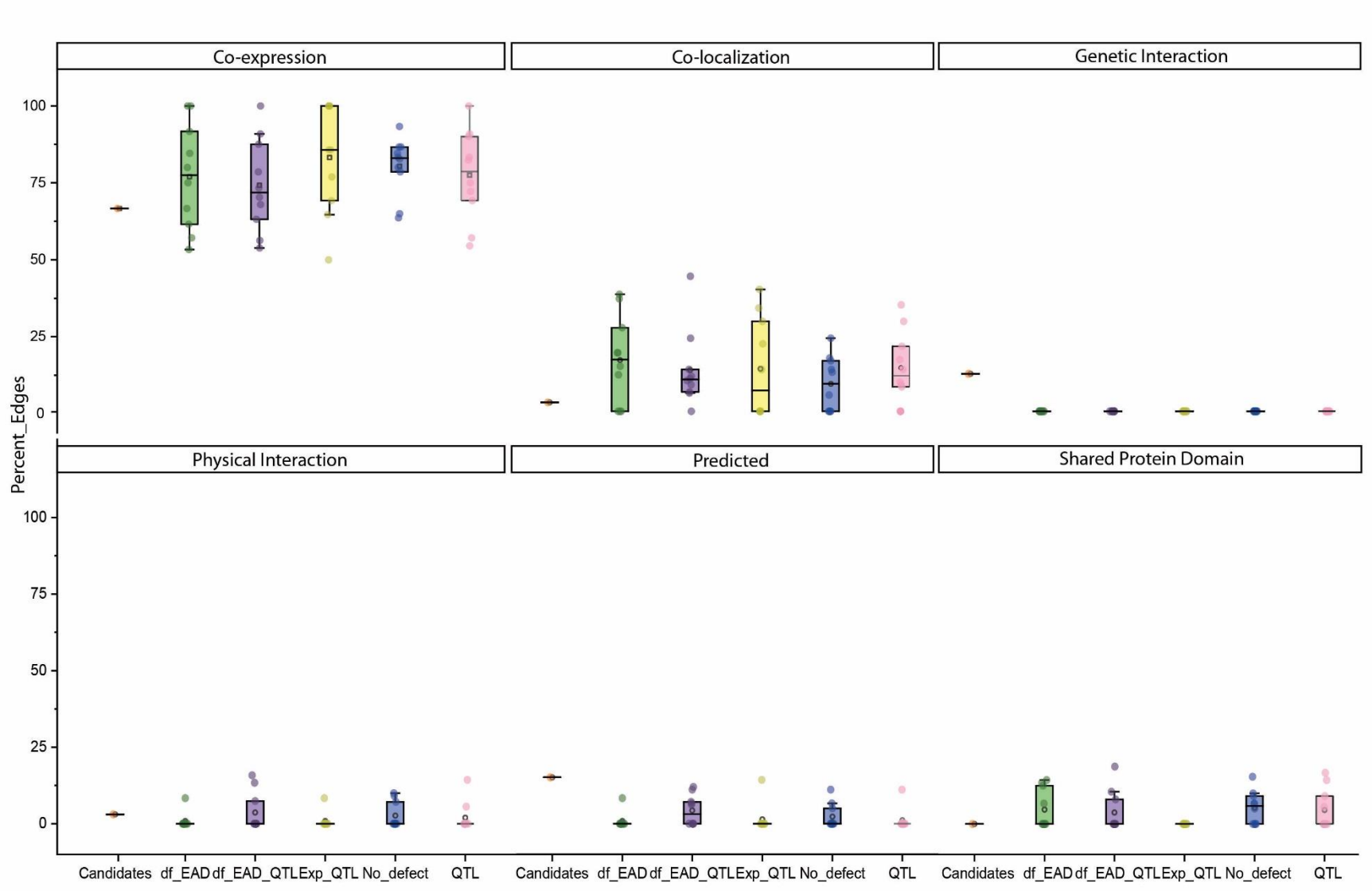

Figure 4.11. The percentage of edges grouped by data type, i.e. co-expression, co-localization, genetic interaction, physical interaction, predicted and shared protein domain. The network constructed by candidate genes has higher percentage of edges from genetic interaction and predicted.

4.5.2. Network extension and GO term analysis

Since the candidate genes seem to be functionally related, I next asked whether the addition more genes to this network allows predicting putative developmental processes in which the candidate genes may act. Therefore, I further added 20 additional genes to the network. Those genes were chosen because they increase the connectivity within the GRN (Figure 4.12, A). Adding these 20 genes resulted in a much higher connectivity (110 edges). Intriguingly, four of these 20 genes were significantly enriched for GO terms related to eye development, i.e. *unpaired* (*upd*) (Tsai and Sun, 2004), *spalt-related* (*salr*) (Barrio et al., 1999; Domingos et al., 2004; Organista and De Celis, 2013), *dachshund* (*dac*) (Tavsanli et al., 2004; Pappu et al., 2005) and *roughex* (*rux*) (Thomas et al., 1994) (Figure 4.12, B). After adding those 20 genes, the pervious unconnected gene *jim* connected to the network through an eye development gene, *upd*. The major biological processes of the additional 20 genes were related to antennal joint development, eye-antennal disc development, and animal organ morphogenesis (Figure 4.12, B), suggesting that genes relevant for eye-antennal disc development were added to the network.

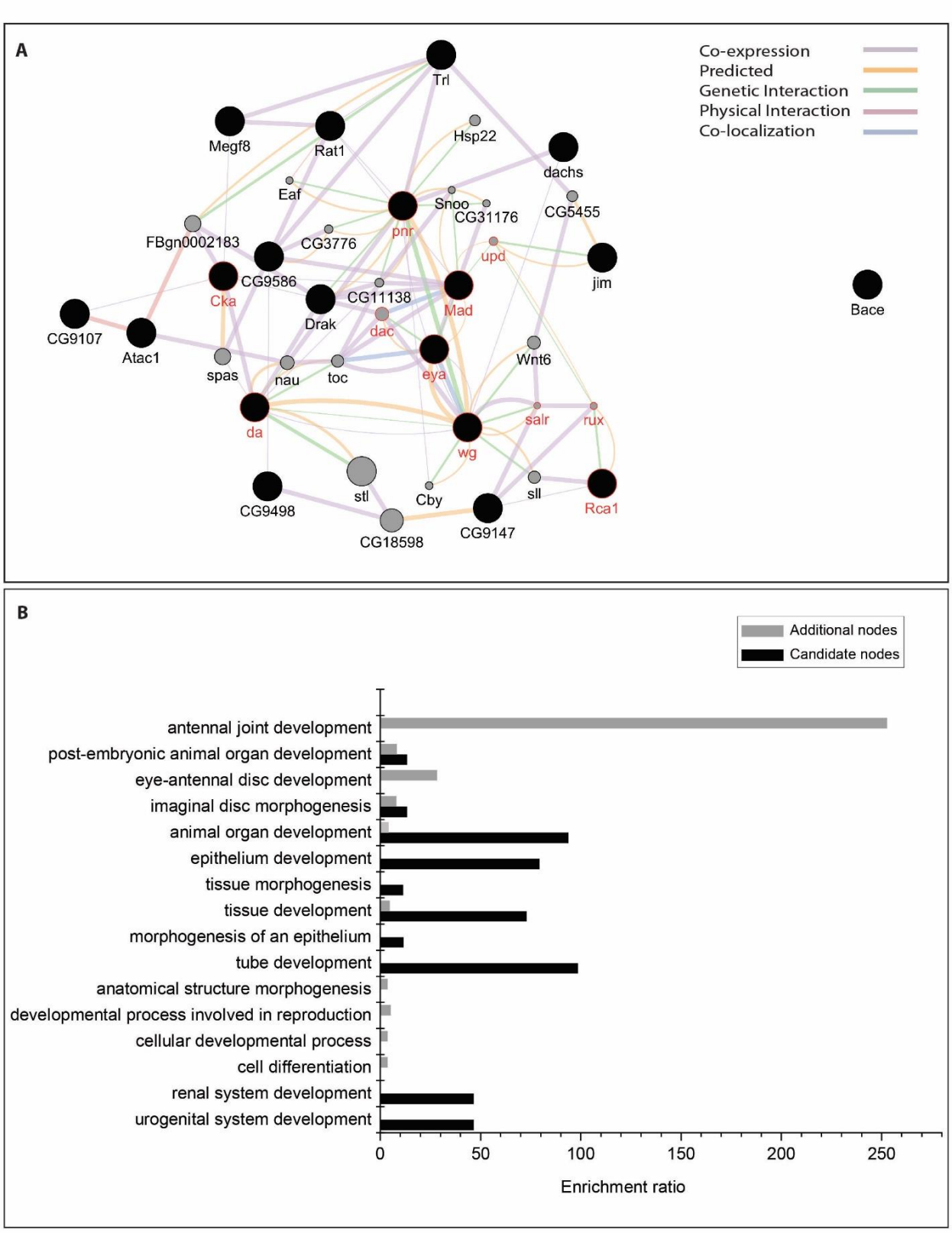

Figure 4.12. (A) The expanded network with additional 20 genes. The black nodes are the candidate genes, and the grey circles are the additional nodes which improve the connectivity. The sizes of grey circle differ with the difference computed

strength of each node, the larger size represent the higher strength for gene function prediction (For instance, Eaf has fewer number of interactions than CG18598) (Warde-Farley et al., 2010). The known eye genes are labelled in red. (**B**) The top 16 GO terms enriched among the genes in the network. The GO terms enriched among additional nodes are shown in grey bar; the GO terms enriched among the candidate genes are shown as black bars. X-axis, the enrichment ratio.

In order to understand whether the connectivity of a candidate gene is correlated to its biological function, I used the phenotypic score defined for adult RNAi phenotypes (Figure 4.4) and tested for a correlation with the unique number of edges for the respective gene (Figure 4.13). I found a trend towards a positive correlation between the phenotypic scores and the number of connections in the GRN (Figure 4.12), although it was not significant ($R^2 = 0.13$; $p = 0{,}24639$; blue line in Figure 4.13). If the four uncharacterized genes (CG-genes), which tend to be less well studied, were removed from the correlation analysis, a clear positive correlation was observed ($R^2 = 0.45$; $p = 0.017393$; Supplementary Figure 6).

Overall, the network analysis provides further support for a functional relationship of the identified candidate genes.

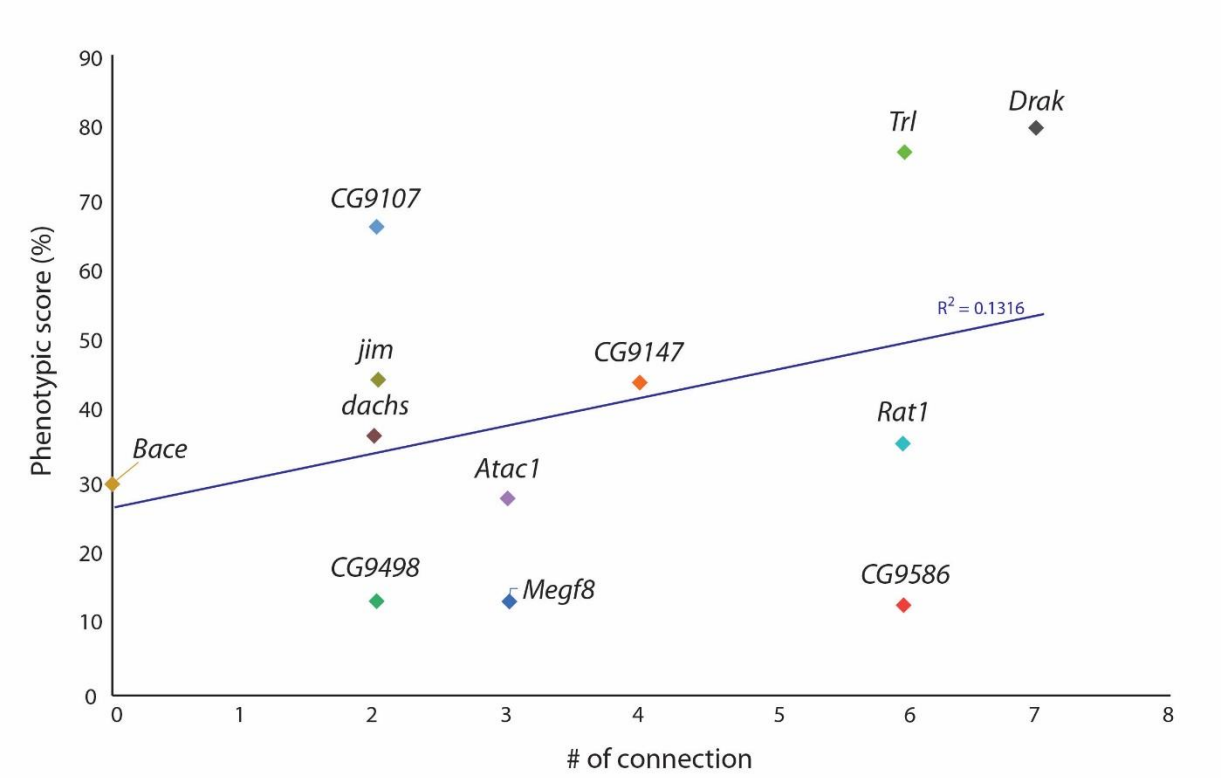

Figure 4.13. Positive, but non-significant (p = 0.24639) correlation between the phenotypic score (adult RNAi phenotype) and the number of connections within the GRN. The Y-axis represents the phenotype score (percentage) of the loss-of-function of each gene in Figure 4.3. The X-axis represents the number of connections of the respective genes based on Figure 4.8, A.

4.6. *jim* plays an important role in eye-antennal disc development

To gain more mechanistic insights into potential developmental processes regulated by the candidate genes, I focused on the candidate gene *jim* for the following reasons: **1)** In my screening pipeline, *jim* was a differentially expressed positional candidate gene involved in *pnr* regulation. **2)** Expression of *jim* was relatively high in the bulk-RNAseq data and RNAi resulted in intermediate to strong reduction of eye size. **3)** In the extended GRN, *jim* was connected to *unpaired*, a gene that has been implicated in the initiation of differentiation in the developing eye-antennal disc (Tsai and Sun, 2004). **4)** A genetic interaction of *jim* and *upd* have been shown (Mukherjee et al., 2006).

4.6.1 Refinement of interactions of *jim*

To further refine the GRN around *jim*, I employed previously published ATACseq data (Buchberger et al., 2021) to reveal candidate genes in the network that may be regulated by Jim and to find putative regulators of *jim* expression (Figure 4.14). First, I found putative Jim binding motifs in accessible regulatory regions of 9 of 19 candidate genes, suggesting that they are downstream targets of Jim (*Rca1*, *eya*, *Mad*, *Drak*, *cka*, *pnr*, *Megf8*, *Trl*, *dachs*; brown arrows in Figure 4.14). Second, in the open chromatin region in the *jim* locus, I found the binding motifs of other eye-related factors, such as Ey (Clements et al., 2009), Forkhead box, sub-group O (Foxo), Klumpfuss (Klu) (Rusconi et al., 2004), Glass (Gl) (Moses and Rubin, 1991; Ellis et al., 1993), atonal (Ato) (Jarman et al., 1994), and Medea (Med) (Das et al., 1998)(white nodes in Figure 4.14). In the *ey* locus I also found Jim motifs, suggesting a bidirectional regulation of both genes. Similar bidirectional relationships were also observed for *Trl* and *Mad*, with *jim*, respectively (yellow arrows in Figure 4.14). The refinement of regulatory interactions of *jim* resulted in many outgoing and incoming connections, confirming a putative central role in the novel network module that governs eye-antennal disc development.

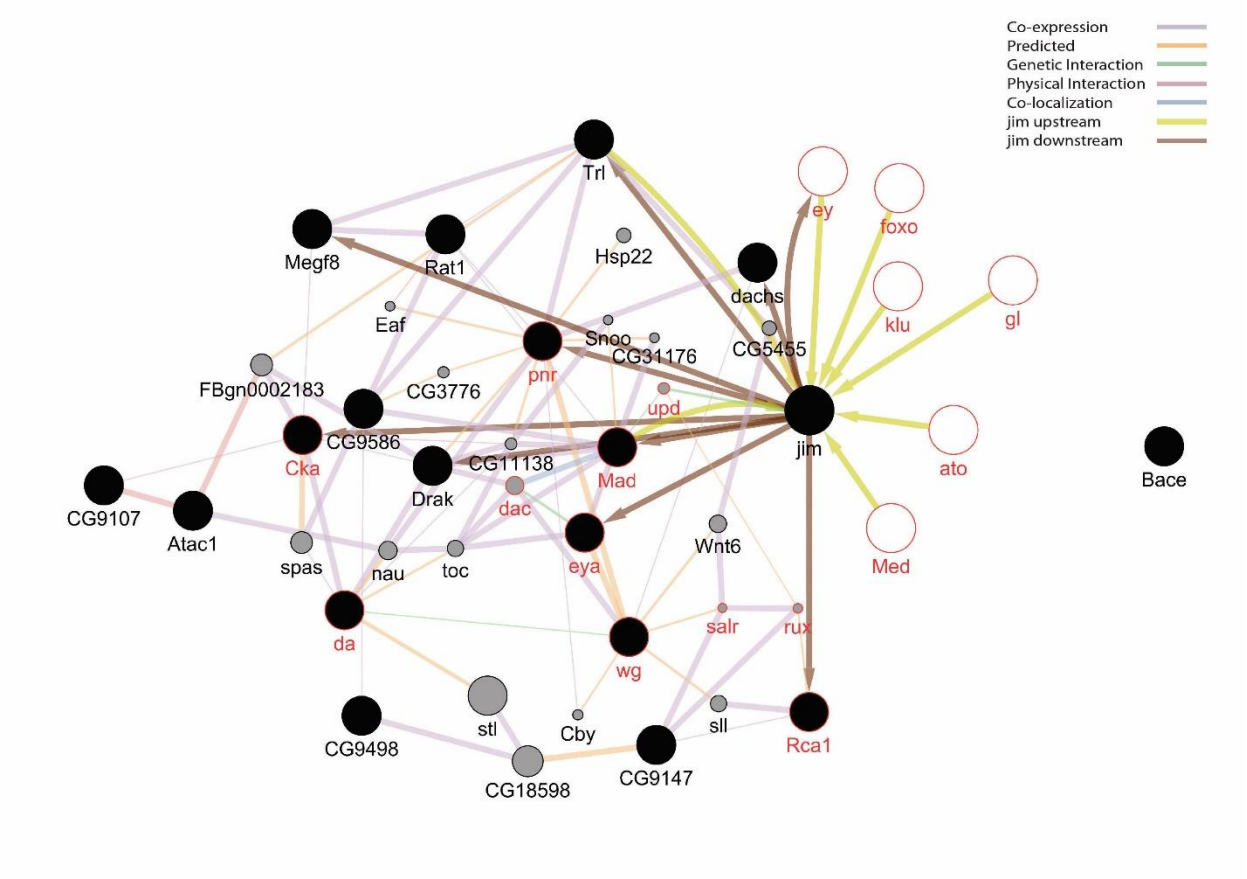

Figure 4.14. Refined regulatory interactions of *jim* after integration of ATACseq data. The black nodes are the candidate genes, and the grey circles are the additional 20 that were added to improve the connectivity. The white nodes represent putative regulators of *jim* expression that have been implicated in eye development. Known eye genes are labelled in red. Factors that may regulate *jim* expression are connected to *jim* with green arrows and genes putatively regulated by Jim are connected via brown arrows.

4.6.2 Expression pattern of *jim*

To further confirm the biological function of *jim* in the network, I performed several experiments to detect the spatial expression pattern of *jim*. Reporter gene expression driven by three *jim*-Gal4 lines (See Material and Methods Table 3.3) showed high expression in photoreceptor cells (Figure 4.15, A-A''). This pattern could be partially confirmed by Hybridization Chain Reaction (HCR) that additionally revealed weaker expression of *jim* in many cells of the disc, but with even weaker expression in the cells in the morphogenetic furrow (yellow arrowhead) and eye-antennal board (white asterisk, Figure 4.15,

C-C'"). Chromogenic *in-situ* hybridization also suggested a weak broad expression with an accumulation in the dorsal region of the eye-antennal disc, which is consistent with a previous study (Mukherjee et al., 2006) (red arrow in Figure 4.15, B). I also identified the *jim* cell lineage and real-time expression using the G-TRACE system (Evans et al., 2009). While real-time expression was detected in developing photoreceptors (Figure 4.15, E'), cells in almost the entire disc were positive for *jim* lineage with, again, an accumulation in the dorsal retinal region (red arrow in Figure 4.15, E). Note that the G-TRACE system was used to test *pnr* expression as positive control (Figure 4.15, D-D'"), because this data has been published before (Buchberger et al., 2021). The broad expression of *jim* with an increased expression in the dorsal region of the eye disc was also confirmed by the sn-RNAseq results (Figure 4.16).

Since Jim seems to regulate *pnr* expression (Figure 4.14), I investigated a potential co-expression between both genes. A clear co-expression pattern was not observed in late larval discs (about 120 h AEL) based on immunohistology, *in situ* hybridization methods and reporter assays (Figure 4.15, A and B). However, the sn-RNAseq data suggests that both genes are co-expressed in ventral PE cells at 84 h, 96 h and 108 h AEL, and in ocelli and dorsal PE cells at 96 h AEL, and also dorsal cells at 120 h AEL (red boxes in Figure 4.16). This co-expression in PE would be found in the cell lineages traced by G-TRACE (Figure 4.15 E and F).

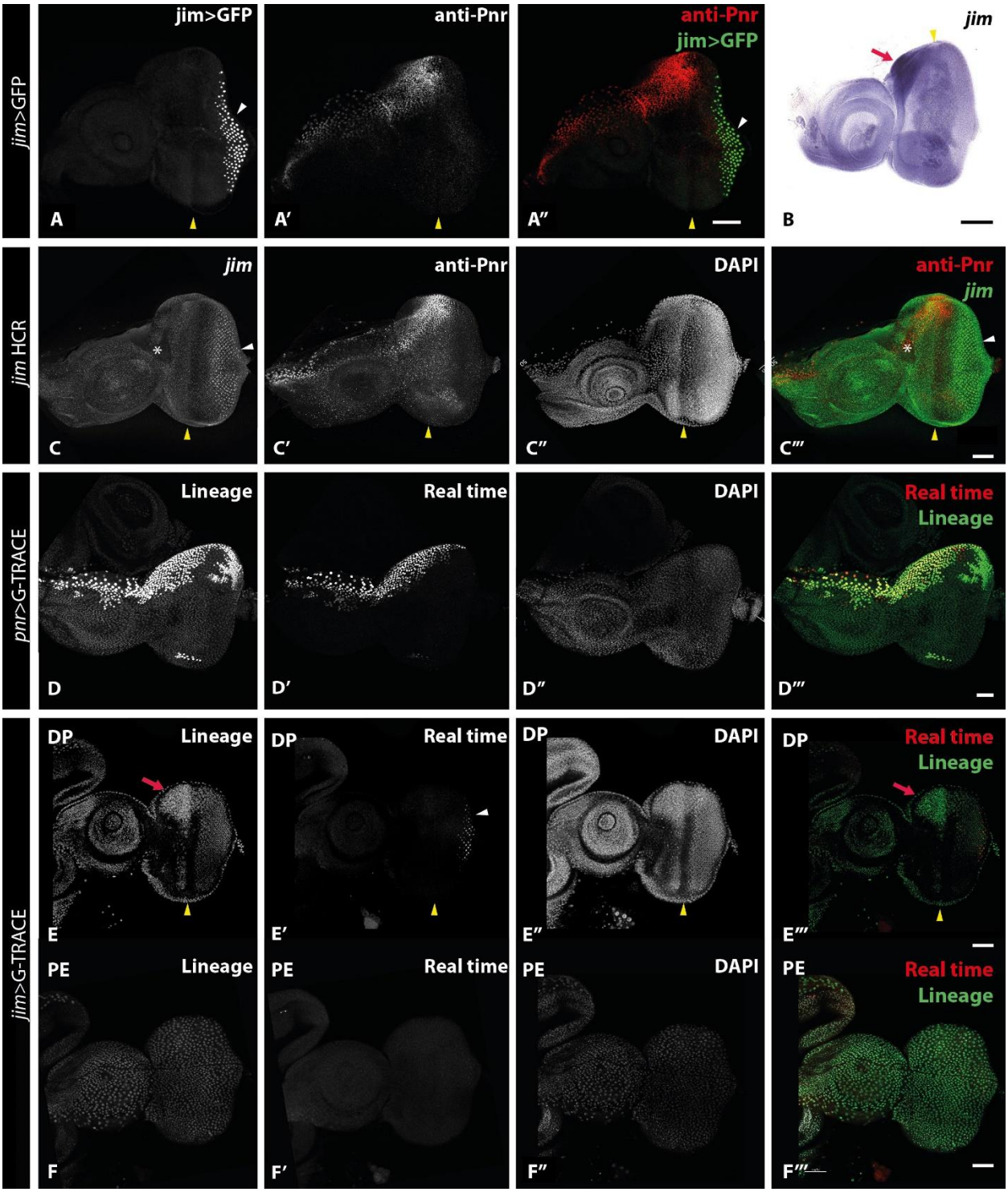

Figure 4.15. *jim* and *pnr* expression in the eye-antennal disc. (**A-A''**) The L3 eye-antennal disc with GFP expression driven by *jim*-Gal4 and stained with rabbit anti-Pnr antibody. (**B**) *jim* RNA expression pattern detected by classic *in-situ* hybridization. (**C-C'''**) *jim* expression is detected by HCR and stained with rabbit anti-Pnr antibody (in red). The asterisk indicates the eye-antennal boarder (**D**) G-TRACE with *pnr*-Gal4. (**E-E'''**) The *jim* lineage (in green) and the *jim* real-time expressed cells (in red) labelled by crossing with GRACE lines, which showed in Disc Proper (DP) The yellow arrow head indicates the MF

location. The red arrow indicates the dorsal accumulation of signal. The white arrow head indicate the expression in photoreceptor cells. **(F-F'')** The *jim* lineage (in green) and the *jim* real-time expressed cells (in red) labelled by crossing with GRACE lines, which showed in Peripodial epithelium (PE). Scale: 50 µm. In all Figures, anterior is to the left. The scale bar is 50 µm. In all figures, anterior is to the left.

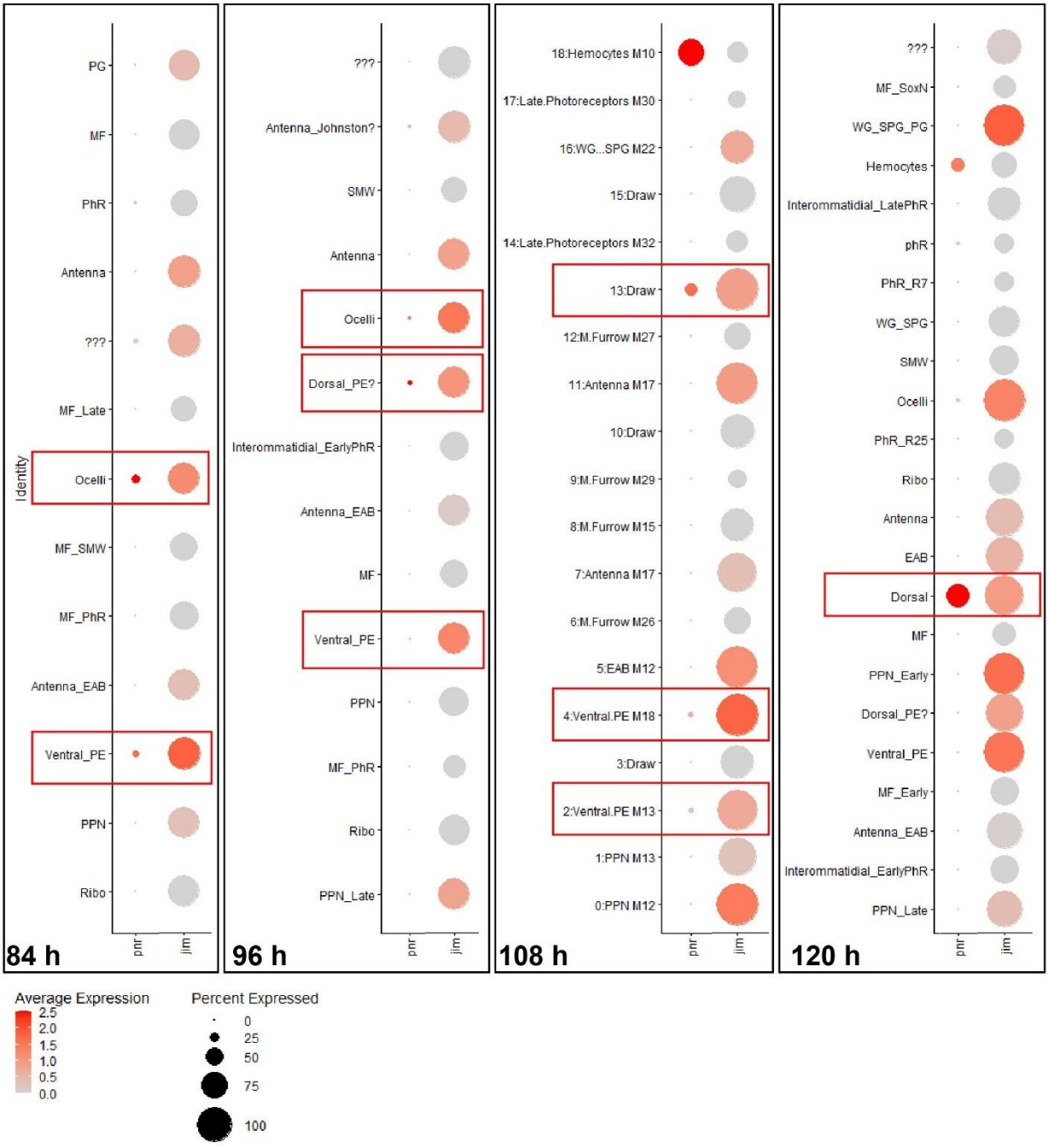

Figure 4.16. *jim* and *pnr* is co-expressed in the PE from sn-RNAseq data. *jim* is expressed in the whole eye-antennal discs from 84 h AEL to 120 h AEL with slightly increased expression in ocelli, PPN dorsal, and ventral PE. PE, Peripodial epithelium; PPN, Pre-proneural. Red boxes indicate the co-expression (Figures provided by Gordon Wiegleb, unpublished).

4.6.3 Genetic interaction between *pnr* and *jim*

Since the novel network module predicted a direct interaction of *jim* and *pnr*, I next performed RNAi experiments to functionally test the prediction. RNAi of *jim* driven by *pnr*-Gal4 resulted in the duplication of the antenna (Figure 4.17, A-A"). The loss-of-function of *pnr* using the same driver line also resulted in antennal duplication (Figure 4.17, B). Interestingly, the similar phenotype of antennal duplication also showed when I performed the loss-of-function of *pnr* in *jim* positive cells (Figure 4.17, C-C").

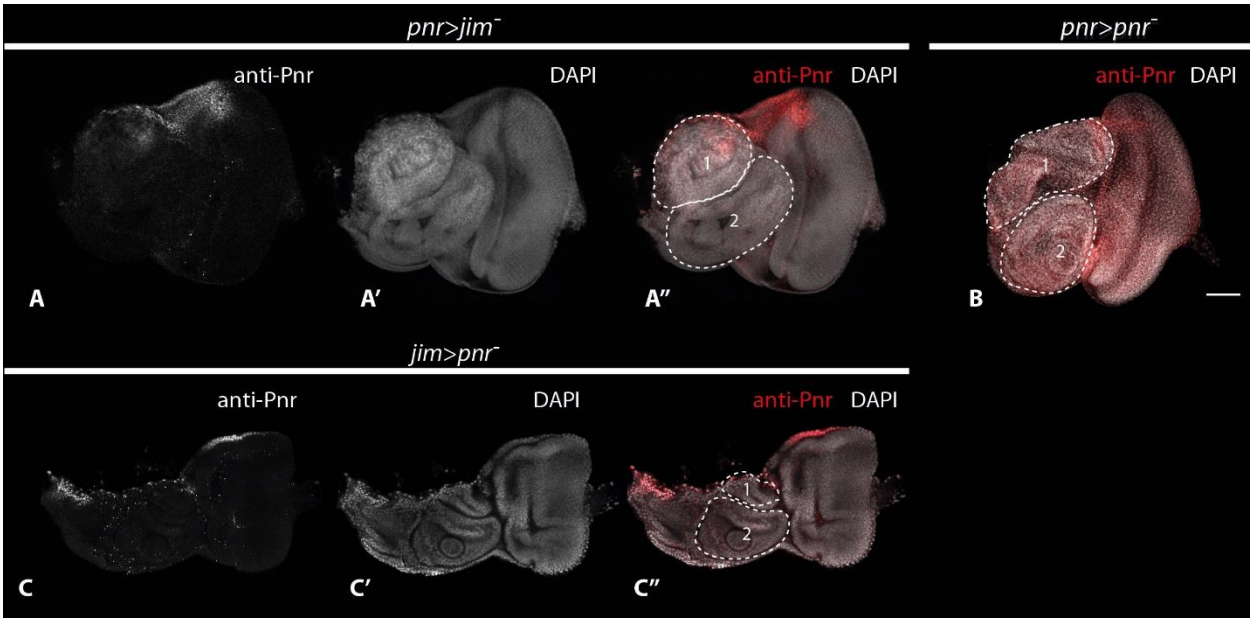

Figure 4.17. *jim* or *pnr* loss-of-function both result in duplication of antenna (1 &2). **(A-C)** Late LIII eye-antennal discs stained with rabbit anti-Pnr and DAPI. (**A-A"**) the loss-of-function of *jim* in *pnr* positive cells (**B**) the loss-of-function of *pnr* in *pnr* positive cells (Buchberger 2019) (**C-C"**) the loss-of-function of *pnr* in *jim* positive cells. Scale: 50 µm.

Next, I tested, whether RNAi of *pnr* in *jim* positive cells affected eye development. RNAi for *pnr* resulted in a slight reduction of the size of the dorsal retinal region in eye-antennal discs (Figure 4.18, A & D) when compared to the wildtype disc (Figure 4.18, B). Note that overexpression of *pnr* in *jim* positive cells resulted in the opposite effect, namely a slight overgrowth the dorsal retinal region (Figure 4.18, C &D).

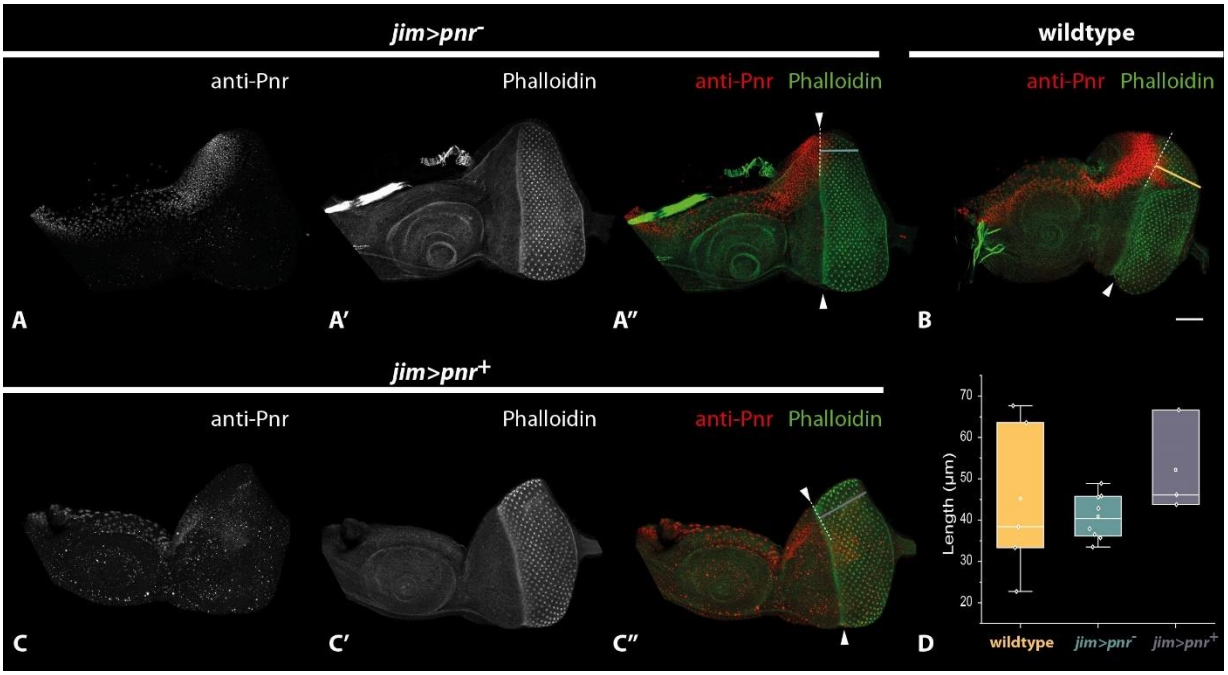

Figure 4.18. *pnr* loss-of-function and gain-of-function in *jim*-positive cells. **(A-C)** Late LIII eye-antennal disc stained with rabbit anti-Pnr antibody and Phalloidin. The arrowhead indicates the morphogenetic furrow. **(D)** The comparison of length of ommatidia region in the respective disc. Scale: 50 µm. In all figures, anterior is to the left.

Previous studies showed that *pnr* is predominantly expressed in the PE (Oros et al., 2010; Buchberger et al., 2021). The suggested interaction of *jim* and *pnr* implies that *jim* may elicit its function in the PE as well. Therefore, I performed *jim* RNAi specifically in the PE driven by the *c311*-Gal4 (BDRC #5937) line (Baker et al., 2018)(Figure 4.19, B and B'). This experiment resulted in the ectopic growth of huge proliferated cells (green arrow in figure 4.19, A'") and the reduced retinal region (green arrow in Figure 4.19), suggesting that the observed role of *jim* during eye development may be caused by its expression in the PE.

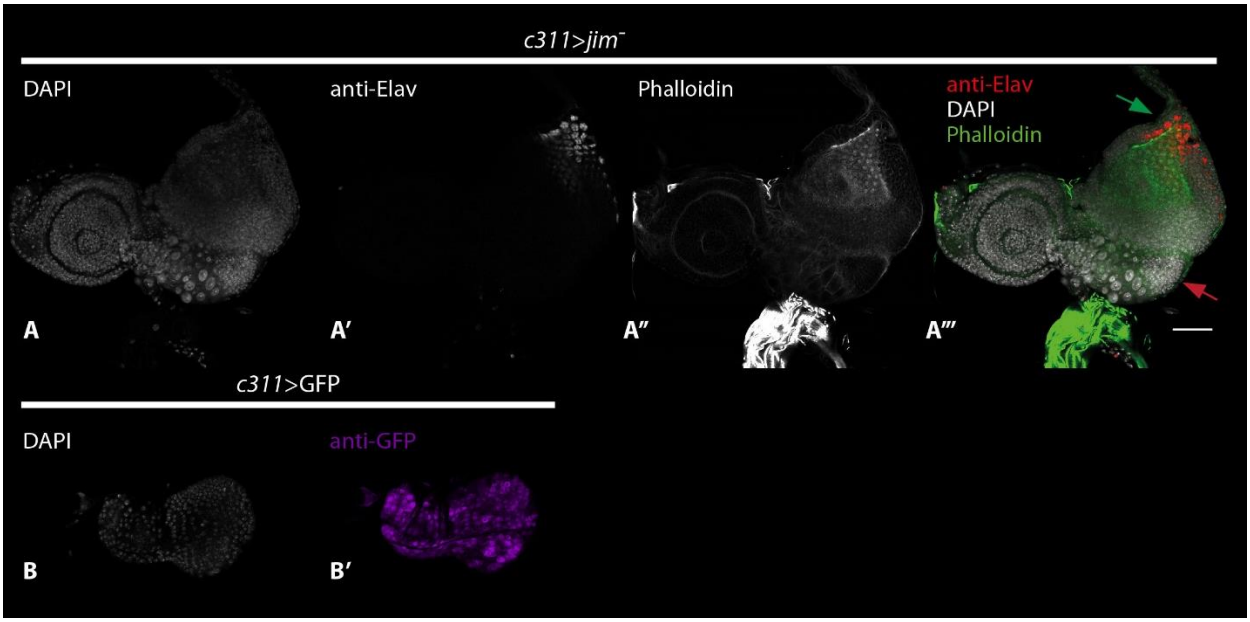

Figure 4.19. (A-A''') the larval eye-antennal disc of loss-of-function of *jim* in peripodial epithelium cells with extra tissue. The Phalloidin was shown in green and the red colour represents the expression of *elav* to label the photoreceptors. **(B-B')** The *c311*-Gal4 induced the UAS-GFP expressed (in purple) in PE. The scale bar is 50 µm. In all Figures, anterior is to the left.

In summary, these experiments suggest that *jim* is co-expressed with *pnr* in the PE. And its expression in the PE plays an important role in the developmental process of eye-antennal discs.

4.6.4 Genetic interaction between *upd* and *jim*

Previous genetic data suggests that *jim* interacts with *upd*, which is involved in the initiation of retinal differentiation (Tsai and Sun, 2004; Mukherjee et al., 2006; Tsai et al., 2007). My GRN approach also suggested an interaction of *jim* with *upd* mediated by *pnr*. To functionally test this regulatory interaction, I performed RNAi of *pnr* and *upd* in *jim* positive cells. Both experiments resulted in the enlargement of adult eyes (Figure 4.20, B &C). A similar enlargement of eyes was also observed for loss-of-function of *upd* in *pnr* positive cells (Figure 4.20, D).

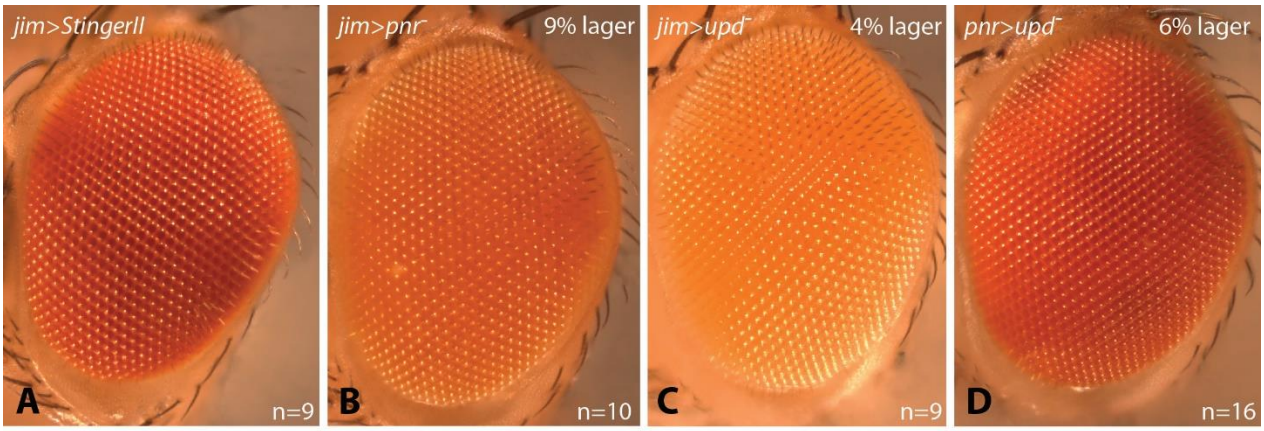

Figure 4.20. the adult eyes of loss-of-function of *pnr* and *upd* both results in the enlargement of eyes **(A)** adult eye of StingerII expressed **(B)** loss-of-function of *pnr* **(C)** loss-of-function of *upd* in *jim* positive cells (*jim*-Gal4, BDSC #62478) **(D)** loss-of-function of *upd* in *pnr* positive cells (*pnr*-Gal4, VDRC #42374). In all Figures, anterior is to the left.

I also analysed eye-antennal discs of *pnr* driven *upd* RNAi to better understand the adult eye enlargement. The discs showed a stripe in the MF and defects in the arrangement of the MF (Figure 4.21). As predicted in the novel module, *pnr* is upstream regulating *upd* in the developing eye-antennal discs. And the result of abnormal discs indicates for the co-expression of *pnr* and *upd* at same stage, which suggests the potential interaction between Pnr and Upd.

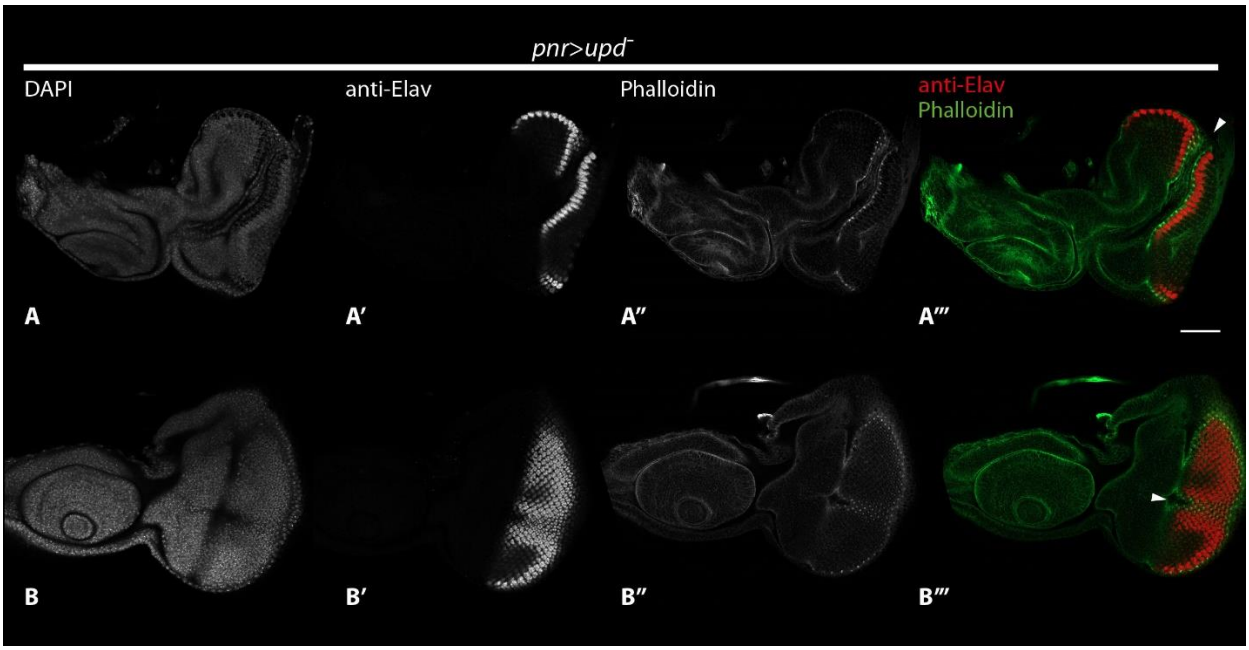

Figure 4.21. the larval eye-antennal disc of loss-of-function of *upd* in *pnr* positive cells with abnormal phenotype. The Phalloidin was shown in green and the red colour represents the expression of *elav* to label the photoreceptors. The scale bar is 50 µm. In all Figures, anterior is to the left.

In summary, my results might indicate co-expression of *jim*, *pnr* and *upd*. And also, the results suggest that they are involved in eye development. However, the genetic mechanism of these genes in the novel network module requires further investigation.

5. Discussion

The novel network module based on integration of several unbiased genome wide datasets in this study provided new insights into the genetic architecture underlying eye and head development and variation of these organs in *Drosophila*. Here I discuss the biological processes those genes are involved in by combining information from previous studies with novel potential interactions within the developmental GRN inferred from my data. Additionally, I discuss the implications of my findings on *jim* expression and function to conclude that this gene is a novel and variable factor in the GRN underlying eye-antennal disc development.

5.1 Novel candidate genes that could underlie natural variation in eye size and head shape between *D. melanogaster* and *D. mauritiana*

Among the 19 candidate genes obtained through my integrative data analysis pipeline, 12 genes had not been implicated in eye-antennal disc development. The observation that they exhibit RNAi phenotypes, however, suggests an involvement in this process. Among those candidate genes, the differentially expressed genes between two species are excellent candidate genes. In the following I will discuss putative novel functions of those genes during eye-antennal disc development.

5.1.1 *CG9107*

In the bulk-RNAseq result, *CG9107* is highly expressed (>50 RPKM) in the developing eye-antennal disc (Figure 4.7) and the loss-of-function of CG9107 resulted in very severe phenotype from reduction of the eye field to missing eyes, which was observed in adults and larval eye-antennal discs (Figure 4.4 & 4.6). The predicted molecular function of CG9107 includes ribosomal RNA- and general nucleotide-binding activity (Larkin et al., 2021). This putative function in conjunction with my experimental observations suggest that CG9107 may play a general role during cellular function in the eye-antennal disc.

Interestingly, the closest human ortholog Ribosomal RNA-processing protein 7A (Rrp7A) plays a role in neurogenesis and proliferation in the developing human brain (Farooq et al., 2020). Moreover, the knockout of the zebrafish ortholog of *Rrp7A* leads to the reduction of the eye, which can be rescued by injection of *Rrp7A* mRNA (Farooq et al., 2020). Therefore, a reduction in retinal tissue upon loss-of-function seems to be conserved feature of CG9107/Rrp7A in vertebrates and flies.

5.1.2 *Ada2a-containing complex component 1 (Atac1)*

In the RNAi knockdown, *atac1* led to the partial reduction of adult eyes, while it also resulted in ectopic growth in the eye-antennal discs (Figure 4.4 and Figure 4.6). These results indicate that the ATAC complex with Atac1 is associated with the developing eye-antennal disc. *atac1* codes for a SANT domain protein in the histone acetyltransferase (HAT) complex (Guelman et al., 2006; Suganuma et al., 2008). The well-known ability of the ATAC complex is to modulate gene transcription (Suganuma et al., 2008). Unlike Atac2, another component of this complex, the detailed regulatory mechanism of Atac1 has not been dissected yet. The ATAC complex has a known function in histone modification (Sheikh and Akhtar, 2019). The histone modification is confirmed its essential role in the developing eye of mouse (Rao et al., 2010) and Xenopus (Xu et al., 2012), and in the eye degeneration of cavefish (*Astyanax mexicanus*, (Gore et al., 2018)). Besides, in *Drosophila*, the histone modification function of CREB-binding protein (CBP) is required to activate *wingless* (*wg*) (Ludlam et al., 2002). Therefore, Atac1 is very likely involved in the developing eye through modulating gene transcription, although it requires detailed experiments to further reveal the mechanism behind this interaction.

5.1.3 *Connector of kinase to AP-1 (Cka)*

In the sn-RNAseq data, *cka* was broadly expressed the eye-antennal disc (Figure 4.8, A) and previous work showed that it plays a role in PE development (Neal et al., 2020). *cka* codes for an essential

component in the STRIPAK-PP2A complexes and the loss of *Cka* function leads to the absence of the peripodial epithelium (PE) and the switch of fate from the PE to the disc proper (DP) (Neal et al., 2020)(Figure 5.1). The mechanism is suggested that Cka as part of the STRIPAK-PP2A complex inactivates the Hippo (Hpo) kinase to promote the PE fate in the eye-antennal disc (Neal et al., 2020). Moreover, Cka and other STRIPAK-PP2A complexes also regulate c-Jun-amino-terminal-(NH2)-Kinase (JNK) signalling in the embryonic epidermis (Chen et al., 2002), in the innate immune system (Liu et al., 2016), and in the gonad (La Marca et al., 2019). And, JNK signalling has also been studied that mediate the cell death during the development of the eye (Tare et al., 2016), and induce glia overmigration (Tavares et al., 2017). Therefore, all those findings suggest that Cka is associated with eye/head development either through Hpo pathway (Neal et al., 2020) (Figure 5.1) or JNK signalling. But, the mechanism is required further experiments.

5.1.4 *Dachs*

In our study, the loss-of-*dachs* resulted in the reduction of the eye field in the adult and also in larval eye-antennal discs (Figure 4.4 and 4.6). *dachs* encodes as a myosin superfamily protein that also regulates the orientation of cell divisions in the wing imaginal discs (Mao et al., 2011; Rodrigues-Campos and Thompson, 2014) and the cell orientation of the ommatidia (Cho et al., 2006; Mao et al., 2006). Dachs is also suggested to interact with the Hpo pathway (Cho and Irvine, 2004; Degoutin et al., 2013). And, it is confirmed that it is involved in the regulation of Wts (Cho et al., 2006). Thus, it is suggested that it also plays its role in the determination of the PE fate (Figure 5.1).

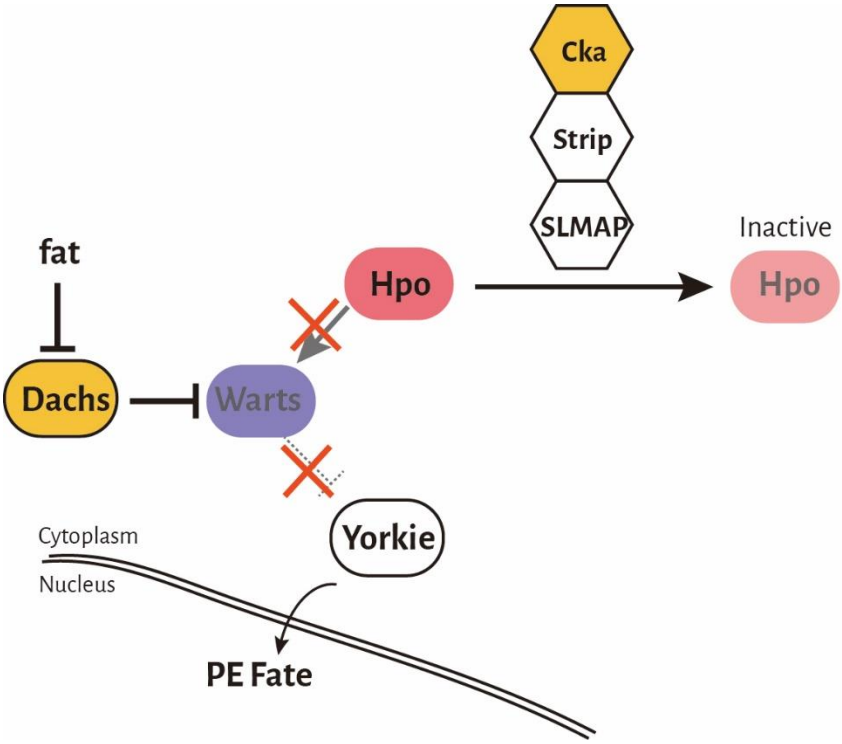

Figure 5.1 Cka and Dachs are involved in Hpo pathway and further affect the PE fate. The Cka/Strip/SLMAP complex will inactivate Hippo (Hpo). With inactived Hpo (red cross), Warts (Wts) will be repressed by Dachs and cannot repress Yorkie (Yki) (red cross). Therefore, Yki will be released into nucleus (black arrow) and suppress retinogenesis of cells and maintain its PE fate; if the Hpo is not inactivated, it will active Wts and further repress Yki and induce the retinogenesis of cells (Figure is modified from Cho et al., 2006; Neal et al., 2020).

5.1.5 *Death-associated protein kinase related (Drak)*

The loss-of-function of Drak led to severe eye reduction, from smaller to missing eyes, and duplication of antenna both in the adult and larval eye-antennal discs (Figure 4.4 and 4.6) and *Drak* was broadly expressed in our sn-RNAseq results (Figure 4.8, B). Drak belongs to the Death-associated protein kinase (DAPK) family and is widely expressed during development in several epithelial tissues (Neubueser and Hipfner, 2010). Drak is involved in shaping epithelium tissue of the wing, leg and haltere imaginal discs (Neubueser and Hipfner, 2010) and loss of Drak function in the developing eye results in abolished ommatida shape and cell sorting, which supports that Drak is involved in the ommatidia morphogenesis during multicellular patterning (Robertson et al., 2012; Chougule et al.,

2016). Drak is also associated with actomyosin dynamics through phosphorylating Myosin Regulatory Light Chain (MRLC, i.e. Spaghetti squash (Sqh)), which is important for the constriction of apical cell profiles (Robertson et al., 2012; Pichaud, 2014; Chougule et al., 2016) (Figure 5.2). Since the constriction of apical cells is a crucial process underlying the morphogenetic furrow (MF) progression and thus retinal differentiation (Schlichting and Dahmann, 2008; Fernandes et al., 2014), this might explain the severe eye phenotype in the absence of photoreceptor cells with loss of Drak function.

5.1.6 *Multiple Epidermal Growth Factor-like Domains 8* (*Megf8*)

The consequences of loss-of-function of Megf8 showed generally subtle defects in the adult eye (Figure 4.4, J) and *Megf8* was only detected in very few cells of the eye-antennal disc and at low expression level (Figure 4.7). The vertebrate ortholog of *Megf8* is broadly expressed based on ISH and it is involved in left-right axis patterning (Engelhard et al., 2013). Previous studies in *Drosophila Megf8* unravelled a potential function in larval mesoderm development (Murray et al., 2012; Lloyd et al., 2018), while there is still little prior knowledge to support the biological function of Megf8 in developing eyes. Interestingly, vertebrate Megf8 is suggested as a modifier of Bone Morphogenetic Protein (BMP) 4 signalling (Engelhard et al., 2013) and this pathway drives the specification of retinal progenitors in vertebrates (Bielen and Houart, 2012; Wong et al., 2015). In mouse, BMP4 is expressed and plays essential role in the developing eye (Furuta and Hogan, 1998). Since Decapentaplegic (Dpp) signalling, as a BMP signalling member, is involved in eye and head formation (Wiersdorff et al., 1996) and it regulates mesoderm development (Staehling-Hampton et al., 1994) in *D. melanogaster*, the observed eye size effects after RNAi of *Rat1* may be linked to Dpp/Mad signalling in the eye-antennal disc.

5.1.7 *Rat1 5'-3' exoribonuclease* (*Rat1*)

In our results, *Rat1* is expressed in relatively specific cells especially in the MF (Supplementary Figure 4). The loss-of-function of Rat1 led to a large range of phenotypes from subtle defects to severe reduction of the eye field and some individuals even had ectopic growth of head tissue and eyes (Figure 4.4 and 4.6). *Rat1* encodes as exoribonuclease that is required for mRNA processing, such as splicing (Chen et al., 2016; Dhoondia et al., 2021). The lack of Rat1 activity could lead to problems during splicing, affecting various genes involved in eye development. Previous results strongly suggest that faulty splicing can have serious effects on eye development. For instance, mutations of a component of the spliceosome, Pre-mRNA processing factor 8 (Prp8) that alters the function of apoptotic genes in eye-antennal discs leading to defects in adult eyes (Stanković et al., 2020). However, there is no further information about potential functions of Rat1 in the developing eye in *Drosophila*.

5.1.8 *CG9586*

Although *CG9586* is very highly expressed (Figure 4.7), the loss-of-function only resulted in very subtle adult eye phenotypes (Figure 4.4). The closest human ortholog is the gene *coiled-coil domain containing 43* (*CCDC43*), which is associated with proliferation in cancer tissue (Wang et al., 2018). In *Drosophila*, there is not much information about the biological function of CG9586. However, a high-resolution protein interaction map showed protein-protein interaction of CG9586 with p38 kinase (Belozerov et al., 2012). P38 kinase plays a role in stress response (Craig et al., 2004; Vrailas-Mortimer et al., 2011), cell growth regulation (Cully et al., 2010), and pathogenic defence (Chen et al., 2010), and different p38 pathways were used in lung, liver, and immune system (Cuadrado and Nebreda, 2010). p38 kinases belong to the mitogen-activated protein kinases (MAPK) family, which are well-investigated to in the

process of the MF initiation (Fernandes et al., 2015). Hence, it may be worth testing, whether observed phenotypes obtained after *CG9586* RNAi could be linked to problems during the MF initiation.

5.1.9 *CG9498*

CG9586 is co-expressed with another uncharacterized candidate gene, *CG9498*. In our RNAseq and sn-RNAseq results, *CG9498* showed low expression levels very specifically in wrapping glia-subperineurial glia (WG-SPG) cell clusters (Figure 4.5 and 4.6, C). Subperineurial glia cells have been shown to influence retinal glia cell migration and differentiation (Silies et al., 2007), but a mechanistic link to the observed strong eye size reduction remains to be established. Additionally, *CG9498* was identified as a down-regulated gene in response to fasting via RNA sequencing (Wang et al., 2021) and it is associated with detoxification (Scanlan et al., 2020). This suggests that CG9498 might lead to the pleiotropic effects in the developing eye/head in *Drosophila*, which needs to be validated.

5.1.10 *CG9147*

From the sn-RNAseq result, *CG9147* is expressed ubiquitously in the eye-antennal disc. The loss-of-function of CG9147 led to a range of adult eye phenotypes (Figure 4.4) that was recapitulated by reduction of the eye field in larval eye-antennal discs (Figure 4.6). *CG9147* is predicted to code for a protein with acyltransferase activity (Larkin et al., 2021). In the vertebrate retina, an enzyme with acyltransferase activity, lecithin:retinol acyltransferase, plays an important role in retinoid production (Kiser et al., 2012). However, there is lacking relationship between CG9147 and eye/head development in *Drosophila*.

5.1.11 *beta-site APP-cleaving enzyme* (*bace*)

RNAi for *Bace* resulted in smaller adult eyes (Figure 4.4). Despite abnormal eye-antennal discs, the larval phenotype was not as extreme as the adult phenotype (Figure 4.6). The expression of *Bace* was

weak and ubiquitous in the developing disc (Figure 4.8). This ubiquitous expression was also shown for the human ortholog of Bace in the human brain and pancreas (Mowrer and Wolfe, 2008). Accordingly, I could not detect Bace via immunohistochemistry (data not shown). Bace is an amyloid precursor protein (APP)-cleaving aspartic protease that cleaves transmembrane proteins. It was shown to have a function in glial cell survival in *D. melanogaster*, especially in the subretinal layer (Bolkan et al., 2012). It was implicated that the knockdown of *Bace* in *D. melanogaster* leads to uncleaved APP and might result in apoptosis of glial cells (Greeve et al., 2004). In the wild-type flies, more than 300 glial cells can be found in the late third instar eye-antennal disc (Silies et al., 2007). Therefore, the absence of *Bace* could potentially affect the migration of glial cells in the disc and this in turn could indirectly affect photoreceptor cell development.

5.1.12 *Trithorax-like (Trl)*

Trithorax-like (*Trl*) is relatively highly expressed in the eye-antennal disc throughout larval development according to bulk-RNAseq data (Figure 4.8). However, smiFISH did not result in a strong signal, and I observed a specific signal in photoreceptors (Supplementary Figure 4, B). *Trl* encodes for a GAGA transcription factor that plays an important role in the chromatin modification (Bhat et al., 1996). Trl could have a direct effect on eye development or it may act as a regulator, since it is a transcription factor and interacts also with other genes, such as Ultrabithorax (Ubx) (Bischof et al., 2018). But, it still leaves the question on its true involvement in the eye development open.

Overall, among the 19 identified candidate genes, 12 genes with unknown functions were identified here. Intriguingly, many of these genes may be linked to interesting cellular and molecular processes that may provide excellent targets for further investigations.

5.2 Regulatory interactions of candidate genes suggest key developmental processes involved in eye size variation

5.2.1 General structure of the novel network module

I reconstructed a network module composed of the 19 candidate genes, 20 additional genes which significantly improved the connectivity of the network and putative regulators of *jim* expression. This network module contains a number of core genes, such as *Mad*, *dac*, *eya*, *ey*, *pnr* (note that *pnr* has been defined as core gene (=hub gene) in Buchberger et al., 2021). Interestingly, many core genes have been shown to function as "eye master control genes" (Braid and Verheyen, 2008; Zhu et al., 2017). This link between connectivity in the network and importance for the trait is nicely recapitulated by my observed positive correlation between number of connections and the phenotypic score (Figure 4.13). The observation that Jim, Trl, Drak and Rat1 were also highly connected core genes and showed severe eye phenotypes upon RNAi, suggests that they are central parts of the GRN underlying eye-antennal disc development. Moreover, the "downstream genes" of those master genes acts as internal nodes, e.g. *da*, *Cka*, *wg*, and *upd* (Bonini, 1997; Shen and Mardon, 1997; Neal et al., 2020), which connects some other candidate genes into the new network module (Figure 4.14).

While some genes are very well-connected, a few candidate genes are only loosely connected within the network. For instance, *CG9498* and *Dachs* have weakly connected in the GRN that fits to their strength of phenotype (Figure 4.13). Moreover, the candidate gene *Bace* is not connected to the network at all (Figure 4.14). This could be due to its previously established roles in neuronal and glia cell development (Greeve et al., 2004; Mowrer and Wolfe, 2008; Bolkan et al., 2012), which is very likely unrelated to eye-antennal disc development. However, the mechanism underlying the observed reduction in eye size after *Bace* RNAi remains to be established. A potential function could be as a

neuronal gene in the differentiation of photoreceptor cells. Its potential biological function in eye/head development is discussed in chapter 5.1.11.

5.2.2 Regulatory loops are found in the GRN

The identified network module contains a number of feed-forward-loops (FFLs) (Figure 4.14), which were only rarely observed in the random networks (Figure 4.9). In Milo et al, 2002, the FFLs also occur more frequently in most of the biological networks than in the randomized networks (Milo et al., 2002). According to the previous studies, the FFLs are the most dominant connections in stable biological networks (Milo et al., 2002; Mangan and Alon, 2003; Mora-Martinez, 2021). Interestingly, in the early third instar larvae, the eye master genes (*Pax-six-eya-dac*, *PSED*) regulate each other in a linear pathway and thereby initiate the MF. In contrast, these *PSED* genes integrate a complex regulatory loop and regulate the MF progression in later stages (Figure 2.4 in chapter 2.5.1) (Desplan, 1997; Baker et al., 2018; Sánchez-Aragón et al., 2019). Similar FFLs are also shown for Glass (Gl) and its targetomes (Potier et al., 2014) and several FFLs connect the newly added gene *jim* to other genes (Figure 4.14). Interestingly, many FFLs within a network suggest that loss-of-function of genes connected by them might lead to the similar phenotypes. This is indeed what I observed for many of the candidate genes in my GRN. In summary, FFLs seem to be an important network feature in the GRN underlying eye-antennal disc development.

5.2.3 Functional implications of established connections

For some genes in the novel network module, we have a very good understanding of the developmental processes they regulate and how they are integrated with other genes involved in eye-antennal disc development. For instance, the core genes, *dac*, *eya*, *ey*, are highly connected to each other and also to other candidate genes in the novel network module and they are associated in the

same regulatory loop to initiate the MF (see chapter 5.2.2). For those candidate genes that have not yet been implicated in eye-antennal disc development, a potential function can be inferred by assessing their molecular function e.g. through predicted protein domains and by transferring knowledge obtained from other tissues in the fly or from orthologous genes in other organisms (see chapter 5.1). However, if we assume that connections within a GRN imply functional relationships (i.e. "guilty-by-association", (Oliver, 2000)) we may be able to predict an involvement in biological processes from known functions of connected genes. And also, those genes that share similar GO terms and biological relationships are very likely be associated to the same biological function (Tian et al., 2008).

For instance, the mutation of human orthologous of *CG9107*, *Rrp7A*, resulted in the down regulation of *Pax6* (Farooq et al., 2020). However, *CG9107* does not directly interact with *Pax6* orthologous (*ey*) in my network module, where the association between *CG9107* and *Pax6* orthologous is mediated through many intermediate steps (Figure 4.14). The regulatory hierarchy remains unclear. The network predicts the co-expression interaction of CG9107 with Cka, which is involved in the PE (Neal et al., 2020) where Ey also plays a major role (Baker et al., 2018). And, among the candidate genes, Dachs and Cka are both found involved in subnetwork (i.e. Hpo) in regulating the PE or the DP fate (see Chapter 5.1, Figure 5.1). Therefore, CG9107 may be relevant to mediate eye development though the PE fate determination.

In the network, *cka* is also connected with other candidate genes such as *da*, *Drak*, *Megf8* (Figure 4.14). Among them, *da* encodes as a basic Helix-Loop-Helix (bHLH) protein and is shown as eye gene in previous studies (Brown et al., 1996; Lim et al., 2008; Melicharek et al., 2008). *da* regulates the progression of MF through affecting the initiation of G_1 (Brown et al., 1996). In our novel network module, the interaction between *da* and *cka* are co-expression in the eye-antennal discs (Figure 4.8).

And interestingly, two genes, i.e., *CG9147* and *Rca1*, were not connected with the core network before adding the additional nodes, *roughex* (*rux*) and *spalt-related* (*salr*) (Figure 4.8 and 4.12). *rux* has a confirmed function in regulating cell cycle progression in the developing eye (Thomas et al., 1994); and *salr* is involved in cell proliferation regulation in wings (Organista and De Celis, 2013). Besides, Rca1 is well-studied as being involved in cell cycle progression via regulation of Cyclin A in the MF (Dong et al., 1997)(Figure 5.2). Taken together, all these findings indicate the potential function of CG9147 in the subnetwork of regulating the cell proliferation (Figure 5.2).

Overall, the results show that the candidate genes are part of a well-connected network module. For instance, *jim*, is found newly in the GRN. But, it has high connection between other candidate genes that indicates its essential role with other genes in well-studied subnetwork (Figure 5.2).

In general, some genes and connections are already well established; at the same time, the new genes and connections are added upon. Therefore, the unbiased screen in combination with regulatory interactions allows identifying key developmental processes that may evolve to result in eye size variation.

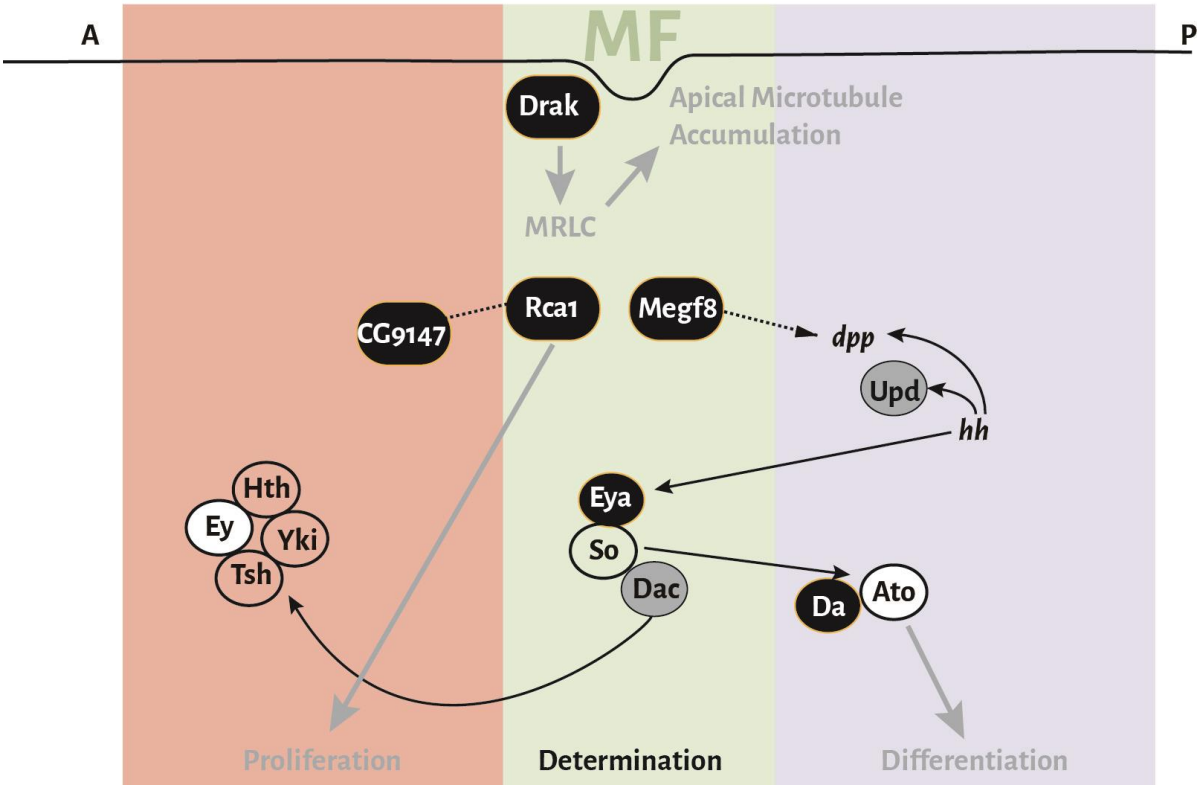

Figure 5.2 The candidate genes are involved in several subnetwork. Protein products are represented by circles; while *dpp* and *hh* as genes. Grey circle represents additional nodes in Figure 4.14; White circle is the eye gene upstream of Jim; Black circle are candidate genes. The dotted line indicates the predicted interaction in the novel network module; the solid line represents the confirmed regulation path. The grey arrow indicates the function of the subnetwork. MRLC, Myosin Regulatory Light Chain (Figure modified from Pichaud, 2014; Casares and Almudi, 2016).

5.2.4 Antennal duplication happens in loss-of-function of few candidate genes

Interestingly, most of the phenotypes caused by the loss-of-function of our candidate genes are only in the eye region (Figure 4.4, 4.5 and 4.6). But, it is noticed that the loss-of-*dachs* and loss-of-*drak* led to the duplication of antennal tissue in eye-antennal discs (Figure 4.4, C, Figure 4.6, C and N). And, the same antennal duplication is shown in adults with loss-of-function of *Trl* and *Drak*. It is suggested that the double antennae phenotype may be the result of early problems in defining the dorsal-ventral axis (antennae are ventral structures in the disc) (Oros et al., 2010). Ey has been shown that it affects eye size by defining where the equator/midline is placed (Baker et al., 2018). This is also an aspect that

causes eye difference in adults between *D. melanogaster* and *D. mauritiana* (Posnien et al., 2012; Buchberger et al., 2021). Besides, the similar antennal duplication results in the perturbation of cell cycle and leads to the consequence of over-proliferation of the antenna disc (Duong et al., 2008).

5.3 A potential new role of Jim during eye development

While the network module (Figure 4.14) allows predicting for some of the candidate genes how they may be linked to known processes regulating eye-antennal disc development, I tested one such link functionally for the candidate gene *jim*, which encodes a Zinc finger C_2H_2 transcription factor (Doerflinger et al., 1999). In the previous studies, the biological function of *jim* is shown in dendrite development (Iyer et al., 2013). This gene was connected to the main part of the network through *upd*. Interestingly, previous genetic data suggests that *jim* interacts with *upd*, which codes for a cytokine involved in the Jak/STAT pathway (Mukherjee et al., 2006). Upd and Jak/STAT pathway activity has been shown to repress *wg* expression causing the initiation of retinal differentiation marked by the MF (Tsai and Sun, 2004; Tsai et al., 2007). During the early larval development, Upd is expressed in the ventral region of eye-antennal disc where it mediates the establishing of D-V midline (Gutierrez-Aviño et al., 2009). Later at Late LII/early LIII, its expression in a few cells at the posterior pole is linked to the initiation of the MF (Reynolds-Kenneally and Mlodzik, 2005) (Figure 5.3). Accordingly, ectopic misexpression of *upd* results in more photoreceptors and larger eyes (Bach et al., 2003). Once removing one copy of the *jim* gene in those JAK/STAT over-expressed flies, *jim* shows only weak/moderate suppression of the overgrowth phenotype (Mukherjee et al., 2006). However, the details of the regulatory process and the exact relationship between Jim and Upd remain unclear.

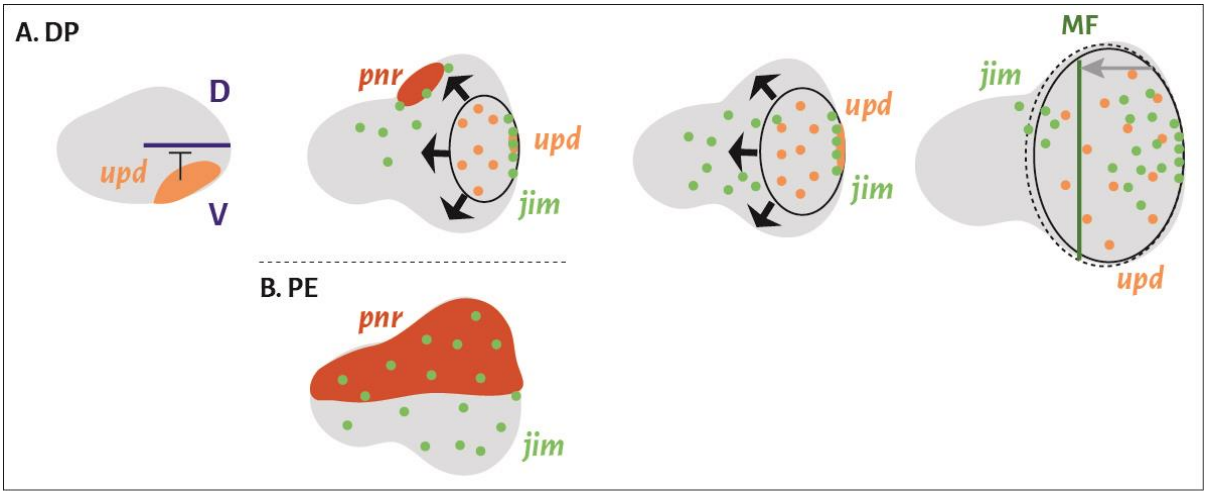

Figure 5.3 The expression pattern of *jim* (in green), *pnr* (in orange) and *upd* (in yellow) in the disc proper (**A**. DP) and peripodial epithelium (**B**. PE). The black arrow shows the direction of the growth of eye region. The morphogenetic furrow progresses from posterior to anterior (grey arrow) (Figure modified from Vollmer et al, 2017; Surkova et al, 2021).

The MF is initiated in the equator region of the eye-antennal disc triggered by signalling from the posterior marginal cells, which connect the DP to the PE (Gibson and Schubiger, 2000; Baker et al., 2018). Previous data from Buchberger et al, 2021 suggests that Pnr acts as a hub in the PE and the posterior margin cells and variation in its expression correlates with eye size differences between *D. melanogaster* and *D. mauritiana* (Buchberger et al., 2021). Jim was identified as putative regulator of *pnr* in developing eye-antennal discs (Figure 4.13) and the loss of *jim* function resulted in duplicated antennal anlagen, which is also a phenotype reminiscent of loss of *pnr* function (Figure 4.16). Additionally, for loss-of-function of *pnr* or *upd* in *jim* positive cells or of *upd* in *pnr* positive cells a similar enlargement of eyes was observed (Figure 4.18). This phenotype was also observed in the previous study when loss-of-function of *pnr* was driven (Singh and Choi, 2003; Singh et al., 2005). These findings suggest a co-localization of Jim, Pnr and Upd and potentially a similar function. Therefore, I hypothesized that Jim and Pnr may interact to regulate MF initiation through Upd/Jak/STAT signalling in the posterior margin cells (Figure 5.4).

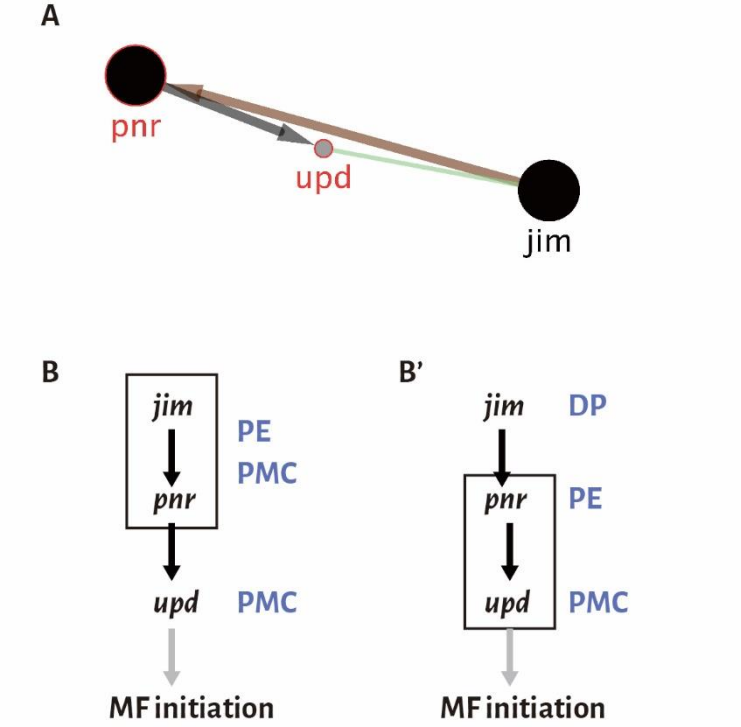

Figure 5.4 (A) Interaction of Jim/Pnr/Upd as inferred from my GRN reconstruction. **(B)** Schematic representation of two potential regulatory mechanism of Jim/Pnr/Upd in the eye-antennal disc. Black arrows indicate genetic or direct interactions; the grey arrow indicates an induced process; blue text indicates expression and function in the peripodial epithelium (PE), in the posterior margin cells (PMC) and in the disc proper (DP).

According to the finding of my experiments, I propose that the Jim/Pnr/Upd interaction could happen in the PE, i.e. hypothesis 1 (Figure 5.4, B), or through the DP to the PE, i.e. hypothesis 2 (Figure 5.4, B'). Support for hypothesis 1 comes from previous data that suggests that *jim* is expressed in the same region as *pnr* (Mukherjee et al., 2006; Kim et al., 2017; Buchberger et al., 2021). I performed *in situ* hybridization (ISH) (Figure 4.15, B) and Hybridization Chain Reaction (HCR) (Figure 4.15, C), and tracing the cell lineages with G-TRACE (Figure 4.15, D and E, F and Figure 5.3) to confirm their co-localization. And their co-localization showed in the G-TRACE results (Figure 4.15, D and E, F and Figure 5.3). Furthermore, the sn-RNAseq data showed *pnr* and *jim* co-expression in PE related clusters (Figure 4.16).

Most importantly, the loss of *jim* specifically in the PE induced by *c311*-Gal4 led to severe phenotype in eye-antennal discs. Overall, my data provides evidence that *jim* is expressed in the PE (Figure 4.19).

Since *jim* is also expressed in other regions of the DP, I cannot exclude the possibility that the expression of *jim* in the DP might affect its downstream genes in the PE. Support for hypothesis 2 comes from previous data. For instance, the communication between DP and PE can happen through juxtacrine and paracrine signalling in the LI and LII larvae when the apical surfaces of the DP and the PE face each other (Pallavi and Shashidhara, 2005). Moreover, the signalling (e.g. Hh, Wg and Dpp signalling) from the PE to the DP that affects the formation of eye-antennal discs has been shown to be mediated through translumenal extensions (Cho et al., 2000). Additionally, it is also suggested EGFR signalling (e.g. Spitz) transmits from the DP to the PE to regulate the expression of genes in the PE (Firth and Baker, 2007). Therefore, Jim may also elicit its function through connections between the DP and the PE.

Overall, I provided the genetic hierarchies of *jim* in the GRN with its upstream and downstream regulatory genes (Figure 4.13 and 5.4, A) and I show that Jim plays important role during eye-antennal disc development in *Drosophila*.

In the study, several staining approaches were used to identify when and where the candidate genes are expressed. Yet according to the bulk-RNAseq (Figure 4.6) and sn-RNAseq result of *jim* and *pnr* (Figure 4.15), the expression varies based on stages and tissues. Therefore, an accurate time course experiments could provide more detail information about candidate genes. To further validate the biological function of all 19 candidate genes and how they interact, it might be interesting to detect

their expression and specifically their co-expression pattern applying HCR, which gave the most consistent results during my project.

5.4 The genetic architecture of eye size variation in Drosophila is in accordance with the omnigenic model

The GRN underlying eye development has been studied for more than two decades and the core genes were identified in *D. melanogaster* (Kumar, 2009b; Bürgy-Roukala et al., 2013; Potier et al., 2014). The integration of large-scale loss- or gain-of-function screens and omics datasets allowed to expand the eye GRN with 241 transcription factors and their 5,632 direct target genes (Potier et al., 2014). In this study, I found 19 genes in this GRN which are essential for eye development, because their loss-of-function leads to similar eye reduction phenotypes. As these genes were either differentially expressed between *D. melanogaster* and *D. mauritiana* during eye-antennal disc development or/and are positional candidates associated with eye size differences in *D. melanogaster*, those genes are excellent candidate genes that may be involved in regulating inter-specific eye size variation. The 19 genes are involved in very different biological and molecular processes. Such a finding is well in line with the recently proposed omnigenic model, that many genes with general cellular functions and ubiquitous expression and few specific genes with specific functions underlie variation in quantitative traits (Boyle et al., 2017). Accordingly, it is almost impossible to reveal individual genes responsible for phenotypic variation in quantitative traits. It has been suggested that meaningful biological insights can be obtained when genes underlying polygenic trait variation are analysed in GRN context. Specifically, a great potential lies in the identification of GRN modules that may contain genes involved in similar biological processes (Fagny and Austerlitz, 2021). Among 19 candidate genes, there is no single gene without effect (i.e. non-zero contribution). This “non-zero” contribution to eye/head

development of those candidate genes supports that those candidate genes are highly interconnected (Fagny and Austerlitz, 2021). And, those genes can be characterized as “core-genes” and “peripheral genes” as previous suggested in omnigenic model (Boyle et al., 2017; Fagny and Austerlitz, 2021). For instance, *atac1* is only directly connected with CG9107 as a less connected peripheral gene. It is found that it is expressed in very few cells during the development of the eye-antennal disc according to the expression level and sn-RNAseq dataset (Figure 4.5 and F). Furthermore, the loss-of-*atac1* leads to a relatively weak phenotype. Yet, except for the well-studied genes, there are other core-genes, such as *Drak*, *pnr* and *jim*. Those core-genes are found highly connected to other candidate genes (Figure 4.14). And the loss-of-function of those core-genes could result in severe loss of eye (Figure 4.5) (Oros et al., 2010).

With my work, I employed a GRN centric approach, which indeed resulted in the identification of interesting biological processes, such as gene expression and function in the PE, cell death control and differentiation that may underlie natural variation in eye size and head shape between *D. melanogaster* and *D. mauritiana*. Therefore, instead of a single master gene, eye and head development is regulated by a group of core-genes and some peripheral genes.

6. Supplementary Tables and Figures

Supplementary Table 1. SmiFISH probes for *Trl* generated by Biosearch Technologies with 28nt FLAP sequence added (CCTCCTAAGTTTCGAGCTGGACTCAGTG).

Name	Sequence
Trl-1	CCTCCTAAGTTTCGAGCTGGACTCAGTGgaattcattggcagcgacat
Trl-2	CCTCCTAAGTTTCGAGCTGGACTCAGTGgcagcgcaacaattggattg
Trl-3	CCTCCTAAGTTTCGAGCTGGACTCAGTGaacgtgcaatcgacgaggtc
Trl-4	CCTCCTAAGTTTCGAGCTGGACTCAGTGctatcttgtgggcgggaaaa
Trl-5	CCTCCTAAGTTTCGAGCTGGACTCAGTGaagtccagcagaaaggggga
Trl-6	CCTCCTAAGTTTCGAGCTGGACTCAGTGcttgcatggtgtattcttta
Trl-7	CCTCCTAAGTTTCGAGCTGGACTCAGTGcagccaacataaccactgga
Trl-8	CCTCCTAAGTTTCGAGCTGGACTCAGTGtccagatcgttcgcattgac
Trl-9	CCTCCTAAGTTTCGAGCTGGACTCAGTGcggtacacaaactccagcag
Trl-10	CCTCCTAAGTTTCGAGCTGGACTCAGTGgtgtagtcgtccttggtaac
Trl-11	CCTCCTAAGTTTCGAGCTGGACTCAGTGatgtgctgcagttgtatcga
Trl-12	CCTCCTAAGTTTCGAGCTGGACTCAGTGttggtcgtgatgttgtggaa
Trl-13	CCTCCTAAGTTTCGAGCTGGACTCAGTGcgatcgtggcaatcagttgg
Trl-14	CCTCCTAAGTTTCGAGCTGGACTCAGTGatgaaccgtttgctgtggag
Trl-15	CCTCCTAAGTTTCGAGCTGGACTCAGTGtgatgatggatgtcctccac
Trl-16	CCTCCTAAGTTTCGAGCTGGACTCAGTGgtcgttgcctggagaatctg
Trl-17	CCTCCTAAGTTTCGAGCTGGACTCAGTGtcggttgtcacaatggtctg
Trl-18	CCTCCTAAGTTTCGAGCTGGACTCAGTGtgaatcactgcctggtcatg
Trl-19	CCTCCTAAGTTTCGAGCTGGACTCAGTGgtttgcgtgccggaagaaaa
Trl-20	CCTCCTAAGTTTCGAGCTGGACTCAGTGgtgacattttctttacgcgt
Trl-21	CCTCCTAAGTTTCGAGCTGGACTCAGTGactttgcttattttcggtgc
Trl-22	CCTCCTAAGTTTCGAGCTGGACTCAGTGcataatcgtatccattcctt
Trl-23	CCTCCTAAGTTTCGAGCTGGACTCAGTGcgtgtgaagaggtcggtgtg
Trl-24	CCTCCTAAGTTTCGAGCTGGACTCAGTGgtgtggatgatagcagttgg
Trl-25	CCTCCTAAGTTTCGAGCTGGACTCAGTGtttgtccttcgctcttgatg
Trl-26	CCTCCTAAGTTTCGAGCTGGACTCAGTGtccatggtcacaatagtctc
Trl-27	CCTCCTAAGTTTCGAGCTGGACTCAGTGttaccggtatcatgttgttg
Trl-28	CCTCCTAAGTTTCGAGCTGGACTCAGTGcttgtgctggtgttatctcg
Trl-29	CCTCCTAAGTTTCGAGCTGGACTCAGTGataggacgccgcttgtattg
Trl-30	CCTCCTAAGTTTCGAGCTGGACTCAGTGcggatgtttagcgcgttttg
Trl-31	CCTCCTAAGTTTCGAGCTGGACTCAGTGtgaacgtggtttctctgttc
Trl-32	CCTCCTAAGTTTCGAGCTGGACTCAGTGagcaggttgttcagattgtg
Trl-33	CCTCCTAAGTTTCGAGCTGGACTCAGTGcagcatagcaaatggggcaa
Trl-34	CCTCCTAAGTTTCGAGCTGGACTCAGTGaggttccgggattgacgaat
Trl-35	CCTCCTAAGTTTCGAGCTGGACTCAGTGaaaatgccgcagctcgagat

Trl-36	CCTCCTAAGTTTCGAGCTGGACTCAGTGttttcttctccttcttcacg
Trl-37	CCTCCTAAGTTTCGAGCTGGACTCAGTGaattgaaagcggagctccac
Trl-38	CCTCCTAAGTTTCGAGCTGGACTCAGTGattgcctatgatctgatggc
Trl-39	CCTCCTAAGTTTCGAGCTGGACTCAGTGagtcagttatattcacctga
Trl-40	CCTCCTAAGTTTCGAGCTGGACTCAGTGaaatgttcttgttgttgccc
Trl-41	CCTCCTAAGTTTCGAGCTGGACTCAGTGttaccgcctttcaaaatgaa
Trl-42	CCTCCTAAGTTTCGAGCTGGACTCAGTGgcctgttgctgtttacgtat
Trl-43	CCTCCTAAGTTTCGAGCTGGACTCAGTGtacgtattattaccgccttt

Supplementary Table 2. SmiFISH probes for *Rca1* generated by Biosearch Technologies with 28nt FLAP sequence added (CCTCCTAAGTTTCGAGCTGGACTCAGTG).

Name	Sequence
rca1-1	CCTCCTAAGTTTCGAGCTGGACTCAGTGcaactcgaaggatgaccctc
rca1-2	CCTCCTAAGTTTCGAGCTGGACTCAGTGtgtagccagactcgttcatc
rca1-3	CCTCCTAAGTTTCGAGCTGGACTCAGTGaattgtgcagcgccaggaag
rca1-4	CCTCCTAAGTTTCGAGCTGGACTCAGTGataaaaatggcgtctccgcg
rca1-5	CCTCCTAAGTTTCGAGCTGGACTCAGTGgatgcattgcgacagttttc
rca1-6	CCTCCTAAGTTTCGAGCTGGACTCAGTGcccgaaagaatgttgtggta
rca1-7	CCTCCTAAGTTTCGAGCTGGACTCAGTGcagtaaaggtcctgctcctg
rca1-8	CCTCCTAAGTTTCGAGCTGGACTCAGTGtgtgttctgggatagggctt
rca1-9	CCTCCTAAGTTTCGAGCTGGACTCAGTGctccgcggaaaatttctttt
rca1-10	CCTCCTAAGTTTCGAGCTGGACTCAGTGgcggagtcatagagaaaggc
rca1-11	CCTCCTAAGTTTCGAGCTGGACTCAGTGttgggcagactatgctcatc
rca1-12	CCTCCTAAGTTTCGAGCTGGACTCAGTGgtgtggcgattgaaagtgtt
rca1-13	CCTCCTAAGTTTCGAGCTGGACTCAGTGcagcttttggacttcttgg
rca1-14	CCTCCTAAGTTTCGAGCTGGACTCAGTGggttcttctatgtggggaaa
rca1-15	CCTCCTAAGTTTCGAGCTGGACTCAGTGcgccgtagaagcgattcttg
rca1-16	CCTCCTAAGTTTCGAGCTGGACTCAGTGacgatatccagcttttcgac
rca1-17	CCTCCTAAGTTTCGAGCTGGACTCAGTGacatgacgcagtatgcactg
rca1-18	CCTCCTAAGTTTCGAGCTGGACTCAGTGgataccttggtcatcacgtc
rca1-19	CCTCCTAAGTTTCGAGCTGGACTCAGTGgcgttggctgcgataaacag
rca1-20	CCTCCTAAGTTTCGAGCTGGACTCAGTGtcaatttgagtcggtggttc
rca1-21	CCTCCTAAGTTTCGAGCTGGACTCAGTGgtgaggattctctttggtta
rca1-22	CCTCCTAAGTTTCGAGCTGGACTCAGTGtatggttcgaggtctgcaat
rca1-23	CCTCCTAAGTTTCGAGCTGGACTCAGTGatcaggtggatgctcgagtt
rca1-24	CCTCCTAAGTTTCGAGCTGGACTCAGTGcgcttatgaaaacccggctg
rca1-25	CCTCCTAAGTTTCGAGCTGGACTCAGTGacaataggttttcgccacac
rca1-26	CCTCCTAAGTTTCGAGCTGGACTCAGTGtgtacgtccaataggcagag
rca1-27	CCTCCTAAGTTTCGAGCTGGACTCAGTGtcatgcaggggaatgtgctg
rca1-28	CCTCCTAAGTTTCGAGCTGGACTCAGTGgacaggaagcgtttgagagg
rca1-29	CCTCCTAAGTTTCGAGCTGGACTCAGTGaagtcctgacctcgtcaaga
rca1-30	CCTCCTAAGTTTCGAGCTGGACTCAGTGaagttatatggcggtccttg
rca1-31	CCTCCTAAGTTTCGAGCTGGACTCAGTGgatgacactggtgcattcgg
rca1-32	CCTCCTAAGTTTCGAGCTGGACTCAGTGtgacgcagaaccgaaactgg
rca1-33	CCTCCTAAGTTTCGAGCTGGACTCAGTGggatgcgacttgcacagaca
rca1-34	CCTCCTAAGTTTCGAGCTGGACTCAGTGtcatcagtttggatggtgtg
rca1-35	CCTCCTAAGTTTCGAGCTGGACTCAGTGttccttgtgattttcggatc
rca1-36	CCTCCTAAGTTTCGAGCTGGACTCAGTGtaaaagcagagccgcttgag

Supplementary Table 3. Detailed gene lists in the QTL region with FlybaseID. https://doi.org/10.25625/HIKEIZ

Supplementary Table 4. Detailed gene lists obtained as part of the candidate gene identification pipeline. https://doi.org/10.25625/HIKEIZ

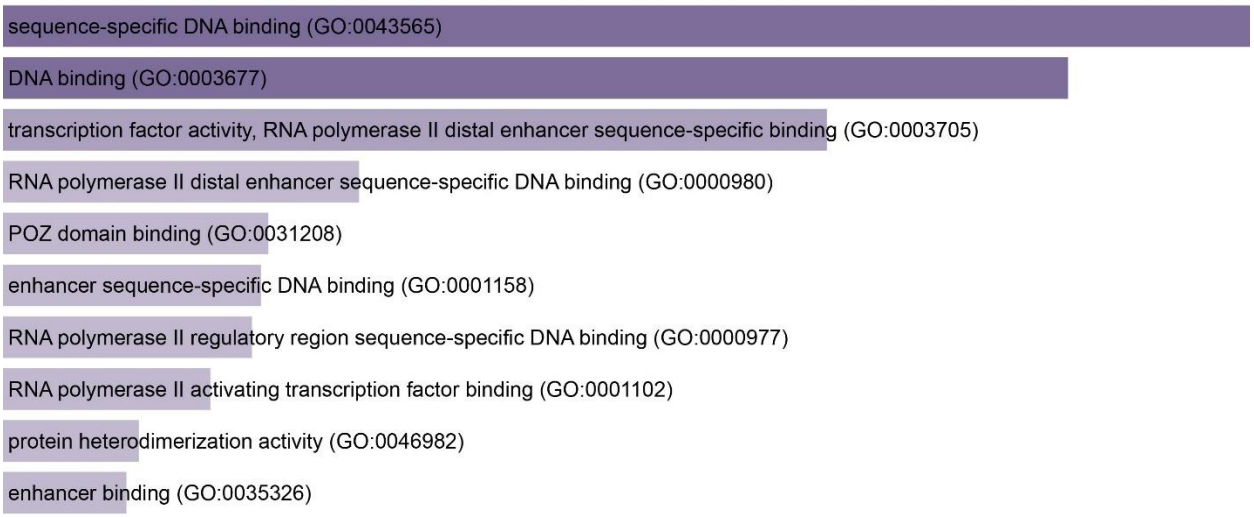

Supplementary Figure 1. GO enrichment of putative *pnr* regulators.

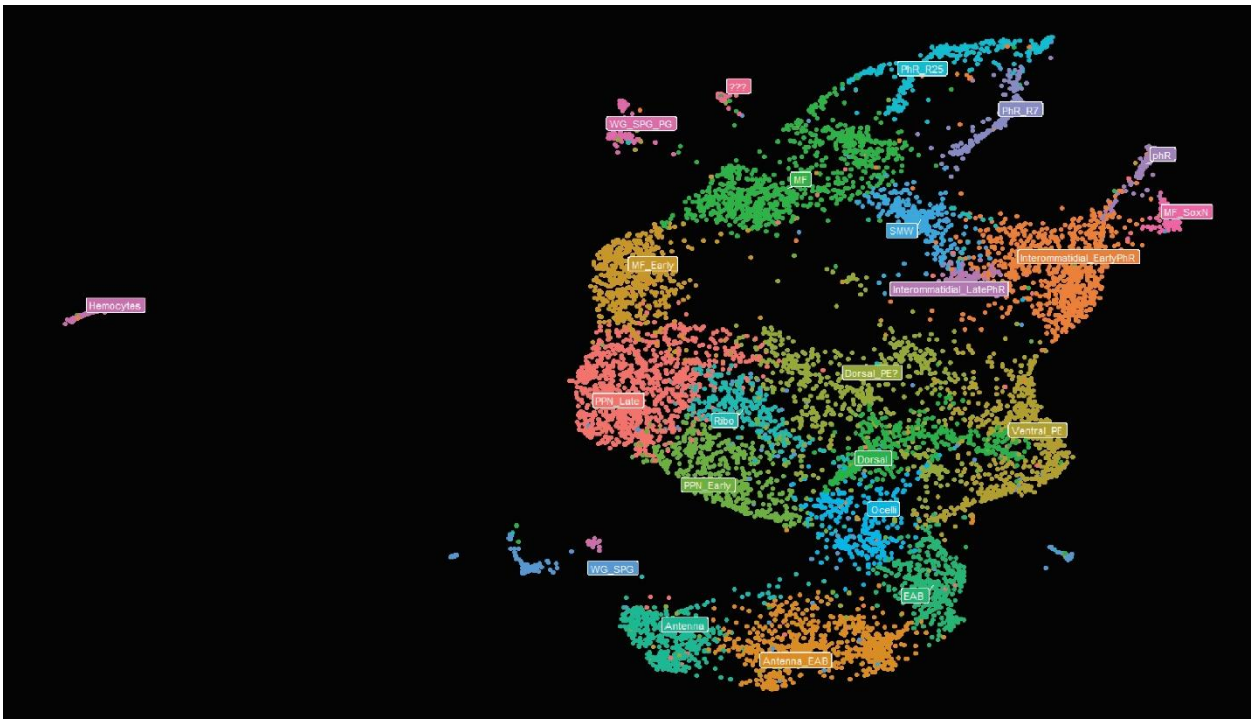

Supplementary Figure 2. UMAP Annotation of sn-RNAseq data in 120 h AEL MF, morphogenetic furrow; MF_SoxN, morphogenetic furrow with SoxN expression; WG, Wrapping glia; PG, Perineurial glia; PhR, Photoreceptor; SMW, Second mitotic wave; EAB, Eye-antennal border; PE, Peripodial epithelium; PPN, Pre-proneural domain; Ribo, cells that express ribosomal genes (Figures provided by Gordon Wiegleb, unpublished).

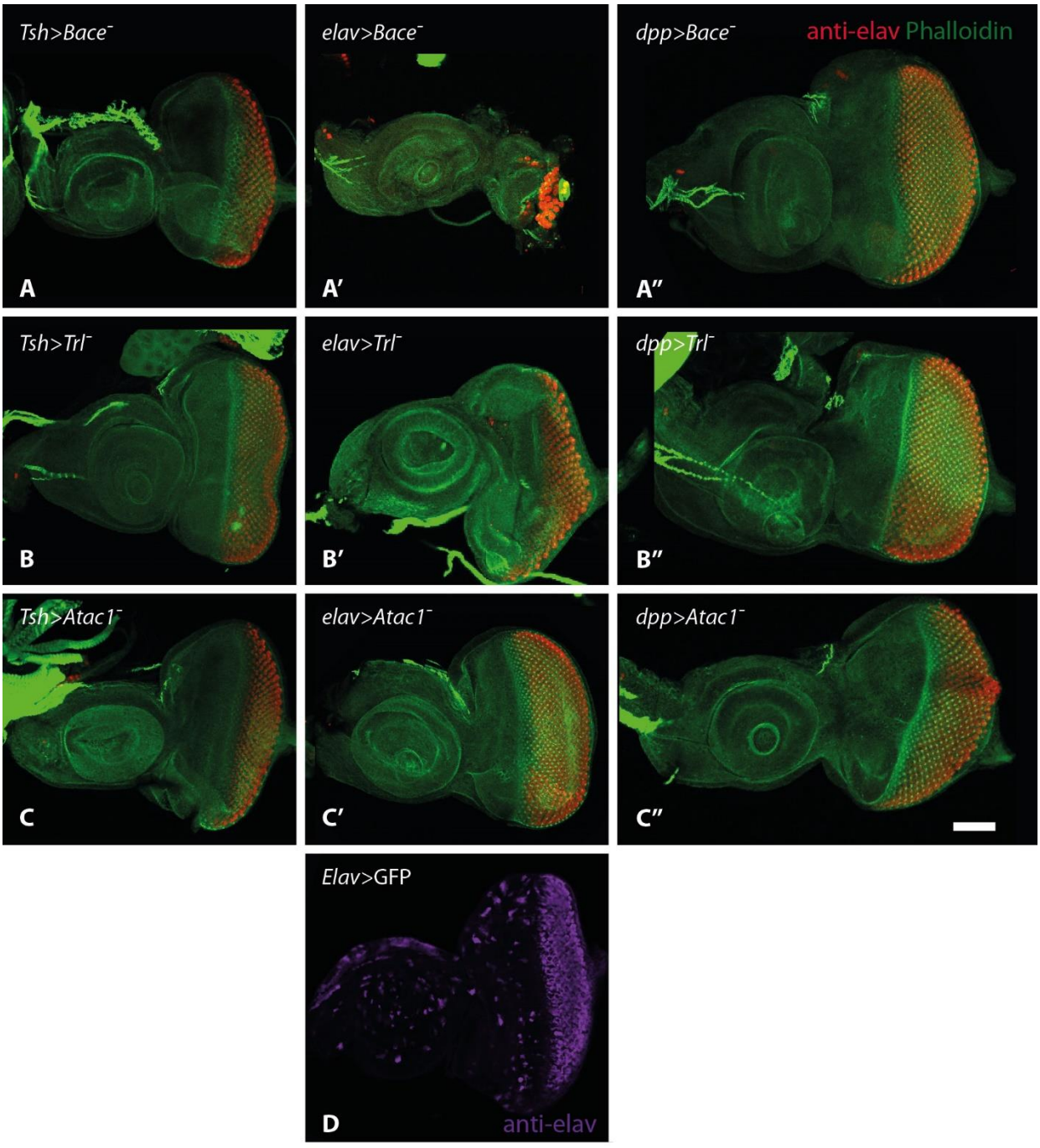

Supplementary Figure 3. (A-A''') *Bace* RNAi induced by different Gal4 driver lines. *Tsh*-Gal4 **(A)**, *Elav*-Gal4 **(A')**, *wg*-Gal4 **(A'')** and *dpp*-Gal4 **(A''')**. The *elav*-Gal4 induced RNAi in the developing photoreceptors (D). Actin detected by Phalloidin is shown in green and the red colour represents the expression of Elav to label the photoreceptors. The scale bar is 50 µm. In all Figures, anterior is to the left. Related to in Figure 4.5.

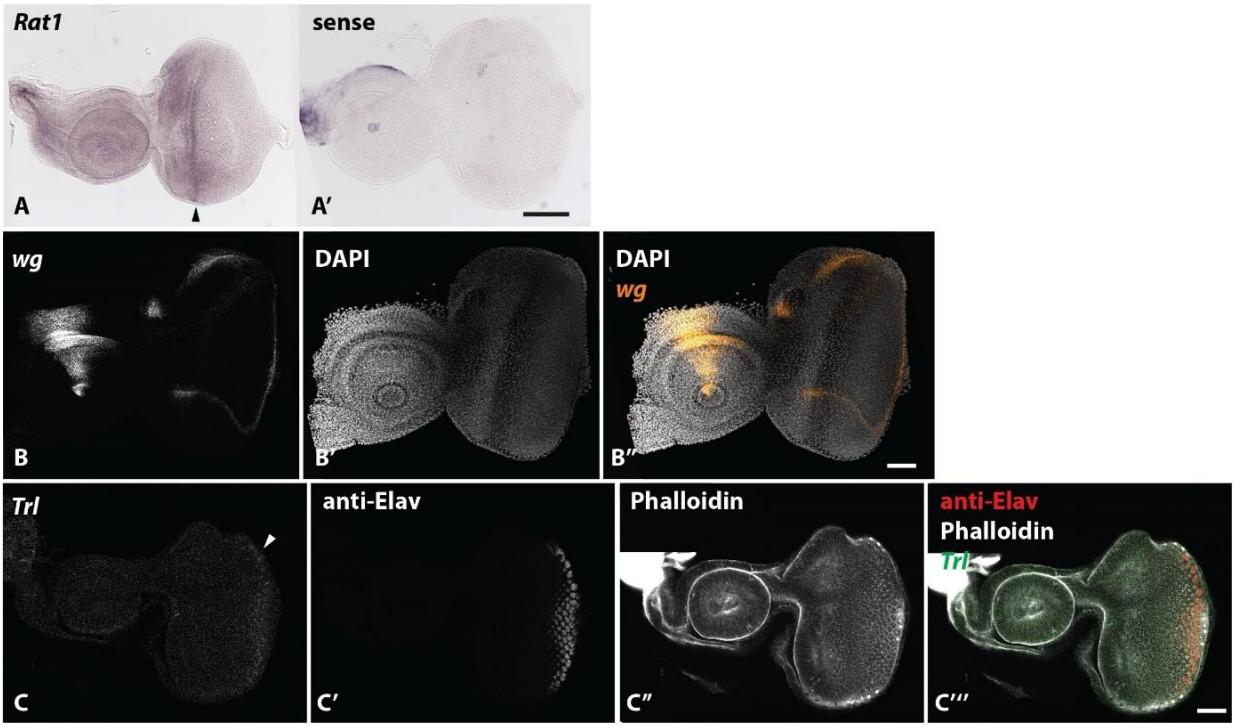

Supplementary Figure 4. Spatial expression of selected candidate genes. *Rat1* **(A)** is detected via classic *in-situ* hybridization with negative control based on hybridisation with a sense probe **(A').** The arrowhead represents the MF region in the eye-antennal disc. **(B-B")** The expression pattern of *wg* detected via HCR. **(C-C‴)** *Trl* expressing cells detected via SmiFISH.

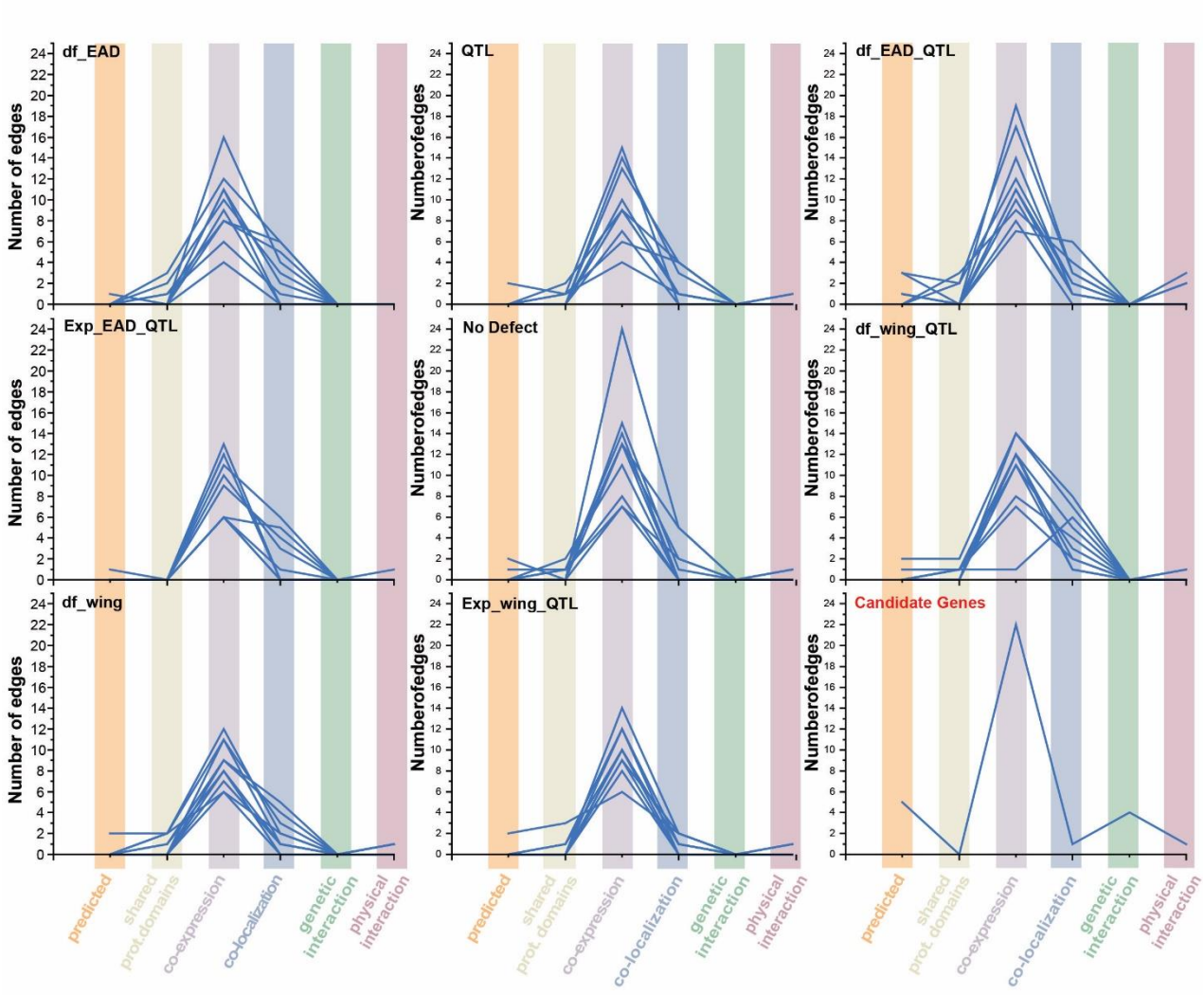

Supplementary Figure 5. (**A-I**) The number of edges of each network. Y-axis is the number of edges. X-axis is 1) predicted interactions, 2) shared protein domains, 3) co-expression, 4) co-localization, 5) genetic interaction and 6) physical interaction. The networks were constructed with gene lists in table 4.1.

Supplementary Table 5 The average numbers and percentage of each type of edges from 10 randomly selected networks among all gene lists (see abbreviation in Table 4.1). The column with grey filling shows the percentage of each type of edges.

	A. df_EAD		B. Exp_EAD_QTL		C. df_EAD_QTL		D. QTL		E. No defect		F. Candidate	
Predicted	0,1	0,77	0,1	0,89	0,9	5,49	0,2	1,63	0,4	2,52	5	15,15
Shared protein domains	0	0,00	0	0,00	0,7	4,27	0,5	4,07	0,7	4,40	0	0,00
Co-expression	9,5	73,08	9,1	81,25	11,8	71,95	9,6	78,05	12,9	81,13	22	66,67
Co-localization	2,7	20,77	1,9	16,96	2,3	14,02	1,9	15,45	1,7	10,69	1	3,03
Genetic Interactions	0	0,00	0	0,00	0	0,00	0	0,00	0	0,00	4	12,12
Physical Interactions	0,7	5,38	0,1	0,89	0,7	4,27	0,1	0,81	0,2	1,26	1	3,03
Total	13	100,00	11,2	100,00	16,4	100,00	12,3	100,00	15,9	100,00	33	100,00

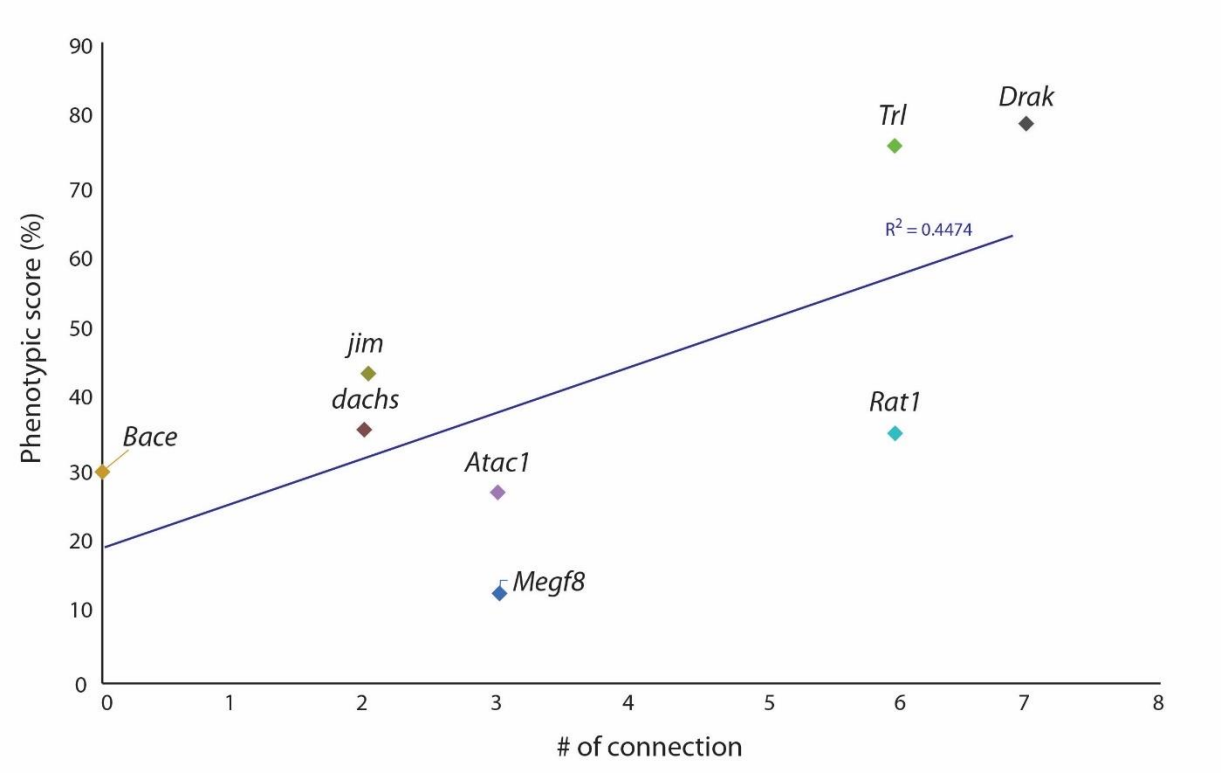

Supplementary Figure 6. Positive correlation (R2 = 0.4474; p = 0.017393) between phenotypic score and the number of connections without uncharacterized genes. Y-axis represents the phenotype score (percentage) of the loss-of-function of each gene in Figure 4.3. X-axis represents the number of connections of the respectively genes.

7. References

Arif, S., Hilbrant, M., Hopfen, C., Almudi, I., Nunes, M.D.S., Posnien, N., Kuncheria, L., Tanaka, K., Mitteroecker, P., Schlötterer, C., et al. (2013). Genetic and developmental analysis of differences in eye and face morphology between Drosophila simulans and Drosophila mauritiana. Evol. Dev. *15*, 257–267.

Ariss, M.M., Islam, A.B.M.M.K., Critcher, M., Zappia, M.P., and Frolov, M.V. (2018). Single cell RNA-sequencing identifies a metabolic aspect of apoptosis in Rbf mutant. Nat. Commun. *9*, 5024.

Auerbach, C. (1935). The development of the legs, wings, and halteres in wild type and some mutant strains of Drosophila melanogaster. Doctoral dissertation.

Bach, E.A., Vincent, S., Zeidler, M.P., and Perrimon, N. (2003). A sensitized genetic screen to identify novel regulators and components of the Drosophila janus kinase/signal transducer and activator of transcription pathway. Genetics *165*, 1149–1166.

Bailey, T.L., and Elkan, C. (1994). Fitting a mixture model by expectation maximization to discover motifs in biopolymers. Proc. Int. Conf. Intell. Syst. Mol. Biol. *2*, 28–36.

Bailey, T.L., and Gribskov, M. (1998). Combining evidence using p-values: application to sequence homology searches. Bioinformatics *14*, 48–54.

Baker, L.R., Weasner, B.M., Nagel, A., Neuman, S.D., Bashirullah, A., and Kumar, J.P. (2018). Eyeless/Pax6 initiates eye formation non-autonomously from the peripodial epithelium. Development *145*.

Barrio, R., de Celis, J.F., Bolshakov, S., and Kafatos, F.C. (1999). Identification of regulatory regions driving the expression of the Drosophila spalt complex at different developmental stages. Dev. Biol. *215*, 33–47.

Beckstead, R.B., Lam, G., and Thummel, C.S. (2005). The genomic response to 20-hydroxyecdysone at the onset of Drosophila metamorphosis. Genome Biol. *6*, R99.

Belozerov, V.E., Lin, Z.-Y., Gingras, A.-C., McDermott, J.C., and Michael Siu, K.W. (2012). High-resolution protein interaction map of the Drosophila melanogaster p38 mitogen-activated protein kinases reveals limited functional redundancy. Mol. Cell. Biol. *32*, 3695–3706.

Bessa, J., and Casares, F. (2005). Restricted teashirt expression confers eye-specific responsiveness to Dpp and Wg signals during eye specification in Drosophila. Development *132*, 5011–5020.

Bessa, J., Gebelein, B., Pichaud, F., Casares, F., and Mann, R.S. (2002). Combinatorial control of Drosophila eye development by eyeless, homothorax, and teashirt. Genes Dev. *16*, 2415–2427.

Bhat, K.M., Farkas, G., Karch, F., Gyurkovics, H., Gausz, J., and Schedl, P. (1996). The GAGA factor is required in the early Drosophila embryo not only for transcriptional regulation but also for nuclear division. Development *122*, 1113–1124.

Bielen, H., and Houart, C. (2012). BMP signaling protects telencephalic fate by repressing eye identity and its Cxcr4-dependent morphogenesis. Dev. Cell *23*, 812–822.

Bischof, J., Duffraisse, M., Furger, E., Ajuria, L., Giraud, G., Vanderperre, S., Paul, R., Björklund, M., Ahr, D., Ahmed, A.W., et al. (2018). Generation of a versatile BiFC ORFeome library for analyzing protein-protein interactions in live Drosophila. Elife *7*.

Bolkan, B.J., Triphan, T., and Kretzschmar, D. (2012). β-secretase cleavage of the fly amyloid precursor protein is required for glial survival. J. Neurosci. *32*, 16181–16192.

Bonini, N.M. (1997). Surviving Drosophila eye development. Cell Death Differ. *4*, 4–11.

Bonini, N.M., Leiserson, W.M., and Benzer, S. (1993). The eyes absent gene: genetic control of cell survival and differentiation in the developing Drosophila eye. Cell *72*, 379–395.

Bonini, N.M., Bui, Q.T., Gray-Board, G.L., and Warrick, J.M. (1997). The Drosophila eyes absent gene directs ectopic eye formation in a pathway conserved between flies and vertebrates. Development *124*, 4819–4826.

Boyle, E.A., Li, Y.I., and Pritchard, J.K. (2017). An expanded view of complex traits: from polygenic to omnigenic. Cell *169*, 1177–1186.

Braid, L.R., and Verheyen, E.M. (2008). Drosophila nemo promotes eye specification directed by the retinal determination gene network. Genetics *180*, 283–299.

Brand, A.H., and Perrimon, N. (1993). Targeted gene expression as a means of altering cell fates and generating dominant phenotypes. Development *118*, 401–415.

Brown, N.L., Paddock, S.W., Sattler, C.A., Cronmiller, C., Thomas, B.J., and Carroll, S.B. (1996). daughterless is required for Drosophila photoreceptor cell determination, eye morphogenesis, and cell cycle progression. Dev. Biol. *179*, 65–78.

Bruce, H., Jerz, G., Kelly, S., McCarthy, J., Pomerantz, A., Senevirathne, G., Sherrard, A., A Sun, D., Wolff, C., and H Patel, N. (2021). Hybridization chain reaction (HCR) in situ protocol v1.

Buchberger, E. (2019). Comparative gene expression to study the developmental basis of organ diversification. Doctoral dissertation.

Buchberger, E., Bilen, A., Ayaz, S., Salamanca, D., Matas de Las Heras, C., Niksic, A., Almudi, I., Torres-Oliva, M., Casares, F., and Posnien, N. (2021). Variation in pleiotropic hub gene expression is associated with interspecific differences in head shape and eye size in Drosophila. Mol. Biol. Evol.

Bürgy-Roukala, E., Miellet, S., Mishra, A.K., and Sprecher, S.G. (2013). Early eye development: specification and determination. In Molecular genetics of axial patterning, growth and disease in the drosophila eye, A. Singh, and M. Kango-Singh, eds. (New York, NY: Springer New York), pp. 1–36.

Cagan, R. (2009). Principles of Drosophila eye differentiation. Curr Top Dev Biol *89*, 115–135.

Calvo, L., Ronshaugen, M., and Pettini, T. (2021). smiFISH and embryo segmentation for single-cell multi-gene RNA quantification in arthropods. Commun. Biol. *4*, 352.

Capani, F., Deerinck, T.J., Ellisman, M.H., Bushong, E., Bobik, M., and Martone, M.E. (2001). Phalloidin-eosin followed by photo-oxidation: a novel method for localizing F-actin at the light and electron microscopic levels. J. Histochem. Cytochem. *49*, 1351–1361.

Carreira, V.P., Imberti, M.A., Mensch, J., and Fanara, J.J. (2013). Gene-by-temperature interactions and candidate plasticity genes for morphological traits in Drosophila melanogaster. PLoS One *8*, e70851.

Carreira, V.P., Mensch, J., Hasson, E., and Fanara, J.J. (2016). Natural Genetic Variation and Candidate Genes for Morphological Traits in Drosophila melanogaster. PLoS One *11*, e0160069.

Casares, F., and Almudi, I. (2016). Fast and furious 800. the retinal determination gene network in drosophila. In Organogenetic Gene Networks, J. Castelli-Gair Hombría, and P. Bovolenta, eds. (Cham: Springer International Publishing), pp. 95–124.

Casares, F., and McGregor, A.P. (2020). The evolution and development of eye size in flies. Wiley Interdiscip Rev Dev Biol e380.

Chen, H.-W., Marinissen, M.J., Oh, S.-W., Chen, X., Melnick, M., Perrimon, N., Gutkind, J.S., and Hou, S.X. (2002). CKA, a novel multidomain protein, regulates the JUN N-terminal kinase signal transduction pathway in Drosophila. Mol. Cell. Biol. *22*, 1792–1803.

Chen, J., Xie, C., Tian, L., Hong, L., Wu, X., and Han, J. (2010). Participation of the p38 pathway in Drosophila host defense against pathogenic bacteria and fungi. Proc. Natl. Acad. Sci. USA *107*, 20774–20779.

Chen, R., Halder, G., Zhang, Z., and Mardon, G. (1999). Signaling by the TGF-beta homolog decapentaplegic functions reiteratively within the network of genes controlling retinal cell fate determination in Drosophila. Development *126*, 935–943.

Chen, Y.-C.A., Stuwe, E., Luo, Y., Ninova, M., Le Thomas, A., Rozhavskaya, E., Li, S., Vempati, S., Laver, J.D., Patel, D.J., et al. (2016). Cutoff Suppresses RNA Polymerase II Termination to Ensure Expression of piRNA Precursors. Mol. Cell *63*, 97–109.

Cho, E., and Irvine, K.D. (2004). Action of fat, four-jointed, dachsous and dachs in distal-to-proximal wing signaling. Development *131*, 4489–4500.

Cho, E., Feng, Y., Rauskolb, C., Maitra, S., Fehon, R., and Irvine, K.D. (2006). Delineation of a Fat tumor suppressor pathway. Nat. Genet. *38*, 1142–1150.

Cho, K.O., Chern, J., Izaddoost, S., and Choi, K.W. (2000). Novel signaling from the peripodial membrane is essential for eye disc patterning in Drosophila. Cell *103*, 331–342.

Choi, H.M.T., Beck, V.A., and Pierce, N.A. (2014). Next-generation in situ hybridization chain reaction: higher gain, lower cost, greater durability. ACS Nano *8*, 4284–4294.

Chougule, A.B., Hastert, M.C., and Thomas, J.H. (2016). Drak is required for actomyosin organization during drosophila cellularization. G3 (Bethesda) *6*, 819–828.

Clements, J., Hens, K., Merugu, S., Dichtl, B., de Couet, H.G., and Callaerts, P. (2009). Mutational analysis of the eyeless gene and phenotypic rescue reveal that an intact Eyeless protein is necessary for normal eye and brain development in Drosophila. Dev. Biol. *334*, 503–512.

Craig, C.R., Fink, J.L., Yagi, Y., Ip, Y.T., and Cagan, R.L. (2004). A Drosophila p38 orthologue is required for environmental stress responses. EMBO Rep. *5*, 1058–1063.

Cuadrado, A., and Nebreda, A.R. (2010). Mechanisms and functions of p38 MAPK signalling. Biochem. J. *429*, 403–417.

Cully, M., Genevet, A., Warne, P., Treins, C., Liu, T., Bastien, J., Baum, B., Tapon, N., Leevers, S.J., and Downward, J. (2010). A role for p38 stress-activated protein kinase in regulation of cell growth via TORC1. Mol. Cell. Biol. *30*, 481–495.

Das, P., Maduzia, L.L., Wang, H., Finelli, A.L., Cho, S.H., Smith, M.M., and Padgett, R.W. (1998). The Drosophila gene Medea demonstrates the requirement for different classes of Smads in dpp signaling. Development *125*, 1519–1528.

Degoutin, J.L., Milton, C.C., Yu, E., Tipping, M., Bosveld, F., Yang, L., Bellaiche, Y., Veraksa, A., and Harvey, K.F. (2013). Riquiqui and minibrain are regulators of the hippo pathway downstream of Dachsous. Nat. Cell Biol. *15*, 1176–1185.

Desplan, C. (1997). Eye development: governed by a dictator or a junta? Cell *91*, 861–864.

Dhoondia, Z., Elewa, H., Malik, M., Arif, Z., Pique-Regi, R., and Ansari, A. (2021). A termination-independent role of Rat1 in cotranscriptional splicing. Nucleic Acids Res. *49*, 5520–5536.

Doerflinger, H., Lepesant, J.-A., and Yanicostas, C. (1999). Differential expression of the Drosophila zinc finger gene jim in the follicular epithelium. Mech. Dev. *86*, 177–182.

Domingos, P.M., Brown, S., Barrio, R., Ratnakumar, K., Frankfort, B.J., Mardon, G., Steller, H., and Mollereau, B. (2004). Regulation of R7 and R8 differentiation by the spalt genes. Dev. Biol. *273*, 121–133.

Dong, P.D.S., Dicks, J.S., and Panganiban, G. (2002). Distal-less and homothorax regulate multiple targets to pattern the Drosophila antenna. Development *129*, 1967–1974.

Dong, X., Zavitz, K.H., Thomas, B.J., Lin, M., Campbell, S., and Zipursky, S.L. (1997). Control of G1 in the developing Drosophila eye: rca1 regulates Cyclin A. Genes Dev. *11*, 94–105.

Duong, H.A., Wang, C.W., Sun, Y.H., and Courey, A.J. (2008). Transformation of eye to antenna by misexpression of a single gene. Mech. Dev. *125*, 130–141.

Ellis, M.C., O'Neill, E.M., and Rubin, G.M. (1993). Expression of Drosophila glass protein and evidence for negative regulation of its activity in non-neuronal cells by another DNA-binding protein. Development *119*, 855–865.

Engelhard, C., Sarsfield, S., Merte, J., Wang, Q., Li, P., Beppu, H., Kolodkin, A.L., Sucov, H.M., and Ginty, D.D. (2013). MEGF8 is a modifier of BMP signaling in trigeminal sensory neurons. Elife *2*, e01160.

Evans, C.J., Olson, J.M., Ngo, K.T., Kim, E., Lee, N.E., Kuoy, E., Patananan, A.N., Sitz, D., Tran, P., Do, M.-T., et al. (2009). G-TRACE: rapid Gal4-based cell lineage analysis in Drosophila. Nat. Methods *6*, 603–605.

Fagny, M., and Austerlitz, F. (2021). Polygenic adaptation: integrating population genetics and gene regulatory networks. Trends Genet. *37*, 631–638.

Farooq, M., Lindbæk, L., Krogh, N., Doganli, C., Keller, C., Mönnich, M., Gonçalves, A.B., Sakthivel, S., Mang, Y., Fatima, A., et al. (2020). RRP7A links primary microcephaly to dysfunction of ribosome biogenesis, resorption of primary cilia, and neurogenesis. Nat. Commun. *11*, 5816.

Fernandes, V.M., McCormack, K., Lewellyn, L., and Verheyen, E.M. (2014). Integrins regulate apical constriction via microtubule stabilization in the Drosophila eye disc epithelium. Cell Rep. *9*, 2043–2055.

Fernandes, V.M., Pradhan-Sundd, T., Blaquiere, J.A., and Verheyen, E.M. (2015). Ras/MEK/MAPK-mediated regulation of heparin sulphate proteoglycans promotes retinal fate in the Drosophila eye-antennal disc. Dev. Biol. *402*, 109–118.

Firth, L.C., and Baker, N.E. (2007). Spitz from the retina regulates genes transcribed in the second mitotic wave, peripodial epithelium, glia and plasmatocytes of the Drosophila eye imaginal disc. Dev. Biol. *307*, 521–538.

Fishman, R.S. (2008). Evolution and the eye: the Darwin bicentennial and the sesquicentennial of the origin of species. Arch. Ophthalmol. *126*, 1586–1592.

Franz, M., Rodriguez, H., Lopes, C., Zuberi, K., Montojo, J., Bader, G.D., and Morris, Q. (2018). GeneMANIA update 2018. Nucleic Acids Res. *46*, W60–W64.

Frise, E., Hammonds, A.S., and Celniker, S.E. (2010). Systematic image-driven analysis of the spatial Drosophila embryonic expression landscape. Mol. Syst. Biol. *6*, 345.

Furuta, Y., and Hogan, B.L. (1998). BMP4 is essential for lens induction in the mouse embryo. Genes Dev. *12*, 3764–3775.

Gaspar, P., Arif, S., Sumner-Rooney, L., Kittelmann, M., Bodey, A.J., Stern, D.L., Nunes, M.D.S., and McGregor, A.P. (2020). Characterization of the Genetic Architecture Underlying Eye Size Variation Within Drosophila melanogaster and Drosophila simulans. G3 (Bethesda) *10*, 1005–1018.

Gehring, W.J. (1996). The master control gene for morphogenesis and evolution of the eye. Genes Cells *1*, 11–15.

Gibson, M.C., and Schubiger, G. (2000). Peripodial cells regulate proliferation and patterning of Drosophila imaginal discs. Cell *103*, 343–350.

Gonzalez-Bellido, P.T., Wardill, T.J., and Juusola, M. (2011). Compound eyes and retinal information processing in miniature dipteran species match their specific ecological demands. Proc. Natl. Acad. Sci. USA *108*, 4224–4229.

Gore, A.V., Tomins, K.A., Iben, J., Ma, L., Castranova, D., Davis, A.E., Parkhurst, A., Jeffery, W.R., and Weinstein, B.M. (2018). An epigenetic mechanism for cavefish eye degeneration. Nat. Ecol. Evol. *2*, 1155–1160.

Greeve, I., Kretzschmar, D., Tschäpe, J.-A., Beyn, A., Brellinger, C., Schweizer, M., Nitsch, R.M., and Reifegerste, R. (2004). Age-dependent neurodegeneration and Alzheimer-amyloid plaque formation in transgenic Drosophila. J. Neurosci. *24*, 3899–3906.

Gross, J.B. (2012). The complex origin of Astyanax cavefish. BMC Evol. Biol. *12*, 105.

Gross, J.B., Meyer, B., and Perkins, M. (2015). The rise of Astyanax cavefish. Dev. Dyn. *244*, 1031–1038.

Guelman, S., Suganuma, T., Florens, L., Swanson, S.K., Kiesecker, C.L., Kusch, T., Anderson, S., Yates, J.R., Washburn, M.P., Abmayr, S.M., et al. (2006). Host cell factor and an uncharacterized SANT domain protein are stable components of ATAC, a novel dAda2A/dGcn5-containing histone acetyltransferase complex in Drosophila. Mol. Cell. Biol. *26*, 871–882.

Gupta, S., Stamatoyannopoulos, J.A., Bailey, T.L., and Noble, W.S. (2007). Quantifying similarity between motifs. Genome Biol. *8*, R24.

Guruharsha, K.G., Rual, J.-F., Zhai, B., Mintseris, J., Vaidya, P., Vaidya, N., Beekman, C., Wong, C., Rhee, D.Y., Cenaj, O., et al. (2011). A protein complex network of Drosophila melanogaster. Cell *147*, 690–703.

Gutierrez-Aviño, F.J., Ferres-Marco, D., and Dominguez, M. (2009). The position and function of the Notch-mediated eye growth organizer: the roles of JAK/STAT and four-jointed. EMBO Rep. *10*, 1051–1058.

Halder, G., Callaerts, P., and Gehring, W.J. (1995). Induction of ectopic eyes by targeted expression of the eyeless gene in Drosophila. Science *267*, 1788–1792.

Halder, G., Callaerts, P., Flister, S., Walldorf, U., Kloter, U., and Gehring, W.J. (1998). Eyeless initiates the expression of both sine oculis and eyes absent during Drosophila compound eye development. Development *125*, 2181–2191.

Hall, B.K. (2012). Evolutionary Developmental Biology (Evo-Devo): Past, Present, and Future. Evo. Edu. Outreach *5*, 184–193.

Hosoishi, S. (2019). A new subterranean Crematogaster with one ommatidium from Cambodia, based on morphology and DNA (Hymenoptera: Formicidae). Acta Entomol Mus Natl Pragae *59*, 507–511.

Iyer, E.P.R., Iyer, S.C., Sullivan, L., Wang, D., Meduri, R., Graybeal, L.L., and Cox, D.N. (2013). Functional genomic analyses of two morphologically distinct classes of Drosophila sensory neurons: post-mitotic roles of transcription factors in dendritic patterning. PLoS One *8*, e72434.

Jang, C.-C., Chao, J.-L., Jones, N., Yao, L.-C., Bessarab, D.A., Kuo, Y.M., Jun, S., Desplan, C., Beckendorf, S.K., and Sun, Y.H. (2003). Two Pax genes, eye gone and eyeless, act cooperatively in promoting Drosophila eye development. Development *130*, 2939–2951.

Jarman, A.P., Grell, E.H., Ackerman, L., Jan, L.Y., and Jan, Y.N. (1994). Atonal is the proneural gene for Drosophila photoreceptors. Nature *369*, 398–400.

Johannsen, W. (1911). The genotype conception of heredity. Am. Nat. *45*, 129–159.

Keesey, I.W., Grabe, V., Gruber, L., Koerte, S., Obiero, G.F., Bolton, G., Khallaf, M.A., Kunert, G., Lavista-Llanos, S., Valenzano, D.R., et al. (2019). Inverse resource allocation between vision and olfaction across the genus Drosophila. Nat. Commun. *10*, 1162.

Keesey, I.W., Grabe, V., Knaden, M., and Hansson, B.S. (2020). Divergent sensory investment mirrors potential speciation via niche partitioning across Drosophila. Elife *9*.

Kenyon, K.L., Yang-Zhou, D., Cai, C.Q., Tran, S., Clouser, C., Decene, G., Ranade, S., and Pignoni, F. (2005). Partner specificity is essential for proper function of the SIX-type homeodomain proteins Sine oculis and Optix during fly eye development. Dev. Biol. *286*, 158–168.

Kim, A.-R., Choi, E.-B., Kim, M.-Y., and Choi, K.-W. (2017). Angiotensin-converting enzyme Ance is cooperatively regulated by Mad and Pannier in Drosophila imaginal discs. Sci. Rep. *7*, 13174.

Kim, J., Johnson, K., Chen, H.J., Carroll, S., and Laughon, A. (1997). Drosophila Mad binds to DNA and directly mediates activation of vestigial by Decapentaplegic. Nature *388*, 304–308.

Kiser, P.D., Golczak, M., Maeda, A., and Palczewski, K. (2012). Key enzymes of the retinoid (visual) cycle in vertebrate retina. Biochim. Biophys. Acta *1821*, 137–151.

Klein, T. (2008). Immunolabeling of imaginal discs. Methods Mol. Biol. *420*, 253–263.

Koushika, S.P., Lisbin, M.J., and White, K. (1996). ELAV, a Drosophila neuron-specific protein, mediates the generation of an alternatively spliced neural protein isoform. Curr. Biol. *6*, 1634–1641.

Kratochwil, C.F., Liang, Y., Gerwin, J., Woltering, J.M., Urban, S., Henning, F., Machado-Schiaffino, G., Hulsey, C.D., and Meyer, A. (2018). Agouti-related peptide 2 facilitates convergent evolution of stripe patterns across cichlid fish radiations. Science *362*, 457–460.

Kumar, J.P. (2009a). The molecular circuitry governing retinal determination. Biochim. Biophys. Acta *1789*, 306–314.

Kumar, J.P. (2009b). The sine oculis homeobox (SIX) family of transcription factors as regulators of development and disease. Cell Mol. Life Sci. *66*, 565–583.

Kumar, J.P. (2012). Building an ommatidium one cell at a time. Dev. Dyn. *241*, 136–149.

Land, M.F., and Fernald, R.D. (1992). The evolution of eyes. Annu. Rev. Neurosci. *15*, 1–29.

Land, M.F., and Nilsson, D.-E. (2006). General-purpose and special-purpose visual systems. In Invertebrate Vision, E. Warrant, and D.-E. Nilsson, eds. (Cambridge, UK: Cambridge University Press), p. 570.

Land, M.F., and Nilsson, D.-E. (2012). Animal Eyes (Oxford Animal Biology Series) (Oxford: Oxford University Press).

Larkin, A., Marygold, S.J., Antonazzo, G., Attrill, H., Dos Santos, G., Garapati, P.V., Goodman, J.L., Gramates, L.S., Millburn, G., Strelets, V.B., et al. (2021). FlyBase: updates to the Drosophila melanogaster knowledge base. Nucleic Acids Res. *49*, D899–D907.

Lim, J., Jafar-Nejad, H., Hsu, Y.-C., and Choi, K.-W. (2008). Novel function of the class I bHLH protein Daughterless in the negative regulation of proneural gene expression in the Drosophila eye. EMBO Rep. *9*, 1128–1133.

Liu, B., Zheng, Y., Yin, F., Yu, J., Silverman, N., and Pan, D. (2016). Toll Receptor-Mediated Hippo Signaling Controls Innate Immunity in Drosophila. Cell *164*, 406–419.

Lloyd, D.L., Toegel, M., Fulga, T.A., and Wilkie, A.O.M. (2018). The Drosophila homologue of MEGF8 is essential for early development. Sci. Rep. *8*, 8790.

Ludlam, W.H., Taylor, M.H., Tanner, K.G., Denu, J.M., Goodman, R.H., and Smolik, S.M. (2002). The acetyltransferase activity of CBP is required for wingless activation and H4 acetylation in Drosophila melanogaster. Mol. Cell. Biol. *22*, 3832–3841.

Ma, C., and Moses, K. (1995). Wingless and patched are negative regulators of the morphogenetic furrow and can affect tissue polarity in the developing Drosophila compound eye. Development *121*, 2279–2289.

Mackay, T.F. (1995). The genetic basis of quantitative variation: numbers of sensory bristles of Drosophila melanogaster as a model system. Trends Genet. *11*, 464–470.

Mandaravally Madhavan, M., and Schneiderman, H.A. (1977). Histological analysis of the dynamics of growth of imaginal discs and histoblast nests during the larval development ofDrosophila melanogaster. Wilhelm Roux'. Archiv. *183*, 269–305.

Mangan, S., and Alon, U. (2003). Structure and function of the feed-forward loop network motif. Proc. Natl. Acad. Sci. USA *100*, 11980–11985.

Mao, Y., Rauskolb, C., Cho, E., Hu, W.-L., Hayter, H., Minihan, G., Katz, F.N., and Irvine, K.D. (2006). Dachs: an unconventional myosin that functions downstream of Fat to regulate growth, affinity and gene expression in Drosophila. Development *133*, 2539–2551.

Mao, Y., Tournier, A.L., Bates, P.A., Gale, J.E., Tapon, N., and Thompson, B.J. (2011). Planar polarization of the atypical myosin Dachs orients cell divisions in Drosophila. Genes Dev. *25*, 131–136.

La Marca, J.E., Diepstraten, S.T., Hodge, A.L., Wang, H., Hart, A.H., Richardson, H.E., and Somers, W.G. (2019). Strip and Cka negatively regulate JNK signalling during Drosophila spermatogenesis. Development *146*.

Maurel-Zaffran, C., and Treisman, J.E. (2000). pannier acts upstream of wingless to direct dorsal eye disc development in Drosophila. Development *127*, 1007–1016.

Melicharek, D., Shah, A., DiStefano, G., Gangemi, A.J., Orapallo, A., Vrailas-Mortimer, A.D., and Marenda, D.R. (2008). Identification of novel regulators of atonal expression in the developing Drosophila retina. Genetics *180*, 2095–2110.

Milo, R., Shen-Orr, S., Itzkovitz, S., Kashtan, N., Chklovskii, D., and Alon, U. (2002). Network motifs: simple building blocks of complex networks. Science *298*, 824–827.

Mora-Martinez, C. (2021). Expression pattern determines regulatory logic. PLoS One *16*, e0244864.

Moses, K., and Rubin, G.M. (1991). Glass encodes a site-specific DNA-binding protein that is regulated in response to positional signals in the developing Drosophila eye. Genes Dev. *5*, 583–593.

Mosimann, C., Hausmann, G., and Basler, K. (2006). Parafibromin/Hyrax activates Wnt/Wg target gene transcription by direct association with beta-catenin/Armadillo. Cell *125*, 327–341.

Mowrer, K.R., and Wolfe, M.S. (2008). Promotion of BACE1 mRNA alternative splicing reduces amyloid beta-peptide production. J. Biol. Chem. *283*, 18694–18701.

Mukherjee, T., Schäfer, U., and Zeidler, M.P. (2006). Identification of Drosophila genes modulating Janus kinase/signal transducer and activator of transcription signal transduction. Genetics *172*, 1683–1697.

Müller, G.B. (2007). Evo-devo: extending the evolutionary synthesis. Nat. Rev. Genet. *8*, 943–949.

Murray, M.J., Ng, M.M., Fraval, H., Tan, J., Liu, W., Smallhorn, M., Brill, J.A., Field, S.J., and Saint, R. (2012). Regulation of Drosophila mesoderm migration by phosphoinositides and the PH domain of the Rho GTP exchange factor Pebble. Dev. Biol. *372*, 17–27.

Narendra, A., Reid, S.F., Greiner, B., Peters, R.A., Hemmi, J.M., Ribi, W.A., and Zeil, J. (2011). Caste-specific visual adaptations to distinct daily activity schedules in Australian Myrmecia ants. Proc. Biol. Sci. *278*, 1141–1149.

Neal, S.J., Zhou, Q., and Pignoni, F. (2020). STRIPAK-PP2A regulates Hippo-Yorkie signaling to suppress retinal fate in the Drosophila eye disc peripodial epithelium. J. Cell Sci. *133*.

Neubueser, D., and Hipfner, D.R. (2010). Overlapping roles of Drosophila Drak and Rok kinases in epithelial tissue morphogenesis. Mol. Biol. Cell *21*, 2869–2879.

Nilsson, D.-E. (1989). Optics and evolution of the compound eye. In Facets of Vision, D.G. Stavenga, and R.C. Hardie, eds. (Berlin, Heidelberg: Springer Berlin Heidelberg), pp. 30–73.

Nilsson, D.-E. (2009). The evolution of eyes and visually guided behaviour. Philos. Trans. R. Soc. Lond. B, Biol. Sci. *364*, 2833–2847.

Nilsson, D.-E. (2013). Eye evolution and its functional basis. Vis Neurosci *30*, 5–20.

Nilsson, D.E., and Pelger, S. (1994). A pessimistic estimate of the time required for an eye to evolve. Proc. Biol. Sci. *256*, 53–58.

Norry, F.M., and Gomez, F.H. (2017). Quantitative trait loci and antagonistic associations for two developmentally related traits in the drosophila head. J. Insect Sci. *17*.

Oliver, S. (2000). Guilt-by-association goes global. Nature *403*, 601–603.

Organista, M.F., and De Celis, J.F. (2013). The Spalt transcription factors regulate cell proliferation, survival and epithelial integrity downstream of the Decapentaplegic signalling pathway. Biol. Open *2*, 37–48.

Oros, S.M., Tare, M., Kango-Singh, M., and Singh, A. (2010). Dorsal eye selector pannier (pnr) suppresses the eye fate to define dorsal margin of the Drosophila eye. Dev. Biol. *346*, 258–271.

Özer, I., and Carle, T. (2020). Back to the light, coevolution between vision and olfaction in the "Dark-flies" (Drosophila melanogaster). PLoS One *15*, e0228939.

Pallavi, S.K., and Shashidhara, L.S. (2005). Signaling interactions between squamous and columnar epithelia of the Drosophila wing disc. J. Cell Sci. *118*, 3363–3370.

Pappu, K.S., Ostrin, E.J., Middlebrooks, B.W., Sili, B.T., Chen, R., Atkins, M.R., Gibbs, R., and Mardon, G. (2005). Dual regulation and redundant function of two eye-specific enhancers of the Drosophila retinal determination gene dachshund. Development *132*, 2895–2905.

Parker, A. (2004). In The Blink Of An Eye: How Vision Sparked The Big Bang Of Evolution (Basic Books).

Pichaud, F. (2014). Transcriptional regulation of tissue organization and cell morphogenesis: the fly retina as a case study. Dev. Biol. *385*, 168–178.

Pignoni, F., Hu, B., Zavitz, K.H., Xiao, J., Garrity, P.A., and Zipursky, S.L. (1997). The eye-specification proteins So and Eya form a complex and regulate multiple steps in Drosophila eye development. Cell *91*, 881–891.

Porter, M.L. (2016). Beyond the eye: molecular evolution of extraocular photoreception. Integr. Comp. Biol. *56*, 842–852.

Posnien, N., Hopfen, C., Hilbrant, M., Ramos-Womack, M., Murat, S., Schönauer, A., Herbert, S.L., Nunes, M.D.S., Arif, S., Breuker, C.J., et al. (2012). Evolution of eye morphology and rhodopsin expression in the Drosophila melanogaster species subgroup. PLoS One *7*, e37346.

Potier, D., Davie, K., Hulselmans, G., Naval Sanchez, M., Haagen, L., Huynh-Thu, V.A., Koldere, D., Celik, A., Geurts, P., Christiaens, V., et al. (2014). Mapping gene regulatory networks in Drosophila eye development by large-scale transcriptome perturbations and motif inference. Cell Rep. *9*, 2290–2303.

Ramaekers, A., Claeys, A., Kapun, M., Mouchel-Vielh, E., Potier, D., Weinberger, S., Grillenzoni, N., Dardalhon-Cuménal, D., Yan, J., Wolf, R., et al. (2019). Altering the Temporal Regulation of One Transcription Factor Drives Evolutionary Trade-Offs between Head Sensory Organs. Dev. Cell *50*, 780–792.e7.

Rao, R.C., Tchedre, K.T., Malik, M.T.A., Coleman, N., Fang, Y., Marquez, V.E., and Chen, D.F. (2010). Dynamic patterns of histone lysine methylation in the developing retina. Invest. Ophthalmol. Vis. Sci. *51*, 6784–6792.

Ready, D.F., Hanson, T.E., and Benzer, S. (1976). Development of the Drosophila retina, a neurocrystalline lattice. Dev. Biol. *53*, 217–240.

Reeves, R.G., and Tautz, D. (2017). Automated Phenotyping Indicates Pupal Size in Drosophila Is a Highly Heritable Trait with an Apparent Polygenic Basis. G3 (Bethesda) *7*, 1277–1286.

Reis, M., Wiegleb, G., Claude, J., Lata, R., Horchler, B., Ha, N.-T., Reimer, C., Vieira, C.P., Vieira, J., and Posnien, N. (2020). Multiple loci linked to inversions are associated with eye size variation in species of the *Drosophila virilis* phylad. BioRxiv.

Rétaux, S., and Casane, D. (2013). Evolution of eye development in the darkness of caves: adaptation, drift, or both? Evodevo *4*, 26.

Reynolds-Kenneally, J., and Mlodzik, M. (2005). Notch signaling controls proliferation through cell-autonomous and non-autonomous mechanisms in the Drosophila eye. Dev. Biol. *285*, 38–48.

Rister, J., Pauls, D., Schnell, B., Ting, C.-Y., Lee, C.-H., Sinakevitch, I., Morante, J., Strausfeld, N.J., Ito, K., and Heisenberg, M. (2007). Dissection of the peripheral motion channel in the visual system of Drosophila melanogaster. Neuron *56*, 155–170.

Robertson, F., Pinal, N., Fichelson, P., and Pichaud, F. (2012). Atonal and EGFR signalling orchestrate rok- and Drak-dependent adherens junction remodelling during ommatidia morphogenesis. Development *139*, 3432–3441.

Rodrigues-Campos, M., and Thompson, B.J. (2014). The ubiquitin ligase FbxL7 regulates the Dachsous-Fat-Dachs system in Drosophila. Development *141*, 4098–4103.

Rogers, E.M., Brennan, C.A., Mortimer, N.T., Cook, S., Morris, A.R., and Moses, K. (2005). Pointed regulates an eye-specific transcriptional enhancer in the Drosophila hedgehog gene, which is required for the movement of the morphogenetic furrow. Development *132*, 4833–4843.

Royet, J., and Finkelstein, R. (1996). hedgehog, wingless and orthodenticle specify adult head development in Drosophila. Development *122*, 1849–1858.

Rusconi, J.C., Fink, J.L., and Cagan, R. (2004). klumpfuss regulates cell death in the Drosophila retina. Mech. Dev. *121*, 537–546.

Sánchez-Aragón, M., Cantisán-Gómez, J., Luque, C.M., Brás-Pereira, C., Lopes, C.S., Lemos, M.C., and Casares, F. (2019). A Toggle-Switch and a Feed-Forward Loop Engage in the Control of the Drosophila Retinal Determination Gene Network. Front. Ecol. Evol. *7*.

Scanlan, J.L., Gledhill-Smith, R.S., Battlay, P., and Robin, C. (2020). Genomic and transcriptomic analyses in Drosophila suggest that the ecdysteroid kinase-like (EcKL) gene family encodes the "detoxification-by-phosphorylation" enzymes of insects. Insect Biochem. Mol. Biol. *123*, 103429.

Schlichting, K., and Dahmann, C. (2008). Hedgehog and Dpp signaling induce cadherin Cad86C expression in the morphogenetic furrow during Drosophila eye development. Mech. Dev. *125*, 712–728.

Schoenemann, B., and Clarkson, E.N.K. (2020). Insights into a 429-million-year-old compound eye. Sci. Rep. *10*, 12029.

Schoenemann, B., and Clarkson, E.N.K. (2021). Points of view in understanding trilobite eyes. Nat. Commun. *12*, 2081.

Schoenemann, B., Pärnaste, H., and Clarkson, E.N.K. (2017). Structure and function of a compound eye, more than half a billion years old. Proc. Natl. Acad. Sci. USA *114*, 13489–13494.

Schwab, I.R. (2018). The evolution of eyes: major steps. The Keeler lecture 2017: centenary of Keeler Ltd. Eye (Lond.) *32*, 302–313.

Sheikh, B.N., and Akhtar, A. (2019). The many lives of KATs - detectors, integrators and modulators of the cellular environment. Nat. Rev. Genet. *20*, 7–23.

Shen, W., and Mardon, G. (1997). Ectopic eye development in Drosophila induced by directed dachshund expression. Development *124*, 45–52.

Silies, M., Yuva, Y., Engelen, D., Aho, A., Stork, T., and Klämbt, C. (2007). Glial cell migration in the eye disc. J. Neurosci. *27*, 13130–13139.

Singh, A., and Choi, K.-W. (2003). Initial state of the Drosophila eye before dorsoventral specification is equivalent to ventral. Development *130*, 6351–6360.

Singh, A., Chan, J., Chern, J.J., and Choi, K.-W. (2005). Genetic interaction of Lobe with its modifiers in dorsoventral patterning and growth of the Drosophila eye. Genetics *171*, 169–183.

Skottheim Honn, J., Johansson, L., and Rasmuson Lestander, Å. (2016). Regulation of twin of eyeless during Drosophila development. Gene Expr Patterns *20*, 120–129.

Staehling-Hampton, K., Hoffmann, F.M., Baylies, M.K., Rushton, E., and Bate, M. (1994). dpp induces mesodermal gene expression in Drosophila. Nature *372*, 783–786.

Stanković, D., Claudius, A.-K., Schertel, T., Bresser, T., and Uhlirova, M. (2020). A Drosophila model to study retinitis pigmentosa pathology associated with mutations in the core splicing factor Prp8. Dis. Model. Mech. *13*.

Stern, D.L., and Orgogozo, V. (2009). Is genetic evolution predictable? Science *323*, 746–751.

Streinzer, M., Brockmann, A., Nagaraja, N., and Spaethe, J. (2013). Sex and caste-specific variation in compound eye morphology of five honeybee species. PLoS One *8*, e57702.

Suganuma, T., Gutiérrez, J.L., Li, B., Florens, L., Swanson, S.K., Washburn, M.P., Abmayr, S.M., and Workman, J.L. (2008). ATAC is a double histone acetyltransferase complex that stimulates nucleosome sliding. Nat. Struct. Mol. Biol. *15*, 364–372.

Supple, J.A., Pinto-Benito, D., Khoo, C., Wardill, T.J., Fabian, S.T., Liu, M., Pusdekar, S., Galeano, D., Pan, J., Jiang, S., et al. (2020). Binocular Encoding in the Damselfly Pre-motor Target Tracking System. Curr. Biol. *30*, 645–656.e4.

Tare, M., Sarkar, A., Bedi, S., Kango-Singh, M., and Singh, A. (2016). Cullin-4 regulates Wingless and JNK signaling-mediated cell death in the Drosophila eye. Cell Death Dis. *7*, e2566.

Tautz, D., Reeves, R., and Pallares, L.F. (2020). New experimental support for long standing concepts of polygenic genetics implies that the Mendelian genetic paradigm needs to be revised. Nationale Akademie der Wissenschaften Leopoldina.

Tavares, L., Correia, A., Santos, M.A., Relvas, J.B., and Pereira, P.S. (2017). dMyc is required in retinal progenitors to prevent JNK-mediated retinal glial activation. PLoS Genet. *13*, e1006647.

Tavsanli, B.C., Ostrin, E.J., Burgess, H.K., Middlebrooks, B.W., Pham, T.A., and Mardon, G. (2004). Structure-function analysis of the Drosophila retinal determination protein Dachshund. Dev. Biol. *272*, 231–247.

Thomas, B.J., Gunning, D.A., Cho, J., and Zipursky, L. (1994). Cell cycle progression in the developing Drosophila eye: roughex encodes a novel protein required for the establishment of G1. Cell *77*, 1003–1014.

Tian, W., Zhang, L.V., Taşan, M., Gibbons, F.D., King, O.D., Park, J., Wunderlich, Z., Cherry, J.M., and Roth, F.P. (2008). Combining guilt-by-association and guilt-by-profiling to predict Saccharomyces cerevisiae gene function. Genome Biol. *9 Suppl 1*, S7.

Torres-Oliva, M. (2016). Identification of the molecular changesunderlying head morphology variation inclosely related Drosophila species. Doctoral dissertation.

Torres-Oliva, M., Schneider, J., Wiegleb, G., Kaufholz, F., and Posnien, N. (2018). Dynamic genome wide expression profiling of Drosophila head development reveals a novel role of Hunchback in retinal glia cell development and blood-brain barrier integrity. PLoS Genet. *14*, e1007180.

Torres-Oliva, M., Buchberger, E., Buffry, A.D., Kittelmann, M., Sumner-Rooney, L., Gaspar, P.M.C., Bullinger, G.C., Guerrero, G., Casares, F., Arif, S., et al. (2021). Differences in *orthodenticle* expression promote ommatidial size variation between *Drosophila* species. BioRxiv.

Treisman, J.E., and Rubin, G.M. (1995). wingless inhibits morphogenetic furrow movement in the Drosophila eye disc. Development *121*, 3519–3527.

Tsai, Y.-C., and Sun, Y.H. (2004). Long-range effect of upd, a ligand for Jak/STAT pathway, on cell cycle in Drosophila eye development. Genesis *39*, 141–153.

Tsai, Y.-C., Yao, J.-G., Chen, P.-H., Posakony, J.W., Barolo, S., Kim, J., and Sun, Y.H. (2007). Upd/Jak/STAT signaling represses wg transcription to allow initiation of morphogenetic furrow in Drosophila eye development. Dev. Biol. *306*, 760–771.

Tyas, D.A., Simpson, T.I., Carr, C.B., Kleinjan, D.A., van Heyningen, V., Mason, J.O., and Price, D.J. (2006). Functional conservation of Pax6 regulatory elements in humans and mice demonstrated with a novel transgenic reporter mouse. BMC Dev. Biol. *6*, 21.

v. Salvini-Plawen, L., and Mayr, E. (1977). On the evolution of photoreceptors and eyes. In Evolutionary Biology, M.K. Hecht, W.C. Steere, and B. Wallace, eds. (Boston, MA: Springer US), pp. 207–263.

Vollmer, J., Fried, P., Aguilar-Hidalgo, D., Sánchez-Aragón, M., Iannini, A., Casares, F., and Iber, D. (2017). Growth control in the Drosophila eye disc by the cytokine Unpaired. Development *144*, 837–843.

Vrailas-Mortimer, A., del Rivero, T., Mukherjee, S., Nag, S., Gaitanidis, A., Kadas, D., Consoulas, C., Duttaroy, A., and Sanyal, S. (2011). A muscle-specific p38 MAPK/Mef2/MnSOD pathway regulates stress, motor function, and life span in Drosophila. Dev. Cell *21*, 783–795.

Wang, C.-W., and Sun, Y.H. (2012). Segregation of eye and antenna fates maintained by mutual antagonism in Drosophila. Development *139*, 3413–3421.

Wang, J., Vasaikar, S., Shi, Z., Greer, M., and Zhang, B. (2017). WebGestalt 2017: a more comprehensive, powerful, flexible and interactive gene set enrichment analysis toolkit. Nucleic Acids Res. *45*, W130–W137.

Wang, J., Liu, G., Liu, M., Xiang, L., Xiao, Y., Zhu, H., Wu, X., Peng, Y., Zhang, W., Jiang, P., et al. (2018). The FOXK1-CCDC43 Axis Promotes the Invasion and Metastasis of Colorectal Cancer Cells. Cell Physiol. Biochem. *51*, 2547–2563.

Wang, T., Wiater, E., Zhang, X., Thomas, J.B., and Montminy, M. (2021). Crtc modulates fasting programs associated with 1-C metabolism and inhibition of insulin signaling. Proc. Natl. Acad. Sci. USA *118*.

Warde-Farley, D., Donaldson, S.L., Comes, O., Zuberi, K., Badrawi, R., Chao, P., Franz, M., Grouios, C., Kazi, F., Lopes, C.T., et al. (2010). The GeneMANIA prediction server: biological network integration for gene prioritization and predicting gene function. Nucleic Acids Res. *38*, W214–20.

Warrant, E.J. (1999). Seeing better at night: life style, eye design and the optimum strategy of spatial and temporal summation. Vision Res. *39*, 1611–1630.

Weasner, B., Salzer, C., and Kumar, J.P. (2007). Sine oculis, a member of the SIX family of transcription factors, directs eye formation. Dev. Biol. *303*, 756–771.

Wiersdorff, V., Lecuit, T., Cohen, S.M., and Mlodzik, M. (1996). Mad acts downstream of Dpp receptors, revealing a differential requirement for dpp signaling in initiation and propagation of morphogenesis in the Drosophila eye. Development *122*, 2153–2162.

Wittkorn, E., Sarkar, A., Garcia, K., Kango-Singh, M., and Singh, A. (2015). The Hippo pathway effector Yki downregulates Wg signaling to promote retinal differentiation in the Drosophila eye. Development *142*, 2002–2013.

Wolff, T., and Ready, D.F. (1991). The beginning of pattern formation in the Drosophila compound eye: the morphogenetic furrow and the second mitotic wave. Development *113*, 841–850.

Wong, K.A., Trembley, M., Abd Wahab, S., and Viczian, A.S. (2015). Efficient retina formation requires suppression of both Activin and BMP signaling pathways in pluripotent cells. Biol. Open *4*, 573–583.

Xu, Y., Xu, C., Kato, A., Tempel, W., Abreu, J.G., Bian, C., Hu, Y., Hu, D., Zhao, B., Cerovina, T., et al. (2012). Tet3 CXXC domain and dioxygenase activity cooperatively regulate key genes for Xenopus eye and neural development. Cell *151*, 1200–1213.

Yao, J.-G., and Sun, Y.H. (2005). Eyg and Ey Pax proteins act by distinct transcriptional mechanisms in Drosophila development. EMBO J. *24*, 2602–2612.

Zhang, W., Reeves, G.R., and Tautz, D. (2021). Testing Implications of the Omnigenic Model for the Genetic Analysis of Loci Identified through Genome-wide Association. Curr. Biol. *31*, 1092–1098.e6.

Zhao, H.W., Zhou, D., Nizet, V., and Haddad, G.G. (2010). Experimental selection for Drosophila survival in extremely high O2 environments. PLoS One *5*, e11701.

Zhu, J., Palliyil, S., Ran, C., and Kumar, J.P. (2017). Drosophila Pax6 promotes development of the entire eye-antennal disc, thereby ensuring proper adult head formation. Proc. Natl. Acad. Sci. USA *114*, 5846–5853.

(2020). Molecular genetics of axial patterning, growth and disease in drosophila eye (Cham: Springer International Publishing).